UNIVERSITY OF CALIFORNIA
RIVERSIDE

Separation of Modified Biomolecules With Synthetic Receptors in Capillary Electrophoresis

A Dissertation submitted in partial satisfaction
of the requirements for the degree of

Doctor of Philosophy

in

Chemistry

by

Jiwon Lee

March 2020

Dissertation Committee:
Dr. Wenwan Zhong, Chairperson
Dr. Joseph Genereux
Dr. Ryan Julian

The Dissertation of Jiwon Lee is approved:

_____

_____

_____

Committee Chairperson

University of California, Riverside

Acknowledgments

I would like to acknowledge my PhD advisor, Dr. Wenwan Zhong, for her guidance and support throughout the years. I have learned so much from her on how to become a better researcher, and her enthusiasm is inspirational. I'd also like to acknowledge the other members of my dissertation committee, Dr. Ryan Julian and Dr. Joseph Genereux, for their time and the advice they have given me.

I'd like to acknowledge Dr. Jikui Song and Linfeng Gao for their permission and help with the instrument for isothermal titration calorimetry. All your training and assistance has been valuable. I'd like to thank Dr. Richard Hooley and the Hooley group members for their resources as well as help on synthetic receptor studies in Chapters 2 through 4. You have been so kind and tremendously helpful. I'd also like to thank Dr. Min Xue and the Xue group members for their resources and help on peptide synthesis in Chapter 3. Thank you for your generosity and sincerity. For providing the tetraphosphonate cavitand as described in Chapter 5, I'd like to thank Dr. Enrico Dalcanale and his lab. I also thank the National Science Foundation (NSF) for funding the projects discussed in this dissertation.

I would like to acknowledge all my former and current co-workers in the Zhong lab for all your advice and support over the years. I would like to provide a special thanks to Junyi Chen for all her technical assistance and contributions in Chapters 3 and 4. Finally, I'd like to acknowledge my parents, Shin Woo Lee and Ji Sun Kim, for their love and support in all my endeavors. Thank you both so much for being there for me, and I appreciate all the sacrifices you have made for our family.

The text and figures in Chapter 2 of this dissertation, in part or in full, has been reprinted (adapted) with permission from *Anal. Chem.* **2018**, *90* (3), 1881–1888. The co-author (Dr. Wenwan Zhong) listed in that publication directed and supervised the research which forms the basis for this chapter.

ABSTRACT OF THE DISSERTATION

Separation of Modified Biomolecules With Synthetic Receptors in Capillary Electrophoresis

by

Jiwon Lee

Doctor of Philosophy, Graduate Program in Chemistry
University of California, Riverside, March 2020
Dr. Wenwan Zhong, Chairperson

Post-translational modifications (PTMs) on histone proteins affect many essential biological processes. With the abundance of PTMs on histone proteins, these modifications can collectively work together to alter chromatin structure and impact gene expression in this complex system. Detection and understanding of these PTMs, as well as the enzymes that mediate them, can elucidate their biological outcomes and connection to pathogenesis. Mass spectrometry (MS) is a powerful tool that is most often used for identification and characterization of modification patterns, and it has greatly expanded the library of histone modifications. However, MS does require coupling to separation techniques, such as reversed-phase liquid chromatography and hydrophilic interaction chromatography, in order to reduce sample complexity and improve analysis. While chromatographic techniques have been widely used, multiple columns and long separation times are required for peptides that are more challenging to separate. For instance, methylation does not alter the charge of lysine residues; in addition, it introduces only subtle changes in size and

hydrophobicity. Recently, there has been an increasing interest in synthetic receptors that have affinity for lysine methylation. Such receptors include water-soluble calixarenes, cucurbiturils, and deep cavitands. Capillary electrophoresis (CE) is an extremely suitable separation method that can be combined with these synthetic receptors, which can be easily included in the separation buffer. In this work, we first developed a method to induce mobility shifts for methylated small guests and peptides. After combining the high resolving power of CE and the selective recognition of host molecules, separation of modified and unmodified peptides was achieved. This host-assisted CE method was able to discriminate between different lysine methylation levels; essentially, this enabled the monitoring of various PTM enzyme reactions, including demethylation, methylation, and phosphorylation. This technique has also demonstrated its capability for analysis of a crosstalk event in which a pre-existing histone modification can impact the activity of an enzyme for another PTM. Furthermore, there is potential of host-assisted CE to separate proteins with PTMs as well.

Table of Contents

List of Figures

List of Tables

Chapter 1: Introduction

1.1 Post-Translational Modifications on Histone Proteins

Histone proteins can condense DNA into chromatin and form nucleosomes. In this structure, DNA is coiled around an octamer comprised of histones H2A, H2B, H3, and H4. Most modifications can occur on the histone tails although some can still appear in the globular portion. These modifications fall under one of the many classifications which include, but are not limited to: acetylation, methylation, phosphorylation, glycosylation, ubiquitylation, and lipidation. Most often, these modifications are facilitated by enzymes, which can act as "writers" to add or as "erasers" to remove post-translational modifications (PTMs).

With the wide range of PTMs that can exist, their combinatorial pattern forms a histone code.[1] Specifically, a single PTM does not act on its own; many PTMs synergistically or antagonistically work together in a signaling network. The histone codes can be interpreted either through direct impacts on the nucleosome or through effector modulation.[2] These effector proteins contain reader domains, which recognize different modifications. Many protein modules, such as bromodomains,[3] chromodomains,[4–6] Tudor domains,[7,8] and plant homeodomains (PHDs)[9–11] have been reported to bind to specific histone marks. The amount, the type, and the combination of these modifications modulate genes (i.e., gene activation or silencing), chromatin organization, and DNA replication, which highlights the importance of PTMs. Furthermore, the addition or removal of histone marks is correlated with neurodegenerative diseases,[12,13] cancer,[14] and cardiovascular diseases.[15]

Discovery and characterization of these PTMs is usually done via mass spectrometry,[16,17] which has significantly expanded the library of known modifications. However, prior treatments such as separation or enrichment techniques are necessary to reduce the sample complexity, which can decrease ion suppression effects and improve identification of low abundance markers when using MS.[18] Current methods include reversed-phase high performance liquid chromatography (RP-HPLC), immobilized metal affinity chromatography (IMAC), and hydrophilic interaction chromatography (HILIC). However, chromatography methods elicit long separation times as well as multiple dimensions,[19] which can require complicated method development. Also, there are still limitations in the amount of coverage, and capillary electrophoresis is a highly efficient separation tool that can uncover additional PTMs.[20] Two PTMs that are covered in this dissertation are lysine methylation and phosphorylation.

1.1.1 Lysine Methylation

Like arginine methylation, lysine methylation is a unique PTM in which there can be multiple levels of methylation (Figure 1.1), each have different downstream biological effects. A lysine residue can be mono-, di-, or tri-methylated. Lysine methyltransferases transfer methyl groups from S-adensoyl-L-methioinine to the residue; on the other hand, lysine demethylases can reverse the reaction to remove the methyl group. There are many different site of methylation including lysine 4, 9, 27, 36, and 79 on histone H3 as well as lysine 20 in histone H4.[4] Depending on the site and level of modification, there are different effects on gene control and relations to disease outcome, as lysine methylation has been

correlated with cancer.[21] So the ease of identifying this modification is vital for disease diagnosis.

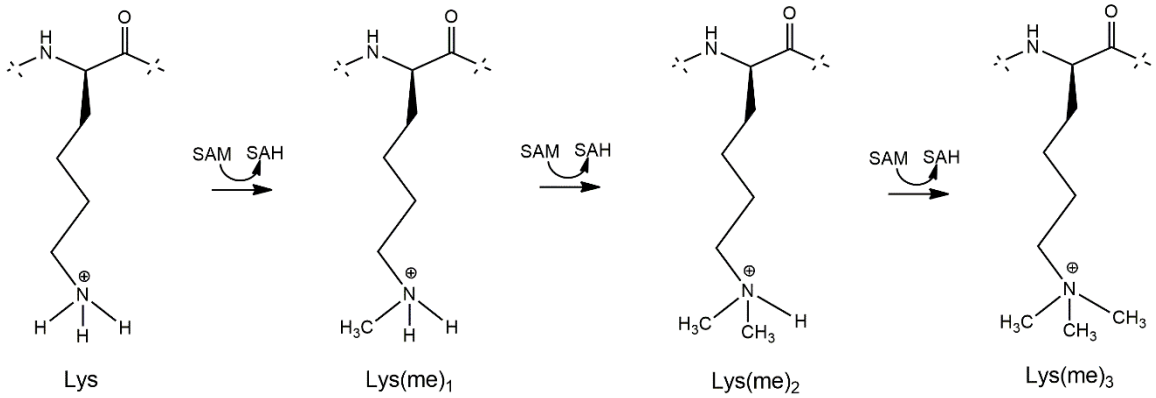

Figure 1.1 The various methylation levels on lysine: no methylation, monomethylation, dimethylation, and trimethylation.

1.1.2 Phosphorylation

Phosphorylation can occur on serine, threonine, or tyrosine residues. It is modulated by kinases that add a phosphoryl group and by phosphatases that remove one. These kinases require adenosine triphosphate to transfer a phosphate group to the amino acid. Phosphorylation can occur on serine 10 and 28 on histone H3 as well as on serine 1 in histone H4.[4] Most focus has been on the phosphorylation of serine 10 and 28, which are both involved in chromosome condensation in mitotic events. Considering the biological impacts in gene activation and deactivation, it is highly important to identify these PTMs.

1.2 Capillary Electrophoresis

Capillary electrophoresis (CE) is an open-channel separation technique with a variety of applications in the analysis of numerous biological molecules. The technique employs a bare fused silica capillary with an inner diameter ranging from 25 μm to 150

μm. Injection of the small nanoliter sample is completed hydrodynamically or electrokinetically; hydrodynamic injection applies pressure differences while electrokinetic injection uses voltage. Upon high voltage application, each component in the sample plug can be separated based on size and charge. Each ion in the sample has its own apparent mobility, which can be calculated by the following:

$$\mu_{app} = \frac{L_d/t_m}{V/L_t} \qquad \textbf{Equation 1.1}$$

L_d is the effective length measured from the inlet to the detection window, L_t is the total length from the inlet to the outlet of the capillary, t_m is the migration time (i.e., the time the analyte takes to reach the detector), and V is the applied voltage during separation.

Another key variable to consider in CE is the electroosmotic flow (EOF). When the inner capillary wall is exposed to the background electrolyte that has a pH above approximately four, the silanol groups become negatively charged. Cations from the running buffer can attach to the ionized silanol groups and form the double electrical layer comprised of a fixed layer and a diffuse layer. The bulk movement of the cations in the diffuse layer causes the EOF, which can be calculated by the following:

$$\mu_{eof} = \frac{\varepsilon\zeta}{4\pi\eta} = \frac{L_d/t_{marker}}{V/L_t} \qquad \textbf{Equation 1.2}$$

ε is the relative permittivity of the buffer, ζ is the zeta potential of the inner capillary wall, and η is the viscosity of the separation buffer. EOF can also be calculated using a similar equation for the apparent mobility with the exception that t_{marker} is the time of an internal

standard or reference marker that is unaffected by the EOF. Taking both the apparent mobility and the electroosmotic flow into account, each ion's electrophoretic mobility value can be obtained with equation 1.3.

$$\mu_{em} = \mu_{app} - \mu_{eof} \qquad \textbf{Equation 1.3}$$

In terms of the EOF, there have been numerous efforts to control or eliminate it by using various coating materials to cover the zeta potential on the capillary wall.[22] The reasoning behind this is that analytes can adsorb to the negatively charged wall which affects the reproducibility of migration time, resolution, and peak shape. All these factors contribute to the efficiency of separation.

When evaluating this efficiency, there are several variables to consider. In this dissertation, we determined the peak resolutions as well as the peak tailing factors to quantitate the value of our results. Peak resolution between two peaks is defined by the ratio of the migration time difference and the average width of those peaks, and t_A is the migration time of peak A, t_B is the migration time of peak B, and $w_{b,avg}$ is the average peak width of the two peaks at baseline.

$$R = \frac{t_A - t_B}{W_{b,avg}} \qquad \textbf{Equation 1.4}$$

The difference in migration time is a way to describe the distance between the peaks and exemplify how well separated they are. The peak width, on the other hand, characterizes band broadening effects. One main advantage in CE, when compared to liquid chromatography, is its flat flow profile as opposed to a parabolic one. This results in more narrow peaks as well as better resolution. In addition, we can also look at the peak tailing factor (as described in Equation 1.5), which can indicate adsorption to the wall or the effect

of a separation buffer additive. In this equation, t_w is the distance in minutes between peak front and the center, and $w_{5.0}$ is the peak width at 5% of peak height (min).

$$t = \frac{w_{5.0}}{t_w \cdot 2} \qquad \textbf{Equation 1.5}$$

Capillary zone electrophoresis (CZE) is the fundamental mode in the suite of CE techniques. Based on this foundation, there have been numerous modes of CE techniques that have been developed over the years, such as micellar electrokinetic chromatography (MEKC), capillary gel electrophoresis, capillary isoelectric focusing, and capillary isotachophoresis. In CZE, the migration order is determined by the charge to size ratio: the most positive and smallest in hydrodynamic diameter reaches the detection window earlier and the most negative, smallest ion reaches the window last. Neutral analytes co-migrate together, regardless of size. Figure 1.2 represents the migration order of analytes that are

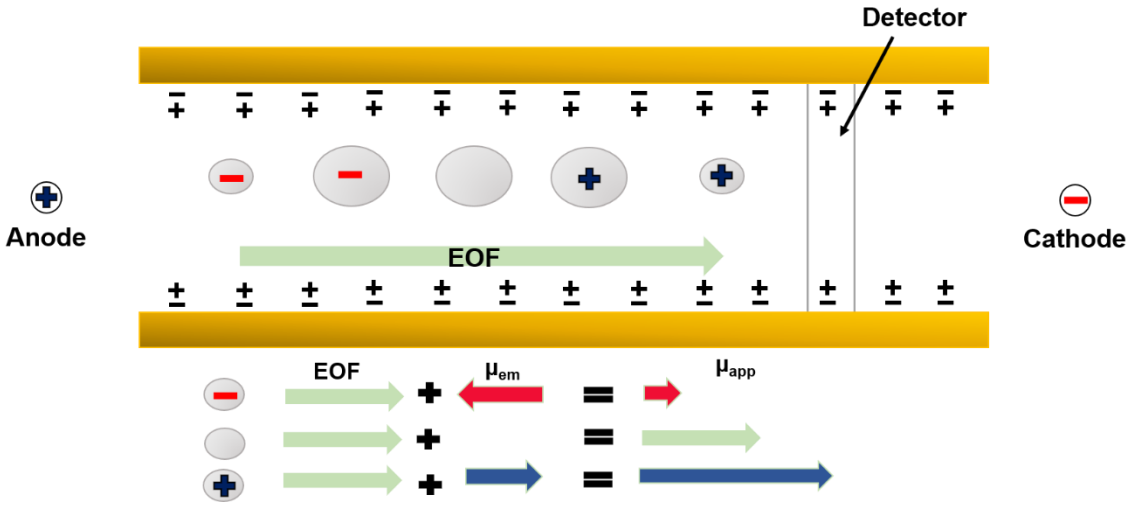

Figure 1.2 Schematic of the separation order in capillary zone electrophoresis.

based on size and charge. In the later chapters of this thesis, we introduce a method we developed that has similar concepts to that of MEKC and affinity capillary electrophoresis (ACE), as described in the following sections.

1.3 Micellar Electrokinetic Chromatography

Building upon the fundamentals of CE, there is a diverse array of techniques customized for different purposes. MEKC is a common technique that employs a pseudostationary phase. When surfactants are included in the background electrolyte above their critical micellar concentration, the micelles act as a pseudostationary phase and analytes can partition between this and the aqueous phase.

There is an assortment of surfactants that can be utilized for the separation of analytes via MEKC. Sodium dodecyl sulfate was the first surfactant used for MEKC,[23] and it is also the most commonly used. The negative charge of SDS migrates towards the cathode at a slow velocity. In general, anions will migrate first due to electrostatic repulsions from the negatively charged SDS micelles. The neutral analytes will be separated based on their hydrophobicity. As mentioned earlier, neutral analytes co-migrate in CZE, so this is one desirable benefit in MEKC. Finally, the cations migrate the slowest due to electrostatic attraction. Of course, there are other variables to consider, such as the hydrophobicity of the charged analytes. Furthermore, this migration order will be different when using other surfactants. Besides SDS, common surfactants include positive (e.g., cetrimonium bromide and tetradecyltrimethylammonium bromide), non-ionic (e.g., Brij-

35 and Tween 20), and zwitterionic (e.g., sulfobetaine) ones. Depending on the analytes and application, the most suitable surfactant can be chosen for separation in CE.

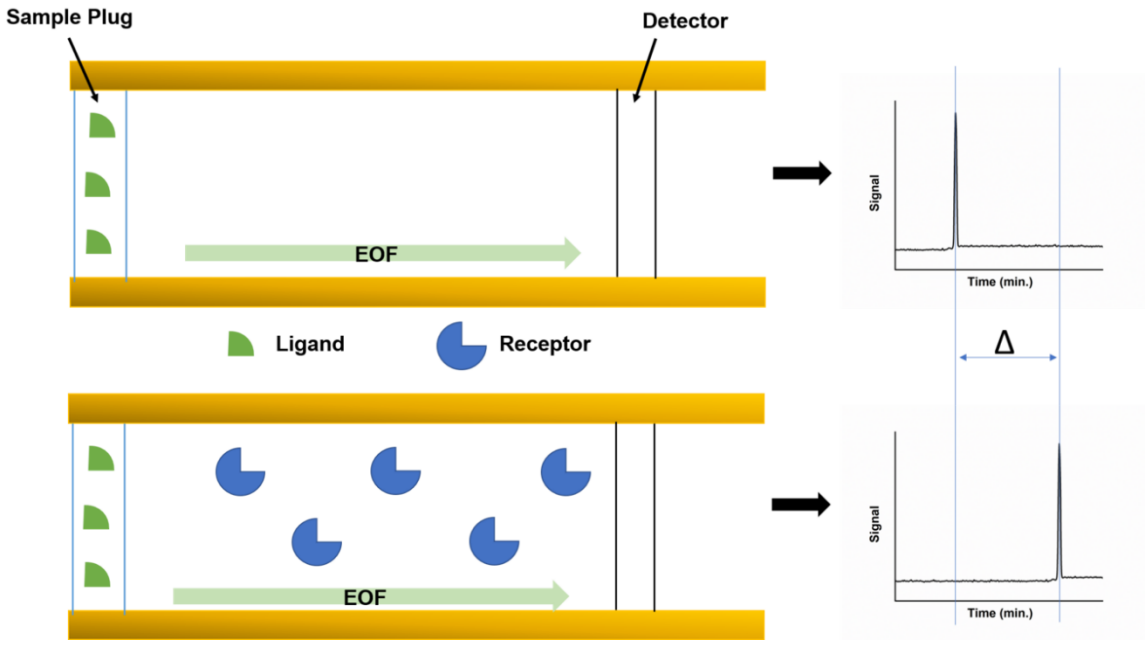

Figure 1.3 Schematic of capillary zone electrophoresis (top) and dynamic equilibrium affinity capillary electrophoresis (bottom). EOF = electroosmotic flow and Δ is the change in migration time.

1.4 Affinity Capillary Electrophoresis

Based on a similar concept to that of MEKC, affinity capillary electrophoresis (ACE) is another method involving molecular interactions; in this case, it can be used to measure affinity constants between a receptor and a ligand. ACE can be used to study the kinetics of different interaction systems. In fact, it has been applied to study many biomolecular interactions such as protein-protein,[24] protein-peptide,[25] DNA-protein,[26,27] and antibody-antigen[28] interactions. There are different derivative methods of ACE in order to study these interactions: non-equilibrium capillary electrophoresis of equilibrium mixtures (NECEEM),[29] dynamic-equilibrium ACE,[30] partial filling ACE,[31] frontal analysis

ACE (FA-ACE), ACE with immobilization,[32] and vacancy ACE (VACE).[33] Mainly, ACE falls under two categories: free solution and immobilized modes. The two prominent modes under free solution ACE include dynamic-equilibrium and pre-equilibrium ACE. In dynamic-equilibrium ACE, the receptor is in the sample and the ligand is dissolved in the running buffer or vice versa (Figure 1.3). There is a retardation in the electrophoretic mobility of the analyte due to formation of the complex. In pre-equilibrium ACE, the receptor and the ligand are pre-incubated in the sample before injection into the capillary and this applied is to slow kinetic interactions. In ACE with immobilization, the receptor can be attached to the wall or to a material on the wall while the ligand is injected as a sample. This mode is primarily for pre-concentration in order to purify or capture the analyte. The disadvantage of the immobilized mode is that it could change the structure and functionality of the attached receptor, which could ultimately affect the binding affinity to the analyte.

1.5 Synthetic Receptors

Synthetic receptors can be used in dynamic-equilibrium ACE to interact with and separate peptides and proteins with PTMs. Several macrocycles have been reported to have binding to PTMs including calixarenes, cucurbiturils, resorcinarenes,[34–36] and cyclophanes.[37] They have been used in multiple techniques such as chemical sensors,[34,38–40] separation tools,[41–43] and surface plasmon resonance spectroscopy;[44–50] they have also been used in the analysis of metal-ion binding,[51,52] PTMs,[39,42,53] fatty acids,[54] steroids,[38] and enzymes.[55] The main driving force for complexation of synthetic receptors with targeted guests is the hydrophobic effect in which there is expulsion of high-energy water

molecules from the cavity of the host.[56–58] The subsequent chapters in this dissertation focus on three synthetic receptors that are able to selectively discriminate different lysine methylation levels: calixarenes, cucurbiturils, and deep cavitands (Figure 1.4).

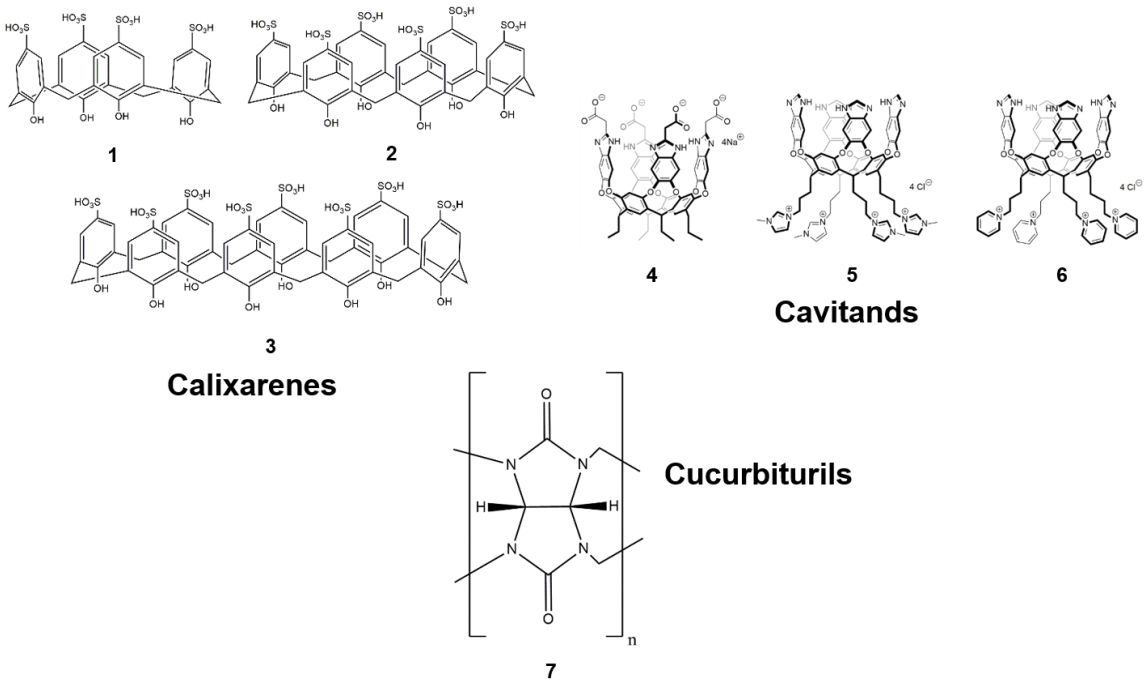

Figure 1.4 Structures of synthetic receptors: *p*-sulfonatocalix[4]arene **1**, *p*-sulfonatocalix[6]arene **2**, *p*-sulfonatocalix[8]arene **3**, tetracarboxylate cavitand **4**, neutral cavitand **5** with imidazolyl feet, neutral cavitand **6** with pyridyl feet, and cucurbit[n]urils **7**.

1.5.1 Calixarenes

Calixarene molecules have a chalice-like shape that can hold small ions and molecules. Out of the existing calixarene molecules in the literature, there has been a growing use of *p*-sulfonatocalix[n]arenes (n = 4, 6, and 8), in particular. They are quite useful in techniques requiring biological conditions due to their high solubility in water. Calixarene molecules have been used to study methylated lysine residues,[59,60] and they are able to discriminate between the different methylation levels.[60] In fact, p-

sulfonatocalix[4]arene macrocycles were able to disrupt the binding of the PHD finger, a binding motif, on the chromodomain helicase DNA-binding protein 4 to a 12-amino acid H3K9me$_3$ peptide.[61] Binding can occur due to the cation-π interactions between the positively charged methyllysine and the hydrophobic cavity of calixarene.

1.5.2 Cucurbiturils

Cucurbiturils also have affinity for lysine methylation and have preferential binding to higher methylation levels[62] although it can also bind to aromatic residues phenylalanine, tyrosine, and tryptophan.[63] These molecules have been involved in numerous studies on drug delivery[64] and imaging.[65,66] They are composed of glycoluril units linked by methylene bridges. Their size can be tuned based on the number of these units; cucurbit[n]urils, where n = 5, 6, 7, 8, or 10, have mainly been reported in publications. In comparison to calixarene and resorcinarene hosts, cucurbiturils have portals on the two entrances of the molecule. The carbonyl groups can form ion-dipole interactions with their cationic targets.

1.5.3 Deep Cavitands

Resorcinarenes are a type of calixarene. Moran et al. created the term "cavitand" to describe rigid, methylene-bridged resorcinarene molecules. It has been exemplified that cavitands can bind to different modifications such as lysine methylation[34,35] and arginine citrullination.[36] The cavitands synthesized by the Hooley group have been used in fluorescent sensors[34,35] as well as supported lipid bilayers,[45,46] and they have demonstrated a wide range in target diversity. Liu et al. was not only able to distinguish between peptides with different methylation levels but peptides with other modifications, such as acetylation

and phosphorylation; furthermore, they were able to differentiate peptides of varying lengths and with different site of modification using cavitands in a sensor.[67]

1.6 Host-Assisted Capillary Electrophoresis

This dissertation provides a method to separate histone modifications, which can help in studying the interactions between them. Our group has developed a host-assisted CE method,[42] akin to MEKC and ACE, based on the affinity between synthetic receptors and their methyllysine targets, and we were able to apply it to several enzyme assays involving a single modification, competing modifications, and inhibitory molecules. We used calixarene, cucurbituril, and cavitand hosts in the background electrolyte to induce a mobility shift and improve the resolution between analyte peaks. The combination of the high resolution in CE and the selectivity of synthetic hosts creates a powerful separation tool to study PTMs, their modulators, and the factors that affect them.

1.7 References

(1) Jenuwein, T.; Allis, C. D. Translating the Histone Code. *Science* **2001**, *293* (5532), 1074–1080.

(2) Cosgrove, M. S.; Boeke, J. D.; Wolberger, C. Regulated Nucleosome Mobility and the Histone Code. *Nat. Struct. Mol. Biol.* **2004**, *11* (11), 1037–1043.

(3) Zeng, L.; Zhou, M. Bromodomain : An Acetyl-Lysine Binding Domain. **2002**, *513*, 124–128.

(4) Lachner, M.; O'Sullivan, R. J.; Jenuwein, T. An Epigenetic Road Map for Histone Lysine Methylation. *J. Cell Sci.* **2003**, *116* (11), 2117–2124.

(5) Kim, C. H.; Kim, J. W.; Jang, S. M.; An, J. H.; Seo, S. B.; Choi, K. H. The Chromodomain-Containing Histone Acetyltransferase TIP60 Acts as a Code Reader, Recognizing the Epigenetic Codes for Initiating Transcription. *Biosci. Biotechnol. Biochem.* **2015**, *79* (4), 532–538.

(6) Wang, T.; Xu, C.; Liu, Y.; Fan, K.; Li, Z.; Sun, X.; Ouyang, H.; Zhang, X.; Zhang, J.; Li, Y.; et al. Crystal Structure of the Human SUV39H1 Chromodomain and Its Recognition of Histone H3K9me2/3. *PLoS One* **2012**, *7* (12).

(7) Lu, R.; Wang, G. G. Tudor: A Versatile Family of Histone Methylation "Readers." *Trends Biochem. Sci.* **2013**, *38* (11), 546–555.

(8) Pek, J. W.; Anand, A.; Kai, T. Tudor Domain Proteins in Development. *Dev.* **2012**, *139* (13), 2255–2266.

(9) Iwase, S.; Lan, F.; Bayliss, P.; de la Torre-Ubieta, L.; Huarte, M.; Qi, H. H.; Whetstine, J. R. R.; Bonni, A.; Roberts, T. M.; Shi, Y. The X-Linked Mental Retardation Gene SMCX/JARID1C Defines a Family of Histone H3 Lysine 4 Demethylases. *Cell* **2007**, *128* (6), 1077–1088.

(10) Li, H.; Ilin, S.; Wang, W.; Duncan, E. M.; Wysocka, J.; Allis, C. D.; Patel, D. J. Molecular Basis for Site-Specific Read-out of Histone H3K4me3 by the BPTF PHD Finger of NURF. *Nature* **2006**, *442* (7098), 91–95.

(11) Shi, X.; Hong, T.; Walter, K. L.; Ewalt, M.; Michishita, E.; Hung, T.; Carney, D.; Peña, P.; Lan, F.; Kaadige, M. R.; et al. ING2 PHD Domain Links Histone H3 Lysine 4 Methylation to Active Gene Repression. *Nature* **2006**, *442* (7098), 96–99.

(12) Anderson, K. W.; Turko, I. V. Histone Post-Translational Modifications in Frontal Cortex from Human Donors with Alzheimer's Disease. *Clin. Proteomics* **2015**, *12* (1), 1–10.

(13) Valor, L. M. Understanding Histone Deacetylation in Huntington's Disease. *Oncotarget* **2017**, *8* (4), 5660–5661.

(14) Shanmugam, M. K.; Arfuso, F.; Arumugam, S.; Chinnathambi, A.; Jinsong, B.; Warrier, S.; Wang, L. Z.; Kumar, A. P.; Ahn, K. S.; Sethi, G.; et al. Role of Novel Histone Modifications in Cancer. *Oncotarget* **2018**, *9* (13), 11414–11426.

(15) Eom, G. H.; Kook, H. Posttranslational Modifications of Histone Deacetylases: Implications for Cardiovascular Diseases. *Pharmacol. Ther.* **2014**, *143* (2), 168–180.

(16) Choudhary, C.; Mann, M. Decoding Signalling Networks by Mass Spectrometry-Based Proteomics. *Nat. Rev. Mol. Cell Biol.* **2010**, *11* (6), 427–439.

(17) Britton, L. M. P.; Gonzales-Cope, M.; Zee, B. M.; Garcia, B. A. Breaking the Histone Code with Quantitative Mass Spectrometry. *Expert Rev. Proteomics* **2011**, *8* (5), 631–643.

(18) Huang, J.; Wang, F.; Ye, M.; Zou, H. Enrichment and Separation Techniques for Large-Scale Proteomics Analysis of the Protein Post-Translational Modifications. *J. Chromatogr. A* **2014**, *1372*, 1–17.

(19) Wu, C. J.; Chen, Y. W.; Tai, J. H.; Chen, S. H. Quantitative Phosphoproteomics Studies Using Stable Isotope Dimethyl Labeling Coupled with IMAC-HILIC-NanoLC-MS/MS for Estrogen-Induced Transcriptional Regulation. *J. Proteome Res.* **2011**, *10* (3), 1088–1097.

(20) Li, Y.; Champion, M. M.; Sun, L.; DiGiuseppe Champion, P. A.; Wojcik, R.; Dovichi, N. J. CZE-ESI-MS/MS as an Alternative Proteomics Platform to UPLC-ESI-MS/MS for Samples of Intermediate Complexity. *Anal. Chem.* **2012**, *84* (3), 1617–1622.

(21) Messier, T. L.; Gordon, J. A. R.; Boyd, J. R.; Tye, C. E.; Browne, G.; Stein, J. L.; Lian, J. B.; Stein, G. S. Histone H3 Lysine 4 Acetylation and Methylation Dynamics Define Breast Cancer Subtypes. *Oncotarget* **2016**, *7* (5), 5094–5109.

(22) Hajba, L.; Guttman, A. Recent Advances in Column Coatings for Capillary Electrophoresis of Proteins. *TrAC - Trends Anal. Chem.* **2017**, *90*, 38–44.

(23) Terabe, S.; Otsuka, K.; Ichikawa, K.; Tsuchiya, A.; Ando, T. Electrokinetic Separations with Micellar Solutions and Open-Tubular Capillaries. *Anal. Chem.* **1984**, *56* (1), 111–113.

(24) Kiessig, S.; Reissmann, J.; Rascher, C.; Küllertz, G.; Fischer, A.; Thunecke, F. Application of a Green Fluorescent Fusion Protein to Study Protein-Protein Interactions by Electrophoretic Methods. *Electrophoresis* **2001**, *22* (7), 1428–1435.

(25) Gomez, F. A.; Chen, J. K.; Tanaka, A.; Schreiber, S. L.; Whitesides, G. M. Affinity Capillary Electrophoresis: Insights into the Binding of SH3 Domains by Peptides Derived from an SH3-Binding Protein. *J. Org. Chem.* **1994**, *59* (10), 2885–2886.

(26) German, I.; Buchanan, D. D.; Kennedy, R. T. Aptamers as Ligands in Affinity Probe Capillary Electrophoresis. *Anal. Chem.* **1998**, *70* (21), 4540–4545.

(27) Huang, C. C.; Cao, Z.; Chang, H. T.; Tan, W. Protein-Protein Interaction Studies Based on Molecular Aptamers by Affinity Capillary Electrophoresis. *Anal. Chem.* **2005**, *76* (23), 6973–6981.

(28) Heegaard, N. H. H. Determination of Antigen-Antibody Affinity by Immuno-Capillary Electrophoresis. *J. Chromatogr. A* **1994**, *680* (2), 405–412.

(29) Berezovski, M.; Krylov, S. N. Nonequilibrium Capillary Electrophoresis of Equilibrium Mixtures - A Single Experiment Reveals Equilibrium and Kinetic Parameters of Protein-DNA Interactions. *J. Am. Chem. Soc.* **2002**, *124* (46), 13674–13675.

(30) Marie, A. L.; Tran, N. T.; Bianchini, E. P.; Saller, F.; Pautus, S.; Abache, T.; Plantier, J. L.; Urbain, R.; Borgel, D.; Taverna, M. A Fast Capillary Electrophoresis Method to Assess the Binding Affinity of Recombinant Antithrombin toward Heparin Directly from Cell Culture Supernatants. *J. Pharm. Biomed. Anal.* **2015**, *111*, 64–70.

(31) Heintz, J.; Hernandez, M.; Gomez, F. A. Use of a Partial-Filling Technique in Affinity Capillary Electrophoresis for Determining Binding Constants of Ligands to Receptors. *J. Chromatogr. A* **1999**, *840* (2), 261–268.

(32) Sroka-Bartnicka, A.; Karlsson, I.; Ndreu, L.; Quaranta, A.; Pijnappel, M.; Thorsén, G. Particle-Based N-Linked Glycan Analysis of Selected Proteins from Biological Samples Using Nonglycosylated Binders. *J. Pharm. Biomed. Anal.* **2017**, *132*, 125–132.

(33) Busch, M. H. A.; Boelens, H. F. M.; Kraak, J. C.; Poppe, H. Vacancy Affinity Capillary Electrophoresis, a New Method for Measuring Association Constants. *J. Chromatogr. A* **1997**, *775* (1–2), 313–326.

(34) Liu, Y.; Perez, L.; Mettry, M.; Easley, C. J.; Hooley, R. J.; Zhong, W. Self-Aggregating Deep Cavitand Acts as a Fluorescence Displacement Sensor for Lysine Methylation. *J. Am. Chem. Soc.* **2016**, *138* (34), 10746–10749.

(35) Liu, Y.; Perez, L.; Gill, A. D.; Mettry, M.; Li, L.; Wang, Y.; Hooley, R. J.; Zhong, W. Site-Selective Sensing of Histone Methylation Enzyme Activity via an Arrayed Supramolecular Tandem Assay. *J. Am. Chem. Soc.* **2017**, *139* (32), 10964–10967.

(36) Gill, A. D.; Hickey, B. L.; Wang, S.; Xue, M.; Zhong, W.; Hooley, R. J. Sensing of Citrulline Modifications in Histone Peptides by Deep Cavitand Hosts. *Chem. Commun.* **2019**, *55* (88), 13259–13262.

(37) Ingerman, L. A.; Cuellar, M. E.; Waters, M. L. A Small Molecule Receptor That Selectively Recognizes Trimethyl Lysine in a Histone Peptide with Native Protein-like Affinity. *Chem. Commun.* **2010**, *46* (11), 1839–1841.

(38) Gill, A. D.; Perez, L.; Salinas, I. N. Q.; Byers, S. R.; Liu, Y.; Hickey, B. L.; Zhong, W.; Hooley, R. J. Selective Array-Based Sensing of Anabolic Steroids in Aqueous Solution by Host–Guest Reporter Complexes. *Chem. - A Eur. J.* **2019**, *25* (7), 1740–1745.

(39) Liu, Y.; Lee, J.; Perez, L.; Gill, A. D.; Hooley, R. J.; Zhong, W. Selective Sensing of Phosphorylated Peptides and Monitoring Kinase and Phosphatase Activity with a Supramolecular Tandem Assay. *J. Am. Chem. Soc.* **2018**, *140* (42), 13869–13877.

(40) Guo, D. S.; Uzunova, V. D.; Su, X.; Liu, Y.; Nau, W. M. Operational Calixarene-Based Fluorescent Sensing Systems for Choline and Acetylcholine and Their Application to Enzymatic Reactions. *Chem. Sci.* **2011**, *2* (9), 1722–1734.

(41) Garnett, G. A. E.; Starke, M. J.; Shaurya, A.; Li, J.; Hof, F. Supramolecular Affinity Chromatography for Methylation-Targeted Proteomics. *Anal. Chem.* **2016**, *88* (7), 3697–3703.

(42) Lee, J.; Perez, L.; Liu, Y.; Wang, H.; Hooley, R. J.; Zhong, W. Separation of Methylated Histone Peptides via Host-Assisted Capillary Electrophoresis. *Anal. Chem.* **2018**, *90* (3), 1881–1888.

(43) Hutchinson, S.; Kearney, G. A.; Horne, E.; Lynch, B.; Glennon, J. D.; Anthony McKervey, M.; Harris, S. J. Solid Phase Extraction of Metal Ions Using Immobilised Chelating Calixarene Tetrahydroxamates. *Anal. Chim. Acta* **1994**, *291* (3), 269–275.

(44) Ghang, Y.-J.; Perez, L.; Morgan, M. A.; Si, F.; Hamdy, O. M.; Beecher, C. N.; Larive, C. K.; Julian, R. R.; Zhong, W.; Cheng, Q.; et al. Anionic Deep Cavitands Enable the Adhesion of Unmodified Proteins at a Membrane Bilayer.

(45) Ghang, Y. J.; Lloyd, J. J.; Moehlig, M. P.; Arguelles, J. K.; Mettry, M.; Zhang, X.; Julian, R. R.; Cheng, Q.; Hooley, R. J. Labeled Protein Recognition at a Membrane Bilayer Interface by Embedded Synthetic Receptors. *Langmuir* **2014**, *30* (34), 10161–10166.

(46) Ghang, Y. J.; Perez, L.; Morgan, M. A.; Si, F.; Hamdy, O. M.; Beecher, C. N.; Larive, C. K.; Julian, R. R.; Zhong, W.; Cheng, Q.; et al. Anionic Deep Cavitands Enable the Adhesion of Unmodified Proteins at a Membrane Bilayer. *Soft Matter* **2014**, *10* (48), 9651–9656.

(47) Perez, L.; Ghang, Y. J.; Williams, P. B.; Wang, Y.; Cheng, Q.; Hooley, R. J. Cell and Protein Recognition at a Supported Bilayer Interface via in Situ Cavitand-Mediated Functional Polymer Growth. *Langmuir* **2015**, *31* (41), 11152–11157.

(48) Perez, L.; Mettry, M.; Hinman, S. S.; Byers, S. R.; McKeating, K. S.; Caulkins, B. G.; Cheng, Q.; Hooley, R. J. Selective Protein Recognition in Supported Lipid Bilayer Arrays by Tailored, Dual-Mode Deep Cavitand Hosts. *Soft Matter* **2017**, *13* (21), 3966–3974.

(49) Liu, Y.; Liao, P.; Cheng, Q.; Hooley, R. J. Protein and Small Molecule Recognition Properties of Deep Cavitands in a Supported Lipid Membrane Determined by Calcination-Enhanced SPR Spectroscopy. *J. Am. Chem. Soc.* **2010**, *132* (30), 10383–10390.

(50) Liu, Y.; Young, M. C.; Moshe, O.; Cheng, Q.; Hooley, R. J. A Membrane-Bound Synthetic Receptor That Promotes Growth of a Polymeric Coating at the Bilayer-Water Interface. *Angew. Chemie - Int. Ed.* **2012**, *51* (31), 7748–7751.

(51) Qureshi, I.; Memon, S. Synthesis and Application of Calixarene-Based Functional Material for Arsenic Removal from Water. *Appl. Water Sci.* **2012**, *2* (3), 177–186.

(52) Rahman, F. U.; Li, Y. S.; Petsalakis, I. D.; Theodorakopoulos, G.; Rebek, J.; Yu, Y. Recognition with Metallo Cavitands. *Proc. Natl. Acad. Sci. U. S. A.* **2019**, *116* (36), 17648–17653.

(53) Garnett, G. A. E.; Starke, M. J.; Shaurya, A.; Li, J.; Hof, F. Supramolecular Affinity Chromatography for Methylation-Targeted Proteomics. *Anal. Chem.* **2016**, *88* (7), 3697–3703.

(54) Mosca, S.; Yu, Y.; Rebek, J. Preparative Scale and Convenient Synthesis of a Water-Soluble, Deep Cavitand. *Nat. Protoc.* **2016**, *11* (8), 1371–1387.

(55) Gober, I. N.; Waters, M. L. Supramolecular Affinity Labeling of Histone Peptides Containing Trimethyllysine and Its Application to Histone Deacetylase Assays. *J. Am. Chem. Soc.* **2016**, *138* (30), 9452–9459.

(56) Dill, K. A. Dominant Forces in Protein Folding. *Biochemistry* **1990**, *29* (31), 7133–7155.

(57) Metherell, A. J.; Cullen, W.; Williams, N. H.; Ward, M. D. Binding of Hydrophobic Guests in a Coordination Cage Cavity Is Driven by Liberation of "High-Energy" Water. *Chem. - A Eur. J.* **2018**, *24* (7), 1554–1560.

(58) Chandler, D. Interfaces and the Driving Force of Hydrophobic Assembly. *Nature* **2005**, *437*, 640–647.

(59) Daze, K. D.; Hof, F. The Cation-π Interaction at Protein-Protein Interaction Interfaces: Developing and Learning from Synthetic Mimics of Proteins That Bind Methylated Lysines. *Acc. Chem. Res.* **2013**, *46* (4), 937–945.

(60) Beshara, C. S.; Jones, C. E.; Daze, K. D.; Lilgert, B. J.; Hof, F. A Simple Calixarene Recognizes Post-Translationally Methylated Lysine. *ChemBioChem* **2010**, *11* (1), 63–66.

(61) Allen, H. F.; Daze, K. D.; Shimbo, T.; Lai, A.; Musselman, C. A.; Sims, J. K.; Wade, P. A.; Hof, F.; Kutateladze, T. G. Inhibition of Histone Binding by Supramolecular Hosts. *Biochem. J.* **2014**, *459* (3), 505–512.

(62) Gamal-Eldin, M. A.; MacArtney, D. H. Selective Molecular Recognition of Methylated Lysines and Arginines by Cucurbit[6]Uril and Cucurbit[7]Uril in Aqueous Solution. *Org. Biomol. Chem.* **2013**, *11* (3), 488–495.

(63) Li, W.; Bockus, A. T.; Vinciguerra, B.; Isaacs, L.; Urbach, A. R. Predictive Recognition of Native Proteins by Cucurbit[7]Uril in a Complex Mixture. *Chem. Commun.* **2016**, *52* (55), 8537–8540.

(64) Park, K. M.; Suh, K.; Jung, H.; Lee, D. W.; Ahn, Y.; Kim, J.; Baek, K.; Kim, K. Cucurbituril-Based Nanoparticles: A New Efficient Vehicle for Targeted Intracellular Delivery of Hydrophobic Drugs. *Chem. Commun.* **2009**, No. 1, 71–73.

(65) Chen, X.-M.; Chen, Y.; Yu, Q.; Gu, B.-H.; Liu, Y. Supramolecular Assemblies with Near-Infrared Emission Mediated in Two Stages by Cucurbituril and Amphiphilic Calixarene for Lysosome-Targeted Cell Imaging. *Angew. Chemie* **2018**, *130* (38), 12699–12703.

(66) Sasmal, R.; Das Saha, N.; Schueder, F.; Joshi, D.; Vasu, S.; Jungmann, R.; Agasti, S. Dynamic Host-Guest Interaction Enables Autonomous Single Molecule Blinking and Super-Resolution Imaging. *Chem. Commun.* **2019**.

(67) Liu, Y.; Perez, L.; Mettry, M.; Gill, A. D.; Byers, S. R.; Easley, C. J.; Bardeen, C. J.; Zhong, W.; Hooley, R. J. Site Selective Reading of Epigenetic Markers by a Dual-Mode Synthetic Receptor Array. *Chem. Sci.* **2017**, *8* (5), 3960–3970.

Chapter 2: Separation of Methylated Histone Peptides via Host-Assisted Capillary Electrophoresis

2.1 Introduction

Post-translational modifications on proteins, including phosphorylation, acetylation, ubiquitination, and methylation, greatly expand the structural and function diversity of the proteome. PTMs impact almost all dynamic cellular processes, and monitoring PTM changes in biological systems is important in determining the regulation mechanisms of cellular signaling networks. Although great effort has been invested in improving PTM identification, it remains challenging due to their large variety in modification type and location.[1] While mass spectrometry is powerful for recognizing different modifications on peptides, prior separation is essential to reduce sample complexity and resolve modified proteins or peptides from the unmodified forms. Chromatographic methods, such as reversed-phase liquid chromatography (RPLC),[2] ion exchange chromatography (IEC), and hydrophilic interaction chromatography (HILIC),[3] have been developed for analyzing PTMs that effect distinguishable changes in charge, M_w, and hydrophobicity of the proteins or peptides. However, for PTMs that induce small overall changes, long separation times, multiple separation dimensions,[4] and extensive method optimization are typically required. An example of a common, yet challenging modification to detect is lysine methylation. Histone lysine modifications have been linked to gene activation and silencing, and they affect cell function, signaling pathways, playing important roles in disease development.[5,6] The modification occurs at different levels: mono-, di-, and tri-methylations can be found on different sites within histones, and occur

at both lysine and arginine residues. Methylation does not change the overall charge of the residue, conferring only small changes in peptide size and hydrophobicity. Thus, discrimination between each methylation level and different methylation sites is challenging. More selective recognition of these modified side chains is required to improve the resolution of different types of PTMs and reduce the complexity in separation methods.

Antibodies are often used as the recognition units for peptide PTMs,[7,8] but they can be costly and time consuming to develop. Individual antibodies are often specific to only one state of modification,[9] and they are also subject to cross-reactivity.[10] Native receptors for PTMs have also been reported, such as the heterochromatin protein 1 (HP1) that can bind to methylated histone peptides with low dissociation constants.[11] These high affinity, high M_w binders are useful in PTM enrichment, but are not effective tools for column separation of diverse PTMs, because their high affinity significantly reduces column efficiency.

Synthetic receptors are attractive alternatives for PTM recognition, as they are more accessible than antibodies. Synthetic receptors such as cyclodextrins[12–14] and crown ethers[15] have been applied in chromatography and capillary electrophoresis (CE) for separation of chemically similar small molecules. CE is ideally suited to the application of synthetic receptors, as it only requires simple addition of the receptors to the separation media and different receptors can be easily employed. The high resolving power of CE can work in tandem with the recognition event, effecting improved PTM separation even if the receptor does not provide sufficient discrimination among targets with similar structures

by itself. Here, we explore the possibility of using synthetic receptors to improve the separation by CE of PTM peptide targets variably methylated at lysine residues (Figure 2.1a). Although CE has been used in the analysis of PTMs such as phosphorylation[16] and acetylation,[17] it has not yet been capable of separating methylated and nonmethylated peptides in the absence of additives.

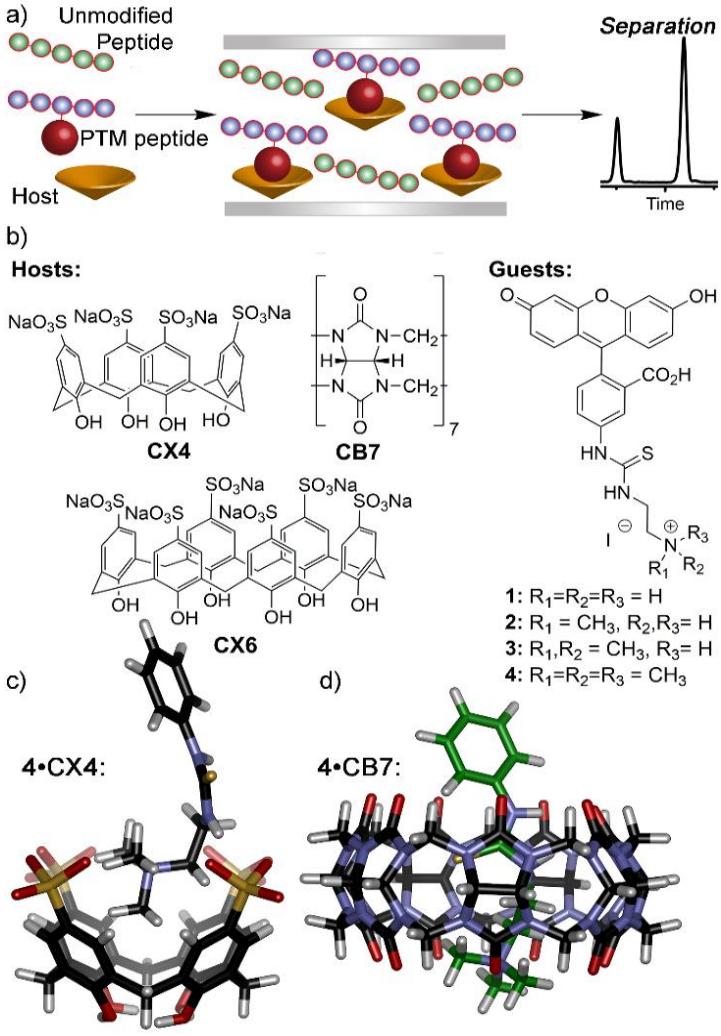

Figure 2.1 a) Representation of the host-assisted CE process. b) Structures of the hosts and guests used in this study; minimized structures of the c) 4•CX4 and 4•CB7 complexes, illustrating the host:guest interactions (SPARTAN, AM1 forcefield).

Synthetic receptors of various types are effective for the molecular recognition of methylation lysine residues. Examples include calixarenes,[8,18–21] cucurbiturils,[22–24] cyclophanes,[25–28] and deep cavitands.[29–31] The molecular recognition events are well-studied, and the receptors have been applied for selective sensing of histone modifications[30,32] as well as in supramolecular tandem assays.[31,33–36] However, the application of synthetic receptors to improve separation of methylated peptides from the unmethylated counterparts is rare, and often requires tethering of the host to the capillary.[8] Covalent attachment of the receptors to solid supports introduces synthetic challenges, and some hosts (especially cucurbiturils) are challenging to derivatize.[37] As CE only requires addition of the host to the running buffer, we were able to test simple, underivatized hosts for the process. We chose tetrasulfonatocalix[4]arene (**CX4**), hexasulfonatocalix[6]arene (**CX6**) and cucurbit[7]uril (**CB7**) in our study, because they are highly water-soluble and contain both a hydrophobic cavity with fixed size and an electron rich upper rim (Figure 2.1b). These hosts were capable of selective, varied molecular recognition of small molecule fluorophores and histone peptides in CE, and CE methods were developed for successful separation of methylated histone peptides that carry different methylation states and sites.

2.2 Materials and Methods

2.2.1 General

All samples and separation buffers were made using ultrapure water (18 MΩ) that was obtained from a Direct-Q Water Purification System (Millipore Sigma, Billerica, MA).

Fluorophores **1-4** were synthesized according to literature procedures.[29,38] 4-Tetrasulfonatocalix[4]arene and cucurbit[7]uril hydrate were purchased from Sigma-Aldrich (St. Louis, MO). 4-Hexasulfonatocalix[6]arene hydrate was purchased from Alfa Aesar (Tewksbury, MA, USA). Lyophilized histone K27 peptides were purchased from AnaSpec, Inc. (Fremont, CA). The sequence is ARTKQTAR-K(me_x)-STGGKAPRKQLA (x = 0, 1, 2, 3). The peptide had either non-, mono-, di-, or trimethylation. Custom labeled nonmethylated and trimethylated histone K9 peptides were purchased from United Biochemical Research, Inc. (Seattle, WA). The sequence of each peptide is FITC-Ahx-AAR-K(me_x)-SAPY-COOH (x = 0 ,3).

UV/vis spectra were obtained with a Varian, Inc. Cary 50 UV-Vis Spectrophotometer from Agilent Technologies (Santa Clara, CA, USA). The absorbance of 3 μM host solutions were measured in a Quartz Spectrophotometer Cell (100 μL, 10 mm, Z = 15 mm) from Starna Cells, Inc. (Atascadero, CA, USA).

2.2.2 Separation of Small Guests and Fluorescently Labeled H3K27 Peptides

The CE experiments on the fluorescent guests were carried out using a homemade instrument equipped with a 488-nm excitation Argon Ion laser (Melles Griot Laser Group, Carlsbad, CA) for laser-induced fluorescence (LIF) detection. Separation power was provided by a TriSep 2100 HV voltage supplier (Unimicro Technologies, Pleasonton, CA). Bare fused-silica capillaries (50 μm i.d., 365 μm o.d.) were purchased from Polymicro Technologies (Phoenix, Arizona). The running buffer was 20 mM phosphate buffer, pH 7.4, with or without the synthetic hosts. The capillary was flushed prior to each separation with 0.1 M NaOH, ultrapure H_2O, and running buffer using a syringe pump. Samples were

injected via gravity pressure. Electrophoresis was driven by an electric field of 250 V/cm with positive polarity. The effective length of the capillary was 45 cm. Electropherograms were acquired using PeakSimple Chromatography Software (SRI Instruments, Torrance, CA). Riboflavin was included as the internal standard for the small guest study. In the peptide study, fluorescein was used as an internal standard in CE-LIF.

2.2.3 Separation of Methylated H3 Peptides in a Coated Capillary

The separation of the non-fluorescently labeled, methylated peptides was performed in a polyvinyl alcohol (PVA)-coated capillary (50 μm inner diameter, 365 μm outer diameter) from Agilent Technologies (Santa Clara, CA). DMSO was included in the sample as an internal standard. Separation was conducted on an Agilent 7100 CE system with a UV absorption detector. Samples were introduced into the PVA capillary (50 μm inner diameter, 365 μm outer diameter, with an effective length of 35 cm) with a 50 mbar injection for 5s. Separation was driven by an electric field of 571 V/cm with positive polarity and 5 mbar of pressure. Prior to each day's experiment, the capillary was flushed with 10 mM phosphoric acid and H_2O. Data was acquired via ChemStation (Agilent Technologies, Santa Clara, CA).

2.2.4 Lysine Demethylation Assay

The demethylation assay was performed using the custom labeled trimethylated peptide, FITC-Ahx-AAR-K(me_3)-SAPY-COOH, and human recombinant demethylase KDM6B (Reaction Biology Corp., Malvern, PA). Two μM of the FITC-labeled H3K27me_3 peptide was incubated with 1 μM KDM6B at room temperature in the reaction buffer (20 mM Tris-HCl, pH 7.4, 100 mM NaCl, 20 μM $(NH_4)_2Fe(SO_4)_2 \cdot 6(H_2O)$, 50 μM α-

ketoglutaric acid, 500 μM ascorbate) with or without 1 μM 2,4-pyridinedicarboxylic acid (Cayman Chemical, Ann Arbor, Michigan). The reaction mixture was injected into the bare fused-silica capillary (50 μm inner diameter, 365 μm outer diameter) at time intervals between 0 and 9 hours. The running buffer was 50 μM **CX4** in 20 mM phosphate buffer, pH 7.4.

Another demethylation assay was performed using an unlabeled H3K27me_3 (23-34) histone peptide purchased from AnaSpec, Inc. (Fremont, CA, USA). The peptide has the sequence, KAAR-K(Me_3)-SAPATGG. Human recombinant demethylase KDM6B was purchased from Reaction Biology Corp., Malvern, PA, USA). 4 μM H3K27me_3 peptide was incubated with 1.6 μM KDM6B at room temperature in the reaction buffer (50 mM Tris-HCl, pH 7.4, 100 mM NaCl, 6 μM $(NH_4)_2Fe(SO_4)_2 \cdot 6(H_2O)$, 50 μM α-ketoglutaric acid, 500 μM ascorbate). The reaction mixture was quenched with formic acid (final, 0.1%). MALDI spectra were obtained with a TOF/TOF 5800 System from AB Sciex (Framingham, MA, USA) on a 96-well MALDI plate insert.

A third demethylation assay was performed using a H3K9me_3 (1-21) histone peptide purchased from AnaSpec, Inc. (Fremont, CA, USA). The peptide has the sequence ARTKQTAR - K(Me3) - STGGKAPRKQLA. Jumonji domain containing 2E (JMJD2E) and its inhibitor 2,4-dicarboxypyridine (2,4-PDCA) were purchased from Cayman Chemical (Ann Arbor, MI, USA). 50 μM H3K27me_3 peptide was incubated with 5 μM KDM6B at room temperature in the reaction buffer (50 mM Tris-HCl, pH 7.4, 100 μM $(NH_4)_2Fe(SO_4)_2 \cdot 6(H_2O)$, 500 μM α-ketoglutaric acid, 5 mM ascorbate) with or without 150 μM 2,4-PDCA. The reaction mixture was stopped by incubating in boiling water for 5

minutes before analysis on MALDI while the reaction mixture was injected *in situ* for analysis on CE. MALDI spectra were obtained with a TOF/TOF 5800 System from AB Sciex (Framingham, MA, USA) on a 96-well MALDI plate insert.

2.2.5 Isothermal Titration Calorimetry Measurements

All ITC experiments were performed using a MicroCal iTC200 (GE Healthcare, Freiburg, Germany) with a stirring rate of 700 rpm. The baseline was stabilized prior to the experiment and a preinjection delay was set to 60 s. The first injection was 0.4 µL while the remaining injections were 2.43 µL, performed every 180s. The reference power was set to 5 µcal/sec. The syringe concentration was 1 mM while the cell concentration was 0.1 mM. All experiments were conducted at 25 °C. Curve fitting was done on Origin using the standard one site model provided by MicroCal. The standard one site model uses the following equation:

$$\Delta Q(i) = Q(i) + \frac{dV_i}{V_0}\left[\frac{Q(i) + Q(i-1)}{2}\right] - Q(i-1) \qquad \textbf{Equation 2.1}$$

where Q(i) is the total heat content at the end of the ith injection, dV_i is the volume at the i^{th} injection, and V_o is the active cell volume.

2.2.6 Mobility, Affinity, and Resolution Calculation

All mobilities in the following text are the electrophoretic mobility after EOF adjustment using the following equation:

$$\mu = \frac{L_t x\, L_d}{V}\left(\frac{1}{t_G} - \frac{1}{t_{IS}}\right) \qquad \textbf{Equation 2.2}$$

with L_t = total length of the capillary, L_d = length of the capillary from the inlet to the detection window, V = voltage, t_G = migration time of the guest, and t_{IS} = migration time

of the internal standard. Binding constants were calculated as reported in affinity CE, using the Hill Equation (Equation 2.3), with n being the Hill coefficient for measurement of the guest's binding cooperativity:[39–41]

$$(\mu_i - \mu_0) = \frac{(\mu_{max} - \mu_0)[L]^n}{K_d + [L]^n} \qquad \textbf{Equation 2.3}$$

The percent change in mobility, %Δμ, was calculated for each host molecule via the following equation:

$$\%\Delta\mu = \frac{\mu_i - \mu_0}{\mu_0} \qquad \textbf{Equation 2.4}$$

with μ_0 being the mobility without the host and μ_i being the mobility with the host at one concentration in the running buffer.

The resolution of two adjacent peaks was calculated with the equation:

$$R = \frac{t_1 - t_2}{\frac{1}{2}(w_1 + w_2)} \qquad \textbf{Equation 2.5}$$

where t_1 is the time of peak 1, t_2 is the time of peak 2, w_1 is the width of peak 1, and w_2 is the width of peak 2.

2.3 Results and Discussion

2.3.1 Analysis of Binding with Small Guests

We initially determined the effectiveness of the three hosts in binding and separating small molecules that varied only in methylation state. Fluorophores **1-4** (Fig. 2.1b) were used as the model compounds to allow simple detection of the separation event:

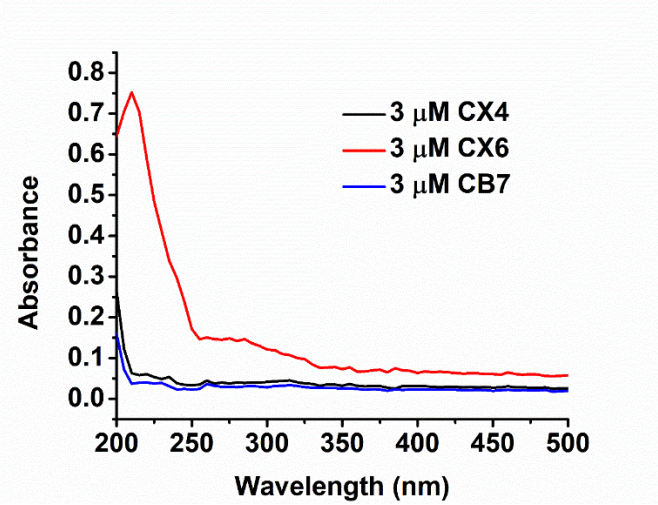

Figure 2.2 Absorbance spectra of 3 μM **CX4**, **CX6**, and **CB7** in water.

guests **1-4**[29,38] were synthesized in 2 or 3 steps from commercial materials, and the fluorescein label permitted LIF detection eliminating the problem of high background UV absorption with increasing host concentration in the background electrolyte (BGE) (Figure 2.2). The three host molecules, **CX4**, **CX6** and **CB7** are all capable of molecular recognition of substituted ammonium species, although their affinities and selectivities are somewhat different. The bowl-shaped, highly anionic **CX4** exploits charge matching cation-π interaction with the guest for maximal affinity. **CX6** has a larger cavity, but is far more flexible, whereas **CB7** is extremely rigid, and relies on a combination of hydrophobic interactions, London Dispersion forces and self-complementary hydrogen bonding at the upper rim to maximize selectivity.[19,22] Their selectivity for the various N-methylated states of lysine is limited, however, as the affinities for K, Kme_1, Kme_2 and Kme_3 are quite similar.[42–44] The best targets for **CB7** is N-terminal phenylalanine residues,[45–47] and functionalized derivatives of **CX4** are most effective at selective recognition of N-

methylated lysines, rather than **CX4** itself.[8,18–21,32] **CX4** shows millimolar affinity for lysine at in buffered PBS at neutral pH,[48] as does **CB7**,[36,44] whereas the more flexible **CX6** favors larger substrates such as arginine, although the affinity for ammonium groups is ~10-fold less than that of **CX4**.[48]

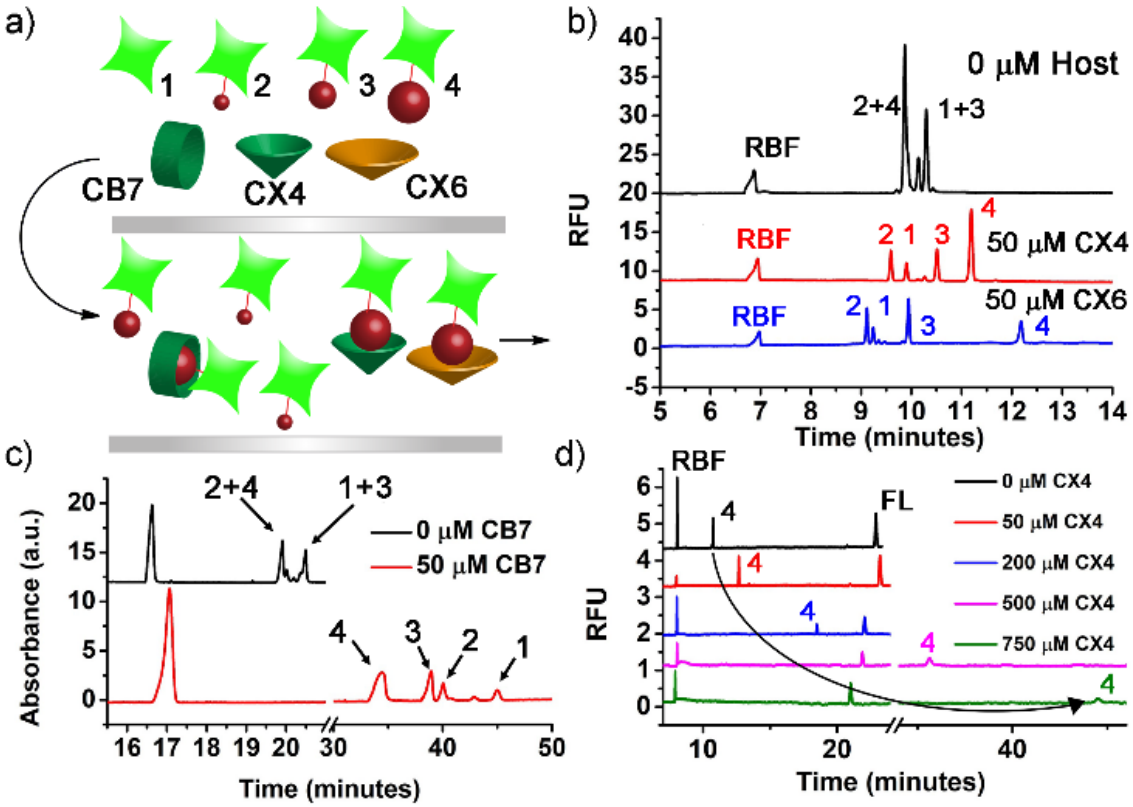

Figure 2.3 a) Small molecule separation via Host-Assisted CE. b) Separation of a small methylated guest mixture in 0 µM host vs. 50 µM **CX4** and **CX6**. [unmethylated guest **1**] = 25 nM, [monomethylated guest **2**] = 50 nM, [dimethylated guest **3**] = 100 nM, [trimethylated guest **4**] = 200 nM. c) Separation of a small methylated guest mixture in 0 µM vs. 50 µM CB7 (detected by UV absorption detector). [**1**] = 50 µM, [**2**] = 100 µM, [**3**] = 200 µM, [**4**] = 500 µM. d) Mobility shift of the small trimethylated guest as more CX4 is added to the BGE. RBF = 10 µM riboflavin, FL = 50 nM fluorescein, [**4**] = 50 nM.

Table 2.1: Mobility changes and dissociation constants for guest fluorophores in the hosts[a]

Mobility Change, %

Guest	**CX4**	**CX6**	**CB7**
1	-6.4	1.8	5.7
2	9.8	-1.8	4.5
3	-9.2	-15.2	14.5
4	-26.0	-54.4	16.0

Guest Affinity

Complex	K_d, μM
2•CX4	299±30
3•CX4	192±7
4•CX4	100±30
4•CX6	135±21
4•CB7	51±4

[a] For mobility change (%), each host was kept at 50 μM for separation of the small guest mixture. With **CX4** or **CX6** in the BGE, [unmethylated guest **1**] = 25 nM, [monomethylated guest **2**] = 50 nM, [dimethylated guest **3**] = 100 nM, [trimethylated guest **4**] = 200 nM**.** With **CB7** in the BGE, [**1**] = 50 μM, [**2**] = 100 μM, [**3**] = 200 μM, [**4**] = 500 μM. BGE = Host in 20 mM sodium phosphate buffer, pH 7.4. Mobility change and guest affinity results are averages of 2-3 replicate measurements. Hill coefficient and fitting R^2 were reported in Table 2.2 in Supporting Information.

To evaluate the binding between each host and the methylated guests, we employed affinity CE by putting the host in the BGE and monitored the migration of the guest (Figure 2.3a). Adding the hosts to the BGE may change the electroosmotic flow (EOF) by altering the charge density of the capillary wall (if the host is adsorbed onto the wall), as well as varying the viscosity of the BGE. Thus, the neutral dye riboflavin (RBF) was used as an internal standard (IS) to determine any changes in EOF. We also added a second IS, fluorescein (FL), to confirm that the label had no specific binding to the host. The resultant electropherograms with 50 μM host in the BGE are shown in Figures 2.3b,c. The guest molecules carry net negative charges at pH 7.4 as they all migrate later than the neutral

marker. In the absence of host, **2** and **4** were not resolved at all, and neither were **1** and **3** (the small peak in between the two overlapped peaks was from impurity in the samples). The addition of **CX4** and **CX6** to the BGE caused the mobility for all methylated guests to become more negative (Table 2.1), due to the interaction between the guest and the multi-anionic hosts. The charge increase exceeds the increase in size, leading to an overall increase in the charge-to-size ratio. Interestingly, **CB7** in the BGE reduces the net mobility of each guest, presumably because the **CB7**-guest complex has a larger hydration size than the guest itself but with no additional charges. The delay in the migration time of the neutral marker also implied a reduction in the EOF with an increase in [**CB7**]. We also tried to measure the binding affinity using the more conventional method of isothermal titration calorimetry (ITC). However, the small molecule-host binding released very small amounts of heat, making accurate measurement difficult. Still, for the binding between **CX4** and guest **3** and **4**, the averaged K_d values obtained (157 μM and 125 μM for **3** and **4**, respectively) were comparable to what measured by CE (Table 2.2, Figure 2.4). Furthermore, we can determine the Hill coefficients, which indicate positive cooperativity in this circumstance. These results highlight the advantage of using CE for measurement of binding between small molecules and synthetic hosts.

The elution order of the four small guests is dependent on their relative affinity to the host in the BGE. The guest that binds to the host with the highest affinity should exhibit the largest change in mobility. For all hosts, the trimethylated guest **4** exhibited the largest mobility shift among the guest molecules, indicating the strongest affinity to the hosts. To

find the binding affinity, the mobility shifts (Δμ) of the methylated guest induced by varying host concentrations in the BGE were measured (Figure 2.3d and Figure 2.5 – 2.9)

Table 2.2: Summary of small guest curve fitting results for small molecular guests binding to the receptors

Guest:Host	**K_d (CE)**	**n**	**R^2**	**K_d (ITC)**
FITC-Me_1 : CX4	299 ± 30 μM	1.6	0.998	Not detected
FITC-Me_2 : CX4	192 ± 7 μM	2.5	0.989	157 μM
FITC-Me_3 : CX4	100 ± 30 μM	1.7	0.995	125 μM
FITC-Me_3 : CB7	51 ± 4 μM	2.0	0.949	Not measured
FITC-Me_3 : CX6	135 ± 21 μM	1.7	0.998	Not measured

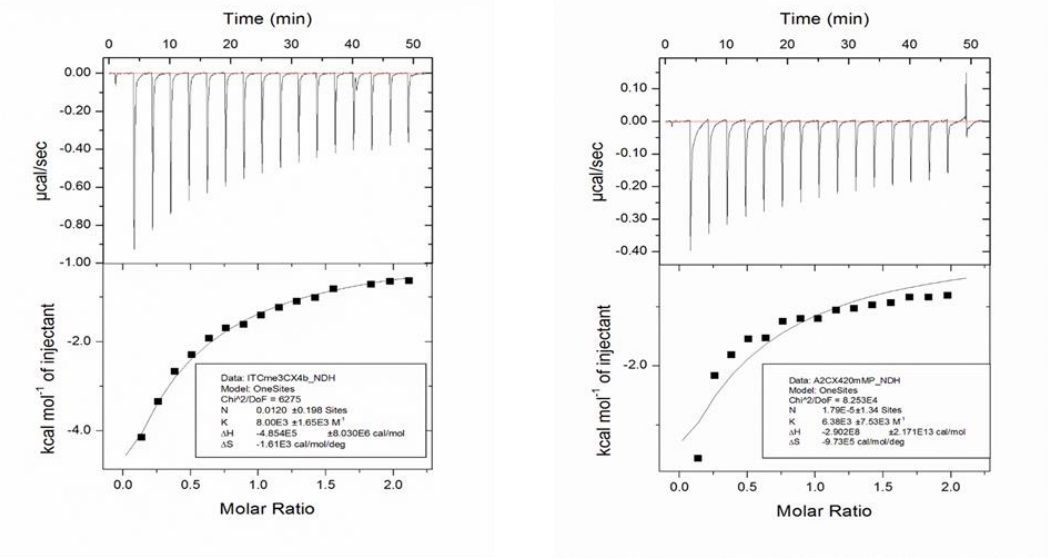

Figure 2.4 Isothermal calorimetry titration curves of guests **4** (left) and **3** (right) with **CX4**.

and plotted vs. [host]. The resultant binding curves were fit with equation 2.3 to allow calculation of dissociation constant K_d for the host:guest complexes (Table 2.1, Figure 2.5-2.9). The non-methylated guest **1** did not show a consistent change in its mobility with any

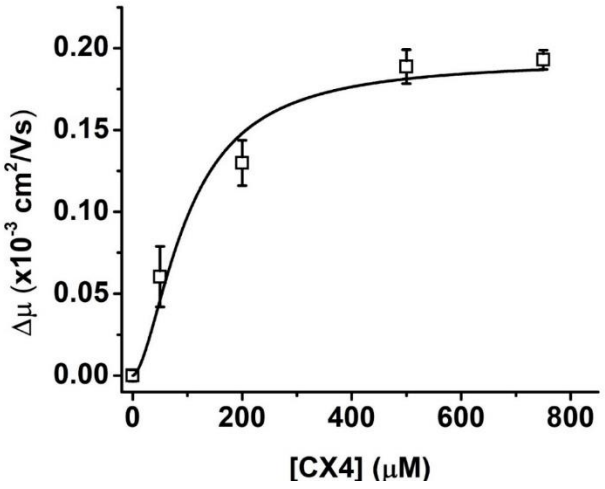

Figure 2.5 A plot of Δμ vs. [**CX4**] for guest **4**. Each data point consists of triplicate measurements.

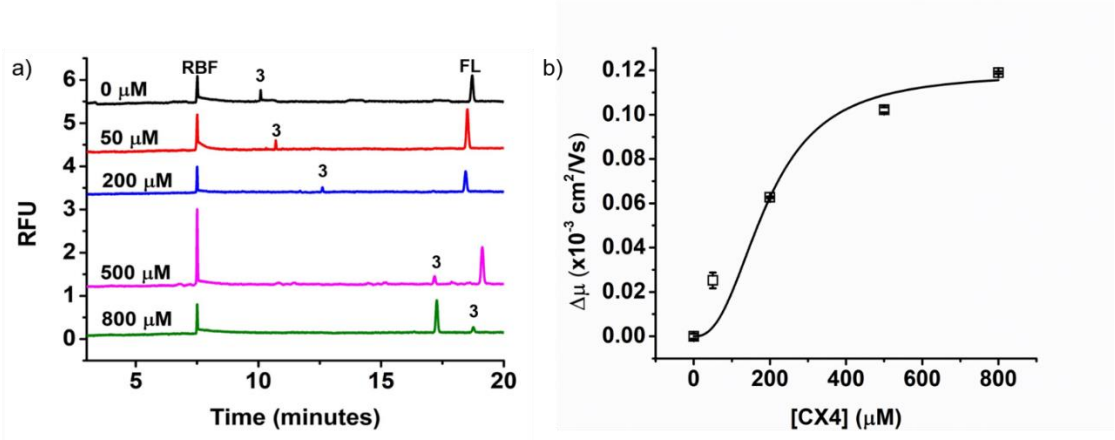

Figure 2.6 a) Mobility shift of the small dimethylated guest **3** as more **CX4** is added to the BGE (20 mM sodium phosphate buffer, pH 7.4). RBF = 10 μM riboflavin, FL = 50 nM fluorescein, [**3**] = 50 nM. b) A plot of Δμ vs. [**CX4**] for guest **3**. Each data point consists of triplicate measurements.

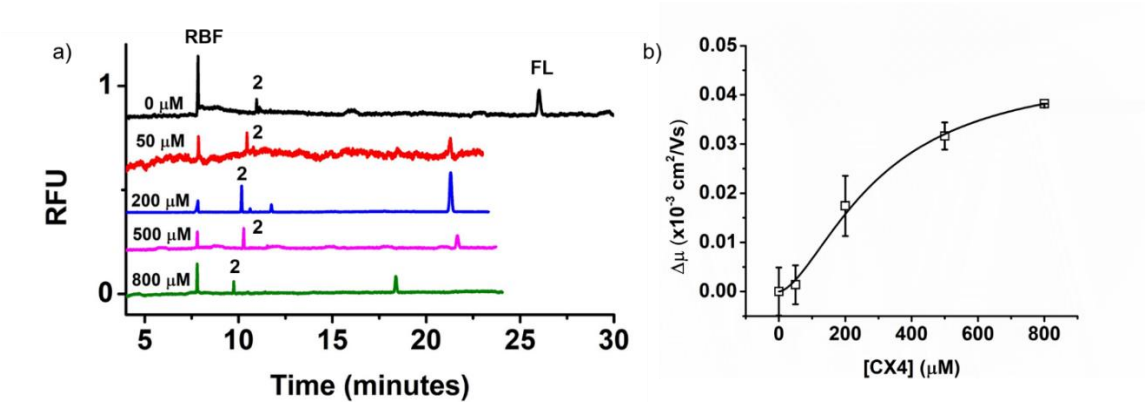

Figure 2.7 a) Mobility shift of the small monomethylated guest **2** as more **CX4** is added to the BGE (20 mM sodium phosphate buffer, pH 7.4). RBF = 10 μM riboflavin, FL = 50 nM fluorescein, [**2**] = 50 nM. b) A plot of Δμ vs. [**CX4**] for guest **2**. Each data point consists of triplicate measurements.

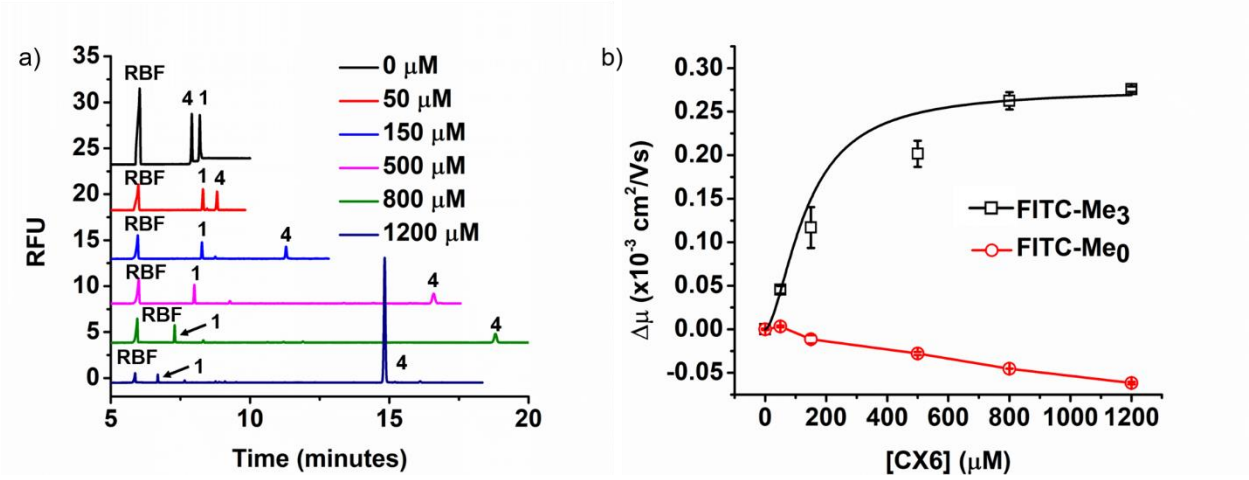

Figure 2.8 a) Mobility shift of the small trimethylated **4** guest as more **CX6** is added to the BGE (20 mM sodium phosphate buffer, pH 7.4). RBF = 10 μM riboflavin, [**1**] = 50 nM, [**4**] = 50 nM. b) A plot of Δμ vs. [**CX6**] for guests 4 and 1. Each data point consists of triplicate measurements.

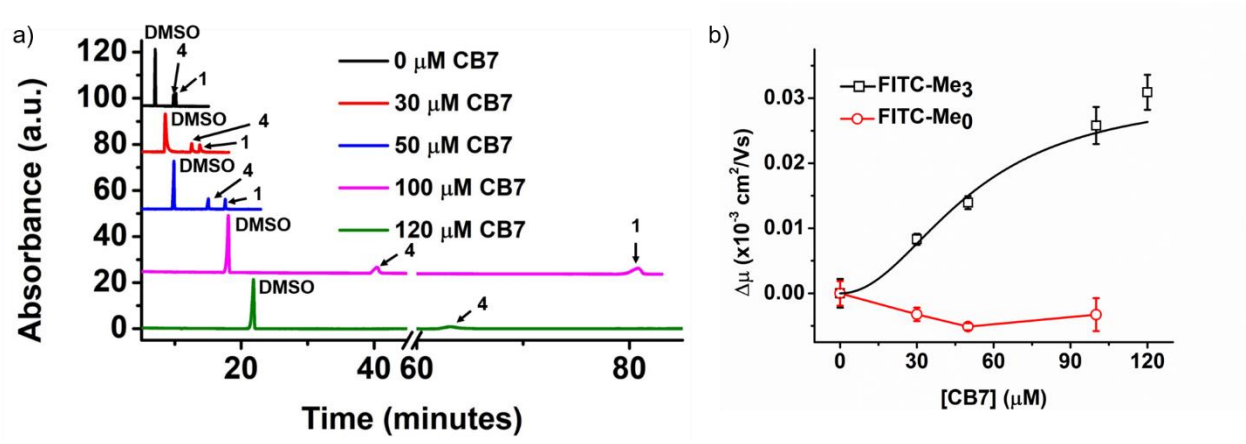

Figure 2.9 a) Mobility shift of the small trimethylated guest **4** as more **CB7** is added to the BGE (20 mM sodium phosphate buffer, pH 7.4). 0.1% DMSO, [**1**] = 50 nM, [**4**] = 50 nM. b) A plot of Δμ vs. [**CB7**] for guests **4** and **1**. Each data point consists of triplicate measurements.

of the host, indicating no binding, thus no K_d was obtained. There is a two-fold variation in affinity between guests **2-4** in **CX4**: the greater the methylation level of the guest, the stronger the affinity for the host, which is consistent with other binding affinity studies.[11,49,50] While the affinity of **4** with **CX4** increased by one fold compared to that of **3**, the difference in the K_d values between **3** and **2** is smaller, about 50%. Addition of the third methyl group significantly enhances the binding between the methylated lysine guests and the receptors. Higher resolution separation of **4** from **3** or **2** was possible than for the guests with lower methylation levels. The affinities of the trimethylated fluorophore **4** vary between the different hosts. The more flexible **CX6** displays a lower affinity for **4**, whereas the more effective host **CB7** binds **4** most strongly (K_d = 51 ± 4 μM), consistent with literature reports for similar species.[22]

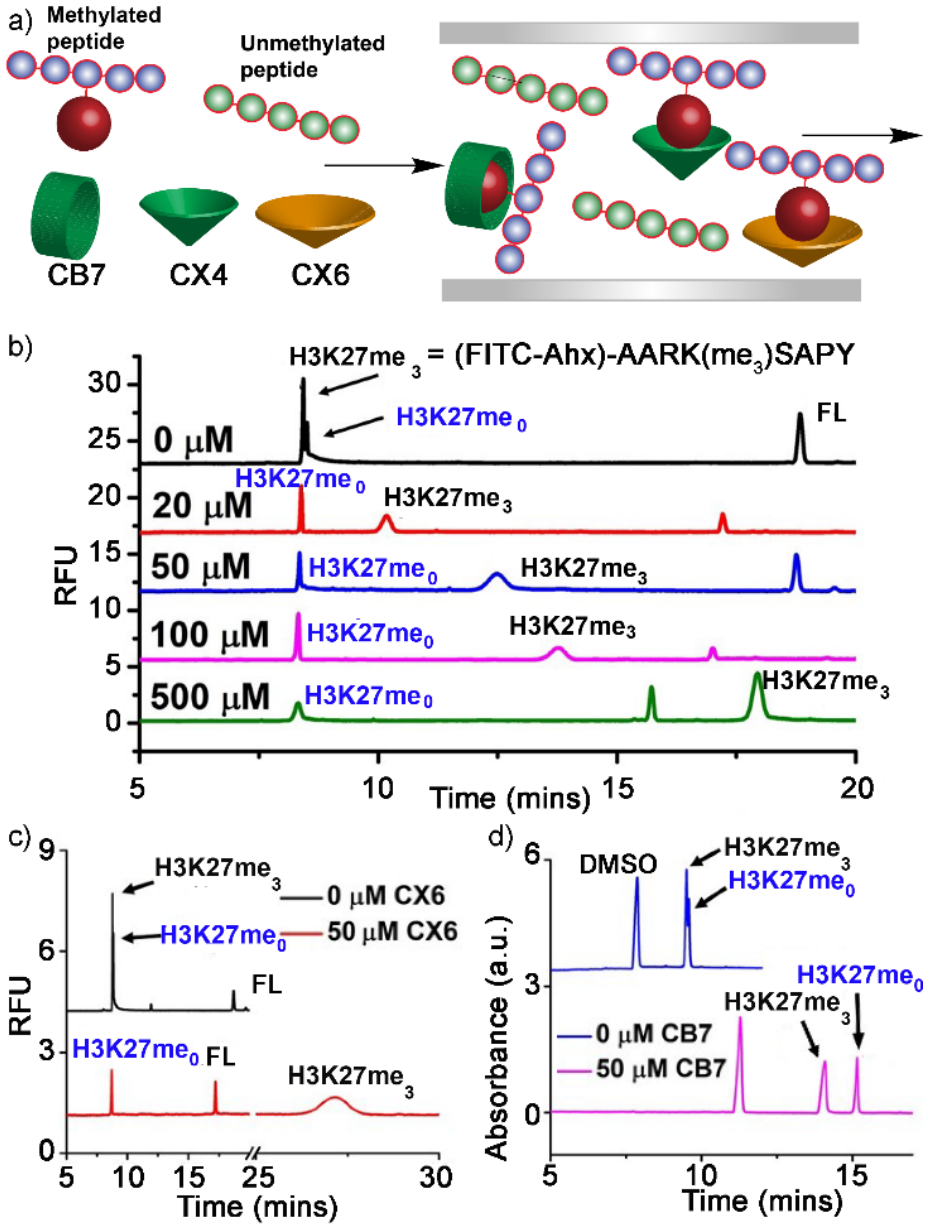

Figure 2.10 a) Methylated peptide separation via Host-Assisted CE. Mobility shift of the labeled H3K27me$_3$ peptide with increasing b) [**CX4**], c) [**CX6**] and d) [**CB7**]. FL = fluorescein as the internal standard. The sequences of the H3K27 peptides are (FITC-Ahx)-AARK(me$_{0/3}$)SAPY. [peptide] = 0.5 μM.

2.3.2 Analysis of Binding With Trimethylated Peptides

The differential binding and separation of the control fluorophores with varying methylation states at N is encouraging and indicates the potential of host-assisted CE for the separation of variably methylated histone peptides. We next analyzed the binding between the four hosts and a trimethylated Histone H3K27 peptide (Figure 2.10a). A fluorescent H3K27(me_3) peptide, N-terminally labeled with fluorescein and an aminohexanoate spacer (FITC-Ahx) was used as target to allow LIF detection, minimizing the background signal from the hosts in BGE. The unmethylated H3K27 peptide equivalent (H3Kme_0) was used as a control. Both cationic peptides migrated faster in the BGE than the anionic fluorescein internal standard. In the absence of any host, the two peptides (0.5 μM) were barely separated (Figure 2.10b). Increasing **CX4** concentration in the BGE extended the migration time of the trimethylated peptide significantly, while the mobility of the unmethylated peptide was essentially unchanged. The mobility change of labeled H3K27(me_3) is 64%, with [**CX4**] = 50 μM, which is more than two times of the 26% decrease of **4** in **CX4**. The resolution (R) value between the H3K27(me_0) and H3K27(me_3) was as large as 4.4 at this host concentration (Table 2.3). Plotting the mobility shift curve against the host concentration and fitting to equation 2.3 (Figure 2.11) showed that the affinity of the H3K27(me_3) peptide for **CX4** was higher than that of **4**, with K_d = 48 ± 7 μM (Table 2.4). In contrast, the nonmethylated H3K27 peptide did not exhibit a sigmoidal relationship between the mobility shift and host concentration, indicating no affinity with **CX4** (Figure 2.11).

Table 2.3 Resolution of various guest and peptide peaks with different hosts in the background electrolyte

Guest/Peptide Pair	0 µM **CX4**	50 µM **CX4**	0 µM **CX6**	50 µM **CX6**	0 µM **CB7**	50 µM **CB7**
1/**3**, **2**/**4**	2.42		2.42		2.00	
2,**1**		1.25		0.85		5.62
1,**3**		3.69		1.97		2.85
3,**4**		2.41		4.98		4.97
$H3K27me_0$, $H3K27me_3$	0.15	4.40	0.15	26.47	0.63	2.65

Table 2.4: Dissociation constants of labeled $H3K27(me_3)$ when bound to the various hosts[a]

Host	K_d, µM	n	R^2
CX4	48.0 ± 7.0	1.3	0.995
CX6	17.7 ± 4.2	1.4	0.999
CB7	5.5 ± 0.7	1.0	0.956

[a][$H3K27(me_3)$] = 0.5 µM in **CX4** and **CX6** BGE. 100 µM $H3K27(me_3)$ in **CB7** BGE. Host in 20 mM sodium phosphate buffer, pH 7.4. Results are averages of triplicate measurements.

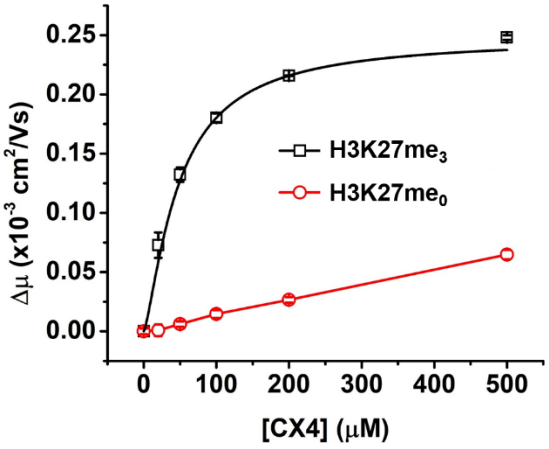

Figure 2.11 Plot of Δμ vs. [**CX4**] for labeled H3K27me$_3$ and H3K27me$_0$. Each data point consists of triplicate measurements.

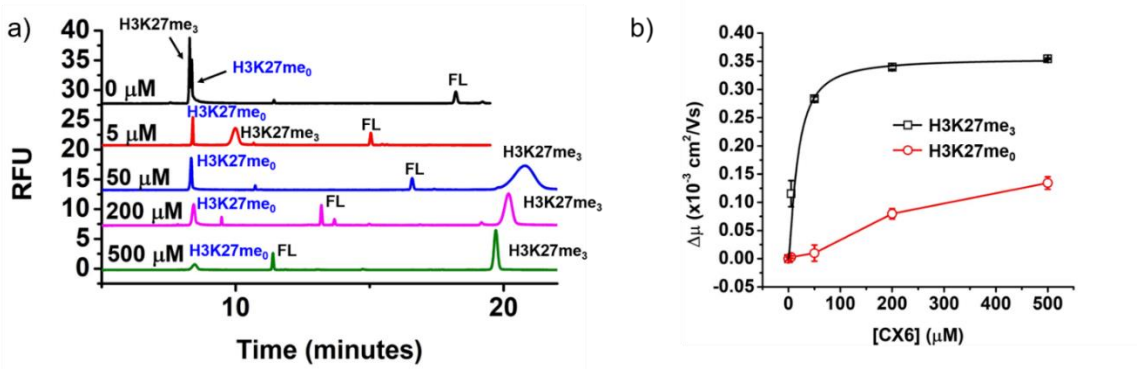

Figure 2.12 a) Mobility shift of labeled H3K27me$_3$ as more CX6 is added to the BGE (20 mM sodium phosphate buffer, pH 7.4). [H3K27me$_3$] = [H3K27me$_0$] = 100 μM, FL = 50 nM fluorescein. b) A plot of Δμ vs. [**CX6**] for labeled H3K27me$_3$ and H3K27me$_0$. Each data point consists of triplicate measurements.

The other hosts were even more effective at binding the H3K27(me$_3$) peptide (Table 2.4, Figures 2.12-2.13). **CB7** was the strongest host, with K_d = 5.5 ± 0.7 μM, and **CX6** was a better host than **CX4**, with K_d = 17.7 ± 4.2 μM. Interestingly, the migration order between H3K27(me$_3$) and H3K27 varied with the type of guest. Both of the

sulfonated calixarene hosts are anionic, causing the calixarene-peptide complex to have a more negative electrophoretic mobility than the free peptide, and migrate slower. In contrast, the neutral cucurbituril effects an increase in overall size upon binding with no global change in charge difference, resulting in a less negative electrophoretic mobility and a faster elution time for the host-peptide complex. However, **CB7** can adsorb to the silica wall and reduce the EOF. With high concentrations (>100 μM) of **CB7** in the BGE (Figure 2.13), the EOF drops significantly and increases the elution time for all analytes, which contributes to peak broadening, lowering the column efficiency. The anionic calixarenes do not adhere to the anionic silica wall, and as such effect minimal EOF change even at high concentrations. Again, the affinity values reported in Table 2.4 were confirmed by ITC measurement (Figure 2.14, Table 2.5), which consumed much more peptides than the CE method.

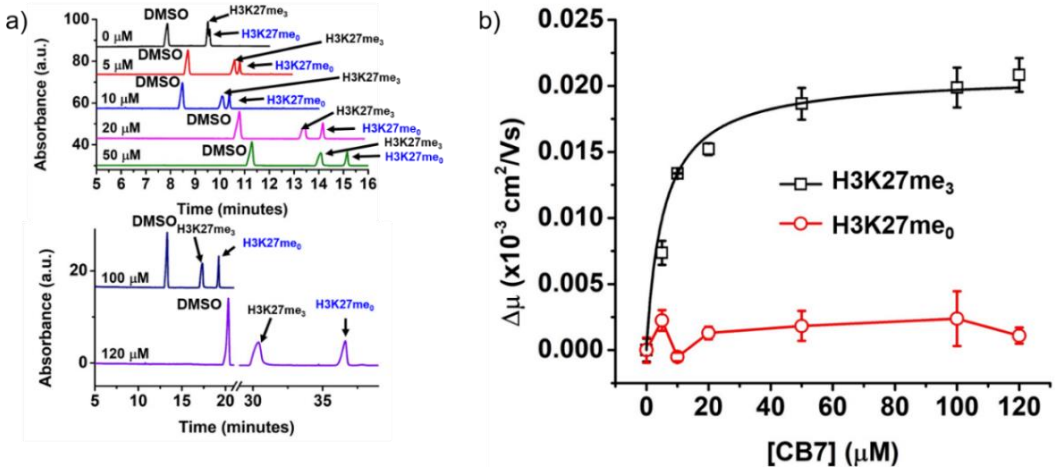

Figure 2.13 a) Mobility shift of labeled H3K27me$_3$ as more **CB7** is added to the BGE (20 mM sodium phosphate buffer, pH 7.4). 0.1% DMSO, [H3K27me$_3$] = [H3K27me$_0$] = 100 μM. b) A plot of Δμ vs. [**CB7**] for labeled H3K27me$_3$ and H3K27me$_0$. Each data point consists of triplicate measurements.

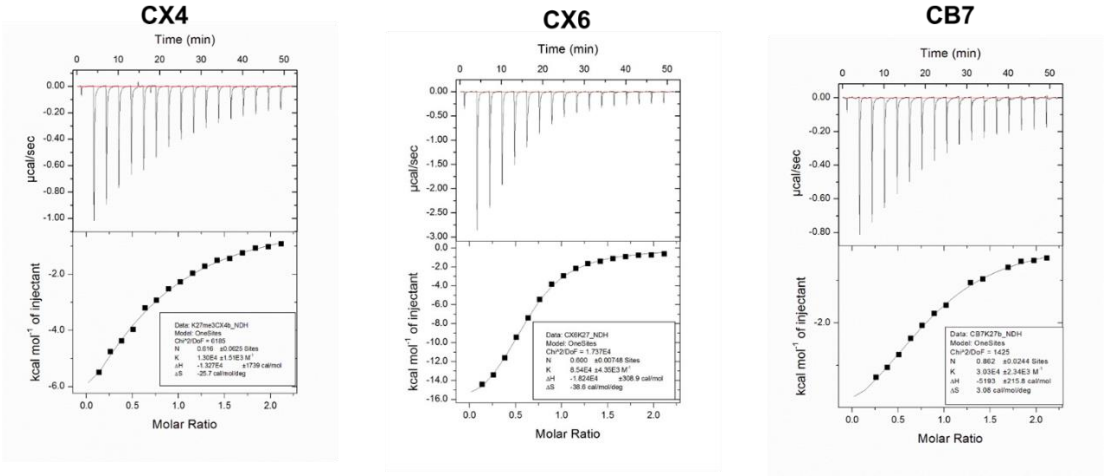

Figure 2.14 ITC titration curves for labeled H3K27(me_3) and hosts, **CX4**, **CX6**, and **CB7**.

Table 2.5 Affinities between receptors and labeled H3K27(me_3) peptides measured by ITC

Host	K_d, µM by ITC
CX4	70.0
CX6	11.7
CB7	33.0

2.3.3 Separation of Peptides with Different Methylation Levels

The host-assisted CE process was highly effective for separation of trimethylated and unmethylated peptides. The more challenging and desirable task is to separate PTM peptides with only slightly different methylation states (i.e. 0, 1, 2 and 3) (Figure 2.15a). We extended the separation process to four peptides based on the H3K9me sequence, with

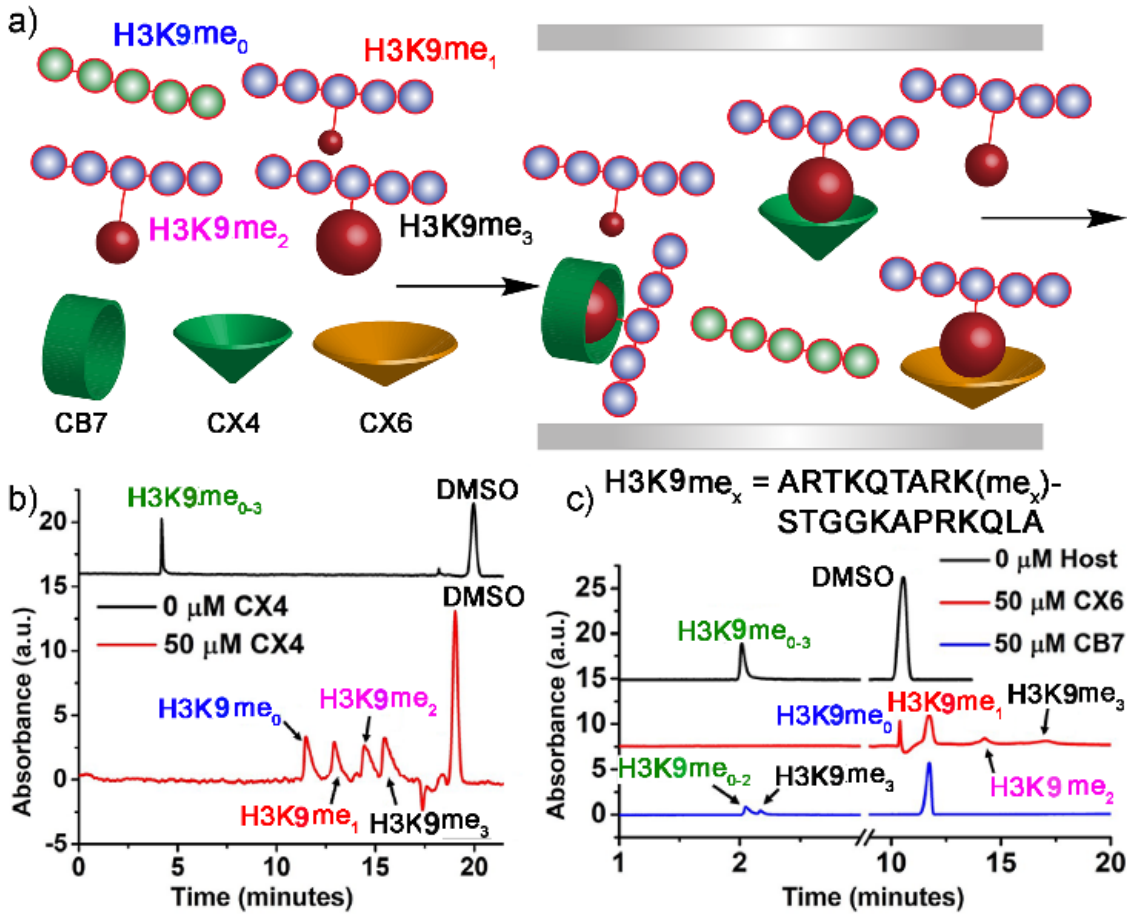

Figure 2.15 a) Separation of H3K9 peptides with varying methylation levels. b) Mobility shifts of the labeled H3K9me$_{0-3}$ peptide mixture with increasing [CX4]; c) Mobility shifts of the labeled H3K9me$_{0-3}$ peptide mixture with increasing [CX6] and [CB7]. 0.1% DMSO as internal standard, [peptide] = 50 μM.

no N-terminal fluorophore and varying K9 methylation levels (0-3), which were more representative of the peptides accessible from biological samples than the fluorescently labeled peptides used previously. These peptides were larger than the K27 counterparts, consisting of 21 amino acid residues with a M_w ~ 2.2 - 2.3 kDa and a pI of 12.14. These longer peptides are more basic, and as such, a polyvinyl alcohol (PVA) coated capillary was employed to prevent adsorption of the highly cationic peptides.[17,51,52] Since the EOF

was almost zero in this coated capillary, hydrodynamic pressure (5 mbar), was applied in addition to the electric field to ensure reasonable separation times for the peptide-host complex.

As shown in Figure 2.15b and c, all four K9 peptides ([peptide] = 50 μM) show identical mobilities in the absence of any host in the BGE. Since the K9 peptides are larger in size, a M_w difference of 14 Da does not induce sufficient change in the electrophoretic mobility between different methylation levels for effective separation. In the presence of 50 μM **CX4** in the BGE, all four peptides could be efficiently separated (Figure 2.15b), with longer elution times being observed as the methylation state increases: H3K9me_0 eluted first, and H3K9me_3 last, indicating increased affinity of the higher methylation states to the host. Identity of each peak was confirmed by spiking the individual peptide to the mixture and observing increase in the peak area (Figure 2.16). The resolution between H3K9me_0 and H3K9me_1 was better than that between H3K9me_2 and H3K9me_3 (Table 2.6). **CX4** absorbs at 214 nm, thus a relatively higher peptide concentration of 100 μM was injected here (compared to 0.5 μM in the separation with the LIF detector) to overcome background signal. Each peptide peak displayed a sharp front and a tailing end, which is induced by the mobility difference between the peptide and the host-peptide complex. For peptides that diffuse out of the sample zone at the front boundary, binding to the host in the BGE slowed down their migration, and thus the peptide is pushed back to the sample zone, forming a sharp peak front. For the peptide diffusing out at the back boundary, binding slowed it down, leading to peak tailing.

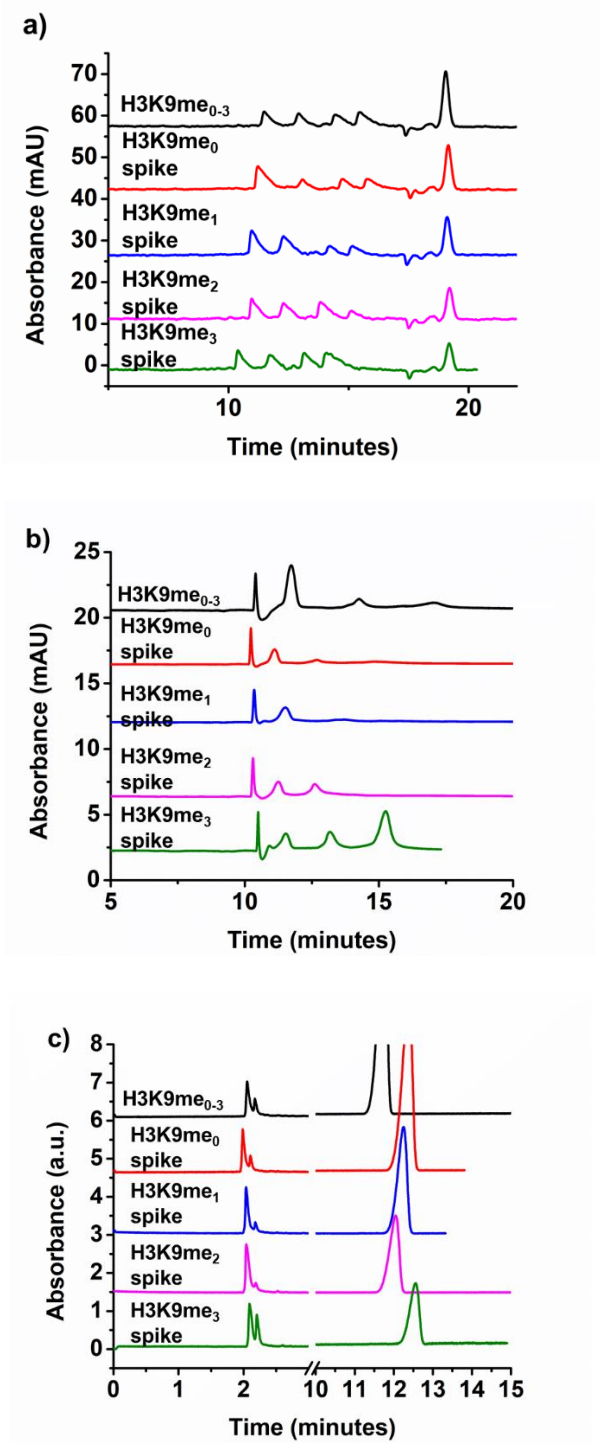

Figure 2.16 Spiked with standard peptides to confirm peak identity in peptide separation using a) **CX4**, b) **CX6**, and c) **CB7**.

Table 2.6 Resolution of the H3K9(me_{0-3}) peptides in the presence of hosts[a]

Peptide Peaks	**CX4**	**CX6**	**CB7**
H3K9me_0/me_1	1.88	2.83	0
H3K9me_1/me_2	1.72	2.42	0
H3K9me_2/me_3	1.06	1.85	0.72

[a] 100 μM H3K9(me_{0-3}) injected into 20 mM sodium phosphate buffer, pH 7.4, [host] = 50 μM. Results are averages of duplicate measurements. See equation 2.5 for resolution definition.

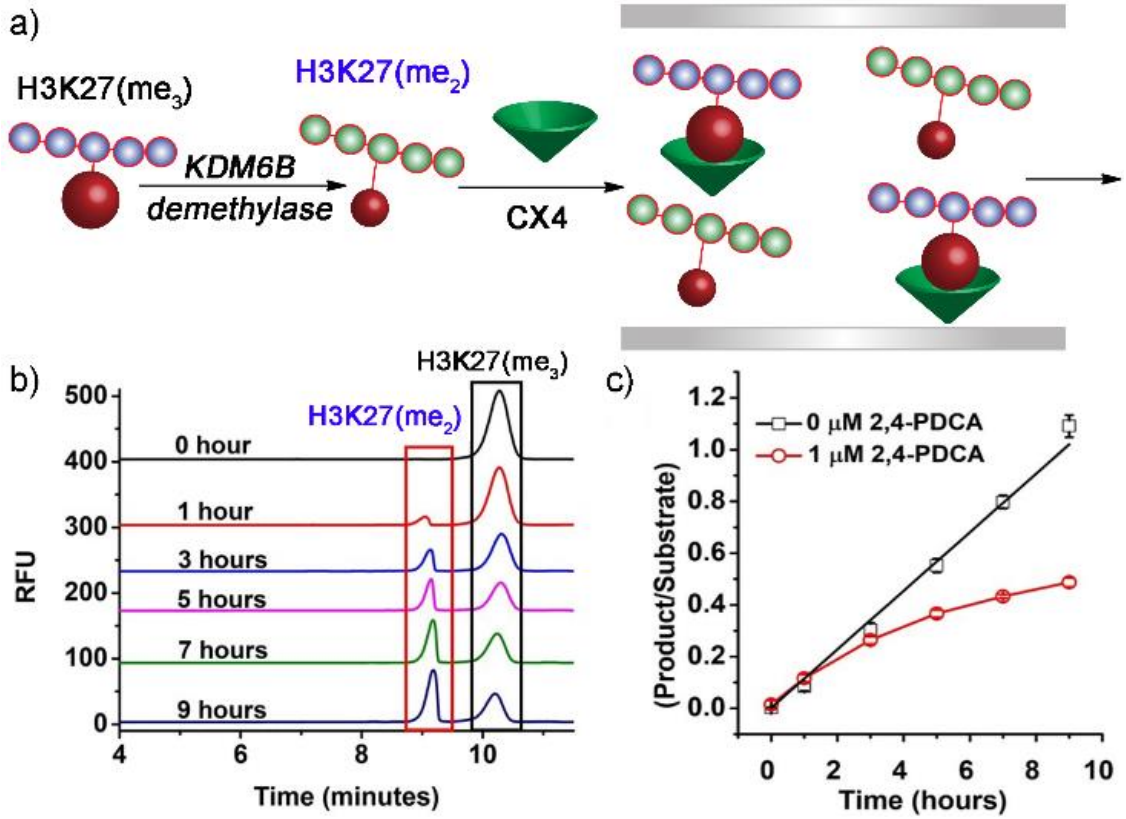

Figure 2.17 a) Host-assisted CE as a KDM6B demethylase assay. b) Separation of demethylated product H3K27(me_2) and H3K27(me_3) substrate after enzyme reaction for various times. c) Inhibitor assay: [H3K27(me_2)]/[H3K27(me_3)] versus time in the presence and absence of 1 μM 2,4-PDCA inhibitor, electropherograms shown in Figure S10.

We also evaluated separation with the other two hosts, keeping the peptide and host concentrations at 50 μM, and separated under the same hydrodynamic pressure of 5 mbar and an electric field of 571 V/cm. **CX6** effected the same migration order of the four H3K9(me_{0-3}) peptides as did **CX4**, but with better resolution (Figure 2.15c, Table 2.6). The broad peak for H3K9(me_1) is large due to overlap with the neutral marker. In contrast, **CB7** was a less effective additive, and only the trimethylated peptide H3K9(me_3) was separated from the mixture (Figure 2.15c), and even then, with a lower resolution of 0.72 (Table 2.6). This is unfortunate, as **CB7** is ideally suited to UV detection due to its minimal absorbance at 214nm. As such, there are no background issues even if high host concentrations are added to the BGE.

The good separation with **CX4** and **CX6** is mainly due to charge changes upon binding. As the H3K9(me_{0-3}) peptides are larger than the control fluorophores and H3K27 peptides, the change in overall size upon binding with the hosts is relatively small. In the case of **CB7**, which only effects a change in size and not charge, the host had less impact on peptide mobility upon binding, and, at 50 μM, it could not resolve the peptides with lower methylation levels.

2.3.4 Enzyme Assay

As the host-assisted CE method could effectively separate peptides of varying methylation level, it is a valuable tool for studying the function of methylation-related enzymes and screening enzyme effectors or inhibitors. To demonstrate this, we applied the CE method to evaluate the activity of KDM6B, a demethylase selective for methylated H3K27 peptides (Figure 2.17a). This enzyme reduces the trimethylated H3K27 peptide to

the demethylated, monomethylated and unmethylated states[53] in the presence of α-ketoglutarate and Fe^{2+} cofactors. Figure 2.17b shows the assay process for the demethylation of 2 μM H3K27(me_3) with 1 μM KDM6B, 50 μM α-ketoglutarate, 500 μM ascorbate, and 20 μM Fe^{2+} in 20 mM tris buffer, pH 7.4. Aliquots were extracted at hourly time points, and subjected to host-assisted CE, with 50 μM **CX4** in the BGE. Fluorescence monitoring prevents interference from the other reaction components and can unambiguously detect the peptide substrate and the corresponding products. As time increased, the H3K27(me_3) substrate was consumed and a single product appeared (Fig. 2.17b). MALDI-MS analysis revealed that the product is dimethylated (Figure 2.18). This demethylase seemed not particularly efficient: a reaction time longer than 5 hours led to only 20% turnover ratio, and only the dimethylated product was produced. Nevertheless, we could use this method to analyze the effect of a demethylase inhibitor, 2,4-pyridinedicarboxylic acid (2,4-PDCA), which is an inhibitor for several JmjC domain-containing enzymes. It targets the active site for iron on α-ketoglutarate, one of the cofactors important in demethylation.[53] Starting at the 3 hour data point, the area ratio of product to substrate decreased with the presence of 2,4-PDCA, indicating reduction of enzyme activity under the action of the inhibitor (Figures 2.17c, 2.19 and Table 2.7).

To prove that our method can also monitor reactions on unlabeled peptides, we applied it to evaluate the demethylation reaction catalyzed by JMJD2E on the non-fluorescently labeled H3K9me_3 as that used in Fig. 2.20. The non-label substrate would be more representative to the peptides obtained from biological samples, and it allows us to

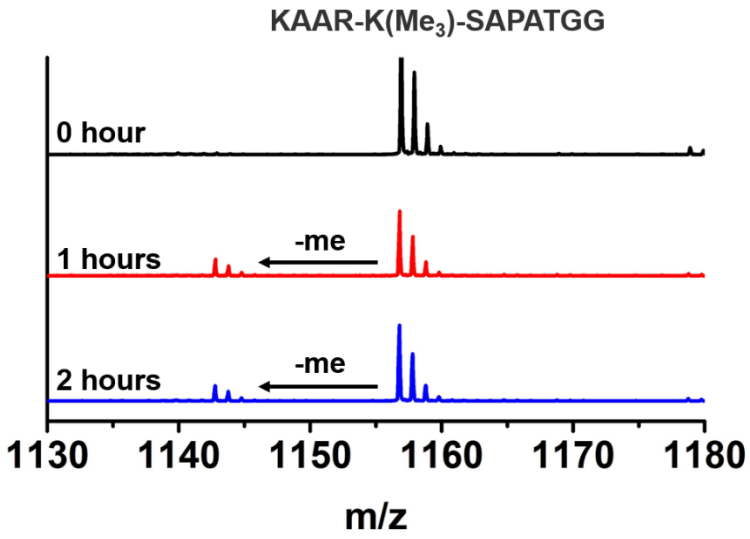

Figure 2.18 MALDI TOF/TOF spectra of substrate H3K27(me_3) and product H3K27(me_2) after demethylase enzyme reaction.

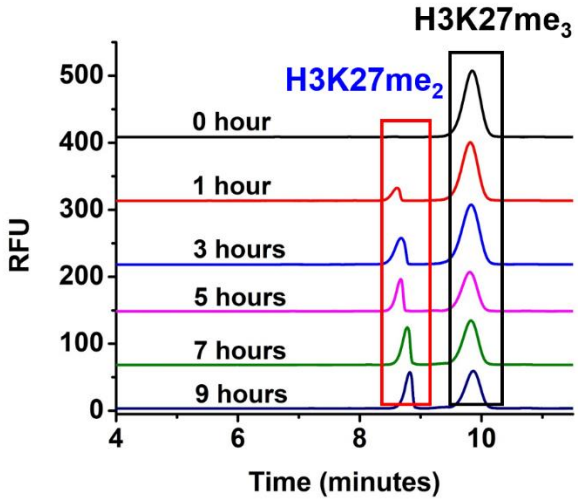

Figure 2.19 Separation of demethylated product H3K27(me_2) and H3K27(me_3) substrate after enzyme reaction for various times in the presence of 1 μM 2,4-PDCA inhibitor. Detection was carried out by the home-built laser induced fluorescence (LIF) system.

Table 2.7: Effect of demethylase inhibitor 2,4-PDCA on the demethylation reaction, monitored by host-assisted CE

Time, h	Product Ratio, 0 μM PDCA[b]	Product Ratio, 1 μM PDCA[b]
0	0.003 ± 0.002	0.014± 0.016
1	0.085 ± 0.017	0.116 ± 0.016
3	0.304 ± 0.026	0.264 ± 0.016
5	0.552 ± 0.026	0.366 ± 0.015
7	0.797 ± 0.025	0.433 ± 0.007
9	1.091 ± 0.043	0.487 ± 0.018

[a] 2 μM H3K27(me_3) incubated with 1 M μM KDM6B, 50 μM α-ketoglutarate, 500 μM ascorbate, and 20 μM Fe^{2+} in 20 mM tris buffer, pH 7.4, 100 mM NaCl. Results are averages of duplicate measurements. Electropherograms shown in Figure S12, Supporting Information.

spike in standard peptides to confirm the identities of the product peaks. A higher substrate concentration of 50 μM was needed to permit UV detection, along with higher enzyme (5 μM JMJD2E) and co-factor concentrations (500 μM α-ketoglutarate, 5 mM ascorbate, and 100 μM Fe^{2+}). CE analysis was carried out at the discrete reaction time points of 0, 20, 60, and 120 min, with 50 μM **CX4** in the BGE. The electropherograms measured at λ_{abs} = 214 nm showed that the peak of H3K9(me_3) decreased dramatically at 20 min, with the appearance of some unresolved product peaks in the region where the peptides with lower methylation levels should locate (Fig. 2.20a). As the reaction went on, the products became better resolved: a clear product peak was observed at reaction duration of 60 min, which decreased with the next 60-min reaction and produced another peak at earlier elution time.

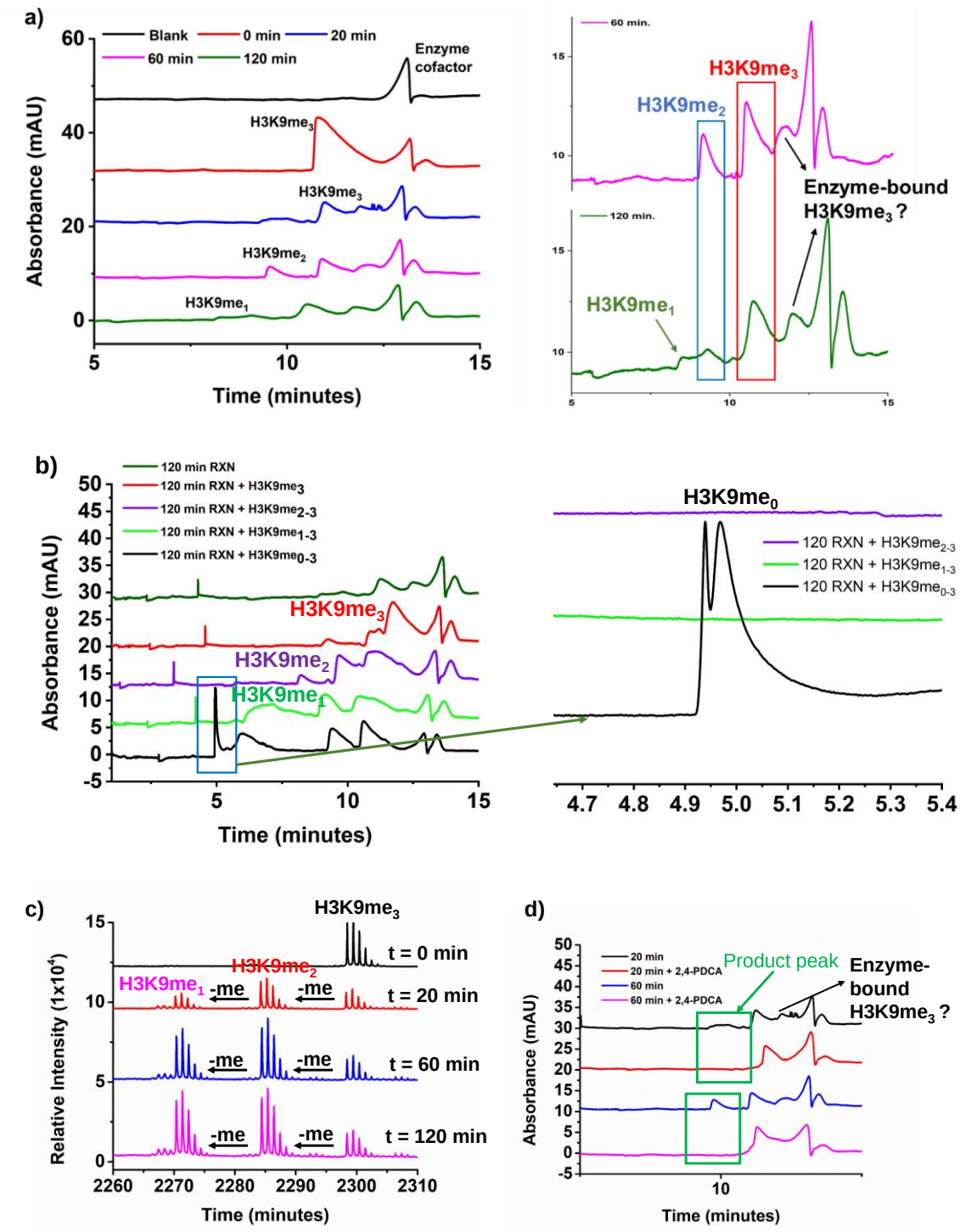

Figure 2.20 Analysis of the demethylation reaction of H3K9me$_3$ catalyzed by JMJD2E. a) Electropherograms collected at multiple reaction time points, with blank being the reaction mixture without addition of enzyme and peptide substrate, and t = 0 min being

the mixture containing the peptide substrate but not enzyme. b) Analysis of the reaction mixture at t = 120 min spiked with H3K9me$_3$, H3K9me$_2$, H3K9me$_1$, and H3K9me$_0$, consecutively for peak identification. The resolution got worse when more peptides were added to the sample due to column overloading. c) MALDI TOF/TOF spectra of substrate H3K9me$_3$ and products of H3K9me$_{1\text{-}2}$ after demethylase enzyme reaction. d) Analysis of reaction mixtures collected at 20 or 60 min. reaction duration with or without the presence of 1 μM 2,4-PDCA inhibitor. Separation was carried out in the Agilent CE system with UV detection at λ = 214 nm.

Spiking the standard peptides of H3K9(me$_{0\text{-}3}$) to the reaction mixture obtained at 120 min helped to confirm the identity of each peak (Fig. 2.20b). The changes occurred in the reaction were also confirmed by MALDI-MS (Fig. 2.20c). With the addition of 2,4-PDCA, obvious inhibition of the enzyme activity took place and no product generation was observed at reaction duration of either 20 or 60 min (Fig. 2.20d). It is interesting to notice that the electropherograms obtained at 20-min reaction duration had one additional peak showing up after adding the enzyme to the reaction mixture, which disappeared if the inhibitor was added (Fig. 2.20d). This peak may indicate the complex formed between the enzyme and the peptide substrate which was disrupted by the addition of 2,4-PDCA. More investigation should be performed on the enzyme reaction to reveal the full power of our method in functional study of methylation enzymes.

The above results support that our method is capable of monitoring enzyme reactions and assessing enzyme activities with either the fluorescently labeled peptides or native peptides. Fluorescence detection is preferred because the peptides (both substrate and products) could be detected unambiguously without interference from other components in the reaction mixture.

2.4 Conclusions

Here, we have shown that capillary electrophoresis is an effective method of separating post-translationally modified histone peptides with only small variations in structure, when combined with a suitable host molecule in the background electrolyte. Even for large, 21-amino acid peptide substrates, the small physical change induced by the addition of only one methyl group to a single lysine residue can be separated. Selective molecular recognition events between calixarene and cucurbituril hosts confer varying changes in size and charge to the peptides. The combination of both molecular recognition and CE magnifies the efficiency of both techniques, allowing high separation efficiency, despite the minimal changes in peptide structure upon modification. Host-assisted CE is fast and consumes a minimal amount of reagents and samples. It is also versatile, as changing the separation medium is simple, and a library of hosts can be applied with no need for covalent attachment to capillary wall surfaces. All these features make host-assisted CE an ideal tool for separation and purification of modified peptides that are challenging to isolate with conventional methods. The host-assisted CE method can also be applied to monitor enzyme reactivity, which is advantageous due to the small sample consumption of CE, and continuous sampling which saves on samples and time. Future work in our laboratories will focus on coupling the host-assisted CE with MS to permit analysis of methylated peptides in more complex mixtures. Examination of protein methylation can then be carried out in biological samples such as cells and tissues for better understanding of the functions of these PTMs.

2.5 References

(1) Olsen, J. V.; Mann, M. Status of Large-Scale Analysis of Posttranslational Modifications by Mass Spectrometry. *Mol. Cell. Proteomics* **2013**, *12* (12), 3444–3452.

(2) Zhang, J.; Corbett, J. R.; Plymire, D. A.; Greenberg, B. M.; Patrie, S. M. Proteoform Analysis of Lipocalin-Type Prostaglandin D-Synthase from Human Cerebrospinal Fluid by Isoelectric Focusing and Superficially Porous Liquid Chromatography with Fourier Transform Mass Spectrometry. *Proteomics* **2014**, *14* (10), 1223–1231.

(3) Zybailov, B.; Sun, Q.; Van Wijk, K. J. Workflow for Large Scale Detection and Validation of Peptide Modifications by RPLC-LTQ-Orbitrap: Application to the Arabidopsis Thaliana Leaf Proteome and an Online Modified Peptide Library. *Anal. Chem.* **2009**, *81* (19), 8015–8024.

(4) Colignon, B.; Raes, M.; Dieu, M.; Delaive, E.; Mauro, S. Evaluation of Three-Dimensional Gel Electrophoresis to Improve Quantitative Profiling of Complex Proteomes. *Proteomics* **2013**, *13* (14), 2077–2082.

(5) Anderton, J. A.; Bose, S.; Vockerodt, M.; Vrzalikova, K.; Wei, W.; Kuo, M.; Helin, K.; Christensen, J.; Rowe, M.; Murray, P. G.; et al. The H3K27me3 Demethylase, KDM6B, Is Induced by Epstein-Barr Virus and over-Expressed in Hodgkin's Lymphoma. *Oncogene* **2011**, *30* (17), 2037–2043.

(6) Hua, K. T.; Wang, M. Y.; Chen, M. W.; Wei, L. H.; Chen, C. K.; Ko, C. H.; Jeng, Y. M.; Sung, P. L.; Jan, Y. H.; Hsiao, M.; et al. The H3K9 Methyltransferase G9a Is a Marker of Aggressive Ovarian Cancer That Promotes Peritoneal Metastasis. *Mol. Cancer* **2014**, *13* (1), 1–13.

(7) Guo, A.; Gu, H.; Zhou, J.; Mulhern, D.; Wang, Y.; Lee, K. A.; Yang, V.; Aguiar, M.; Kornhauser, J.; Jia, X.; et al. Immunoaffinity Enrichment and Mass Spectrometry Analysis of Protein Methylation. *Mol. Cell. Proteomics* **2014**, *13* (1), 372–387.

(8) Garnett, G. A. E.; Starke, M. J.; Shaurya, A.; Li, J.; Hof, F. Supramolecular Affinity Chromatography for Methylation-Targeted Proteomics. *Anal. Chem.* **2016**, *88* (7), 3697–3703.

(9) Santos-Rosa, H.; Schneider, R.; Bannister, A. J.; Sherriff, J.; Bernstein, B. E.; Emre, N. C. T.; Schreiber, S. L.; Mellor, J.; Kouzarides, T. Active Genes Are Tri-Methylated at K4 of Histone H3. *Nature* **2002**, *419* (6905), 407–411.

(10) Rothbart, S. B.; Dickson, B. M.; Raab, J. R.; Grzybowski, A. T.; Krajewski, K.; Guo, A. H.; Shanle, E. K.; Josefowicz, S. Z.; Fuchs, S. M.; Allis, C. D.; et al. An Interactive Database for the Assessment of Histone Antibody Specificity. *Mol. Cell* **2015**, *59* (3), 502–511.

(11) Nielsen, P. R.; Nietlispach, D.; Mott, H. R.; Callaghan, J.; Bannister, A.; Kouzarides, T.; Murzin, A. G.; Murzina, N. V.; Laue, E. D. Structure of the HP1 Chromodomain Bound to Histone H3 Methylated at Lysine 9. *Nature* **2002**, *416* (6876), 103–107.

(12) Gong, Y.; Lee, H. K. Application of Cyclam-Capped β-Cyclodextrin-Bonded Silica Particles as a Chiral Stationary Phase in Capillary Electrochromatography for Enantiomeric Separations. *Anal. Chem.* **2003**, *75* (6), 1348–1354.

(13) Wu, S. H.; Ding, W. H. Application of Cyclodextrin-Mediated Capillary Electrophoresis to Determine the Apparent Binding Constants and Thermodynamic Parameters of the Alkylnaphthalene Derivatives. *Electrophoresis* **2005**, *26* (18), 3528–3537.

(14) Mitchell, C. R.; Armstrong, D. W. Cyclodextrin-Based Chiral Stationary Phases for Liquid Chromatography. In *Chiral Separations: Methods and Protocols*; Gübitz, G., Schmid, M. G., Eds.; Humana Press: Totowa, NJ, 2004; pp 61–112.

(15) Yongzhu, J.; Hirose, K.; Nakamura, T.; Nishioka, R.; Ueshige, T.; Tobe, Y. Preparation and Evaluation of a Chiral Stationary Phase Covalently Bound with a Chiral Pseudo-18-Crown-6 Ether Having a Phenolic Hydroxy Group for Enantiomer Separation of Amino Compounds. *J. Chromatogr. A* **2006**, *1129* (2), 201–207.

(16) Lindner, H.; Helliger, W.; Dirschlmayer, A.; Talasz, H.; Wurm, M.; Sarg, B.; Jaquemar, M.; Puschendorf, B. Separation of Phosphorylated Histone H1 Variants by High-Performance Capillary Electrophoresis. *J. Chromatogr. A* **1992**, *608* (1), 211–216.

(17) Lindner, H.; Helliger, W.; Dirschlmayer, A.; Jaquemar, M.; Puschendorf, B. High-Performance Capillary Electrophoresis of Core Histones and Their Acetylated Modified Derivatives. *Biochem. J.* **1992**, *283* (2), 467–471.

(18) Beshara, C. S.; Jones, C. E.; Daze, K. D.; Lilgert, B. J.; Hof, F. A Simple Calixarene Recognizes Post-Translationally Methylated Lysine. *ChemBioChem* **2010**, *11* (1), 63–66.

(19) Daze, K. D.; Hof, F. The Cation-π Interaction at Protein-Protein Interaction Interfaces: Developing and Learning from Synthetic Mimics of Proteins That Bind Methylated Lysines. *Acc. Chem. Res.* **2013**, *46* (4), 937–945.

(20) Hof, F. Host-Guest Chemistry That Directly Targets Lysine Methylation: Synthetic Host Molecules as Alternatives to Bio-Reagents. *Chem. Commun.* **2016**, *52* (66), 10093–10108.

(21) Daze, K. D.; Pinter, T.; Beshara, C. S.; Ibraheem, A.; Minaker, S. A.; Ma, M. C. F.; Courtemanche, R. J. M.; Campbell, R. E.; Hof, F. Supramolecular Hosts That Recognize Methyllysines and Disrupt the Interaction between a Modified Histone Tail and Its Epigenetic Reader Protein. *Chem. Sci.* **2012**, *3* (9), 2695–2699.

(22) Barrow, S. J.; Kasera, S.; Rowland, M. J.; Del Barrio, J.; Scherman, O. A. Cucurbituril-Based Molecular Recognition. *Chem. Rev.* **2015**, *115* (22), 12320–12406.

(23) Assaf, K. I.; Nau, W. M. Cucurbiturils: From Synthesis to High-Affinity Binding and Catalysis. *Chem. Soc. Rev.* **2015**, *44* (2), 394–418.

(24) Gamal-Eldin, M. A.; MacArtney, D. H. Selective Molecular Recognition of Methylated Lysines and Arginines by Cucurbit[6]Uril and Cucurbit[7]Uril in Aqueous Solution. *Org. Biomol. Chem.* **2013**, *11* (3), 488–495.

(25) Ingerman, L. A.; Cuellar, M. E.; Waters, M. L. A Small Molecule Receptor That Selectively Recognizes Trimethyl Lysine in a Histone Peptide with Native Protein-like Affinity. *Chem. Commun.* **2010**, *46* (11), 1839–1841.

(26) Pinkin, N. K.; Waters, M. L. Development and Mechanistic Studies of an Optimized Receptor for Trimethyllysine Using Iterative Redesign by Dynamic Combinatorial Chemistry. *Org. Biomol. Chem.* **2014**, *12* (36), 7059–7067.

(27) James, L. I.; Beaver, J. E.; Rice, N. W.; Waters, M. L. A Synthetic Receptor for Asymmetric Dimethyl Arginine. *J. Am. Chem. Soc.* **2013**, *135* (17), 6450–6455.

(28) Gober, I. N.; Waters, M. L. Supramolecular Affinity Labeling of Histone Peptides Containing Trimethyllysine and Its Application to Histone Deacetylase Assays. *J. Am. Chem. Soc.* **2016**, *138* (30), 9452–9459.

(29) Liu, Y.; Perez, L.; Mettry, M.; Easley, C. J.; Hooley, R. J.; Zhong, W. Self-Aggregating Deep Cavitand Acts as a Fluorescence Displacement Sensor for Lysine Methylation. *J. Am. Chem. Soc.* **2016**, *138* (34), 10746–10749.

(30) Liu, Y.; Perez, L.; Mettry, M.; Gill, A. D.; Byers, S. R.; Easley, C. J.; Bardeen, C. J.; Zhong, W.; Hooley, R. J. Site Selective Reading of Epigenetic Markers by a Dual-Mode Synthetic Receptor Array. *Chem. Sci.* **2017**, *8* (5), 3960–3970.

(31) Liu, Y.; Perez, L.; Gill, A. D.; Mettry, M.; Li, L.; Wang, Y.; Hooley, R. J.; Zhong, W. Site-Selective Sensing of Histone Methylation Enzyme Activity via an Arrayed Supramolecular Tandem Assay. *J. Am. Chem. Soc.* **2017**, *139* (32), 10964–10967.

(32) Minaker, S. A.; Daze, K. D.; Ma, M. C. F.; Hof, F. Antibody-Free Reading of the Histone Code Using a Simple Chemical Sensor Array. *J. Am. Chem. Soc.* **2012**, *134* (28), 11674–11680.

(33) Florea, M.; Kudithipudi, S.; Rei, A.; González-Úlvarez, M. J.; Jeltsch, A.; Nau, W. M. A Fluorescence-Based Supramolecular Tandem Assay for Monitoring Lysine Methyltransferase Activity in Homogeneous Solution. *Chem. - A Eur. J.* **2012**, *18* (12), 3521–3528.

(34) Peacor, B. C.; Ramsay, C. M.; Waters, M. L. Fluorogenic Sensor Platform for the Histone Code Using Receptors from Dynamic Combinatorial Libraries. *Chem. Sci.* **2017**, *8* (2), 1422–1428.

(35) Praetorius, A.; Bailey, D. M.; Schwarzlose, T.; Nau, W. M. Design of a Fluorescent Dye for Indicator Displacement from Cucurbiturils: A Macrocycle-Responsive Fluorescent Switch Operating through a PKa Shift. *Org. Lett.* **2008**, *10* (18), 4089–4092.

(36) Nau, W. M.; Ghale, G.; Hennig, A.; Bakirci, H.; Bailey, D. M. Substrate-Selective Supramolecular Tandem Assays: Monitoring Enzyme Inhibition of Arginase and Diamine Oxidase by Fluorescent Dye Displacement from Calixarene and Cucurbituril Macrocycles. *J. Am. Chem. Soc.* **2009**, *131* (32), 11558–11570.

(37) Lucas, D.; Minami, T.; Iannuzzi, G.; Cao, L.; Wittenberg, J. B.; Anzenbacher, P.; Isaacs, L. Templated Synthesis of Glycoluril Hexamer and Monofunctionalized Cucurbit[6]Uril Derivatives. *J. Am. Chem. Soc.* **2011**, *133* (44), 17966–17976.

(38) Liu, Y.; Liao, P.; Cheng, Q.; Hooley, R. J. Protein and Small Molecule Recognition Properties of Deep Cavitands in a Supported Lipid Membrane Determined by Calcination-Enhanced SPR Spectroscopy. *J. Am. Chem. Soc.* **2010**, *132* (30), 10383–10390.

(39) Rundlett, K. L.; Armstrong, D. W. Methods for the Determination of Binding Constants by Capillary Electrophoresis. *Electrophoresis* **2001**, *22* (7), 1419–1427.

(40) Chen, Z.; Weber, S. G. Determination of Binding Constants by Affinity Capillary Electrophoresis, Electrospray Ionization Mass Spectrometry and Phase-Distribution Methods. *TrAC - Trends Anal. Chem.* **2008**, *27* (9), 738–748.

(41) Colquhoun, D. The Quantitative Analysis of Drug-Receptor Interactions: A Short History. *Trends Pharmacol. Sci.* **2006**, *27* (3 SPEC. ISS.), 149–157.

(42) McGovern, R. E.; Fernandes, H.; Khan, A. R.; Power, N. P.; Crowley, P. B. Protein Camouflage in Cytochrome C-Calixarene Complexes. *Nat. Chem.* **2012**, *4* (7), 527–533.

(43) McGovern, R. E.; Snarr, B. D.; Lyons, J. A.; McFarlane, J.; Whiting, A. L.; Paci, I.; Hof, F.; Crowley, P. B. Structural Study of a Small Molecule Receptor Bound to Dimethyllysine in Lysozyme. *Chem. Sci.* **2015**, *6* (1), 442–449.

(44) Bailey, D. M.; Hennig, A.; Uzunova, V. D.; Nau, W. M. Supramolecular Tandem Enzyme Assays for Multiparameter Sensor Arrays and Enantiomeric Excess Determination of Amino Acids. *Chem. - A Eur. J.* **2008**, *14* (20), 6069–6077.

(45) Li, W.; Bockus, A. T.; Vinciguerra, B.; Isaacs, L.; Urbach, A. R. Predictive Recognition of Native Proteins by Cucurbit[7]Uril in a Complex Mixture. *Chem. Commun.* **2016**, *52* (55), 8537–8540.

(46) Lee, J. W.; Lee, H. H. L.; Ko, Y. H.; Kim, K.; Kim, H. I. Deciphering the Specific High-Affinity Binding of Cucurbit[7]Uril to Amino Acids in Water. *J. Phys. Chem. B* **2015**, *119* (13), 4628–4636.

(47) Lee, J. W.; Shin, M. H.; Mobley, W.; Urbach, A. R.; Kim, H. I. Supramolecular Enhancement of Protein Analysis via the Recognition of Phenylalanine with Cucurbit[7]Uril. *J. Am. Chem. Soc.* **2015**, *137* (48), 15322–15329.

(48) Douteau-Guével, N.; Coleman, A. W.; Morel, J. P.; Morel-Desrosiers, N. Complexation of the Basic Amino Acids Lysine and Arginine by Three Sulfonatocalix[n]Arenes (n = 4, 6 and 8) in Water: Microcalorimetric Determination of the Gibbs Energies, Enthalpies and Entropies of Complexation. *J. Chem. Soc. Perkin Trans. 2* **1999**, No. 3, 629–633.

(49) Hughes, R. M.; Wiggins, K. R.; Khorasanizadeh, S.; Waters, M. L. Recognition of Trimethyllysine by a Chromodomain Is Not Driven by the Hydrophobic Effect. *Proc. Natl. Acad. Sci. U. S. A.* **2007**, *104* (27), 11184–11188.

(50) Taverna, S. D.; Li, H.; Ruthenburg, A. J.; Allis, C. D.; Patel, D. J. How Chromatin-Binding Modules Interpret Histone Modifications: Lessons from Professional Pocket Pickers. *Nat. Struct. Mol. Biol.* **2007**, *14* (11), 1025–1040.

(51) Horvath, J.; Dolník, V. Polymer Wall Coatings for Capillary Electrophoresis. *Electrophoresis* **2001**, *22* (4), 644–655.

(52) Belder, D.; Deege, A.; Husmann, H.; Kohler, F.; Ludwig, M. Cross-Linked Poly(Vinyl Alcohol) as Permanent Hydrophilic Column Coating for Capillary Electrophoresis. *Electrophoresis* **2001**, *22* (17), 3813–3818.

(53) Rose, N. R.; McDonough, M. A.; King, O. N. F.; Kawamura, A.; Schofield, C. J. Inhibition of 2-Oxoglutarate Dependent Oxygenases. *Chem. Soc. Rev.* **2011**, *40* (8), 4364–4397.

Chapter 3: Monitoring Lysine Methyltransferase and Kinase Activity with Host-Assisted Capillary Electrophoresis

3.1 Introduction

Post-translational modifications (PTMs) on proteins greatly increase their diversity by changing the structures, properties, and interactions, leading to substantial effects on activity. There are various PTM classifications including phosphorylation, methylation, glycosylation, and ubiquitylation. While PTMs can occur on all proteins, the ones on histone proteins that condense DNA into chromatin can affect gene expression. These PTMs are important epigenetic factors to regulate cellular functions like development, differentiation, proliferation, and apoptosis. They also respond to different stimuli, leading to altered biological processes and development of pathological conditions. Therefore, monitoring PTM changes in cells is essential for better understanding of the regulation mechanisms of cellular processes.

PTMs are controlled by modification enzymes, which can act as "writers" to add the specific PTM or as "erasers" to remove it. Furthermore, the activity of PTM enzymes can be affected by pre-existing modification sites nearby, termed crosstalk. In crosstalk events, one PTM can directly interfere with or enhance the addition of another mark located within the same histone tail[1] or another histone protein,[2,3] leading to downstream effects in chromatin regulation and structure as well as potential disease outcomes. To elucidate cross talk events, we can compare the activity of enzymes on substrates with or without other modifications.

Current methods for monitoring enzymatic activity include spectrophotometric[4,5] and radiometric[6–8] techniques; however, there can be overlap in product and other signals or safety concerns about radioactive waste. It is also difficult to use these techniques to inspect competition between the peptide substrates with or without other modifications in a mixture and detect modification on one of them. Separation techniques that can resolve the peptides with different PTMs are suitable studying PTM crosstalk. In particular, capillary electrophoresis (CE) has been widely applied in study of enzyme activity,[9] because of its low sample consumption, real-time reaction monitoring, and possibility to be operated in a high-throughput manner. More importantly, its high resolving power is essential in the context of PTMs conferring only small changes in hydrophobicity, size, and charge. CE has been used for separation of peptides in a simpler setting (i.e., single modification, such as phosphorylation or methylation);[10–12] however, it is still challenging to separate substrates from products with multiple modifications. Therefore, a separation additive is necessary for improved resolution.

Synthetic receptors can be included in CE, because of their quick on-and-off binding rate, lower molecular weight than protein receptors, and good water solubility. With understanding of their interaction with guest molecules, their structures can be designed to improve binding strength and selectivity; and they can be synthesized with low cost in large scales. These features are beneficial for obtaining high separation efficiency with simple and low-expense operation. Several supramolecular host molecules, including calixarenes,[12–14] cucurbiturils,[15] and cavitands,[16–18] have shown selectivity for PTMs like methylation and phosphorylation, which can be exploited to improve CE-based PTM

analysis. While phosphorylation changes the charge of the peptide, it is more challenging for CE to resolve peptides carrying methylation which only adds one to three methyl groups without charge alteration.

In the previous chapter, we successfully developed the host-assisted CE methods that employed 4-tetrasulfonatocalix[4]arene (CX4), 4-hexasulfonatocalix[6]arene (CX6), or cucurbit[7]uril (CB7) in the running buffer of CE to separate peptides with various degrees of lysine methylation. We also briefly demonstrated that, this method can be applied to study the activity of methylation enzymes, using histone demethylases as the example. In this study, we demonstrated that the host-assisted CE method can be applied to analyze enzyme crosstalk in one-pot reaction by simultaneously monitoring the changes on the peptides with or without the pre-existing modification. Using a capillary coated in-house with linear polyacrylamide (LPA) and fluorescently labeled peptides synthesized in the lab, we proved that the host-assisted CE method could resolve the peptides carrying multiple modifications. The activities of G9a methyltransferase or Aurora B kinase, which have been reported to be involved in crosstalk events,[19–22] were examined at the presence of an antagonistic modification on the adjacent residue, revealing the effect of phosphorylation on methyltransferase activity and vice versa.

3.2 Materials and Methods

3.2.1 General

All samples and separation buffers were made using ultrapure water (18 MΩ) from a Direct-Q Water Purification System (Millipore Sigma, Billerica, MA). α-Lactalbumin,

lysozyme, cytochrome c, hemoglobin, 4-tetrasulfonatocalix[4]arene, cucurbit[7]uril hydrate, 3-(trimethoxysilyl)propyl methacrylate, acrylamide, ammonium persulfate, α-cyano-4-hydroxycinnamic acid (α-CHCA), adenosine 5′-triphosphate disodium salt hydrate, *s*-(5′-adenosyl)-*L*-methionine (SAM) chloride dihydrochloride, and magnesium chloride hexahydrate were purchased from Sigma-Aldrich (St. Louis, MO). 4-Hexasulfonatocalix[6]arene hydrate was purchased from Alfa Aesar (Tewksbury, MA). 5(6)-Carboxyfluorescein was purchased from ACROS Organics (Morris Plains, NJ). All 9-fluorenylmethyloxycarbonyl-protected amino acids were purchased from AAPPTec (Louisville, KY) except for Fmoc-N-ε-dimethyl-L-lysine hydrochloride (ChemPep Inc., Wellington, FL) and N-α-Fmoc-O-benzyl-L-phosphoserine (Millipore Sigma, Billerica, MA). Lyophilized, non-labeled histone K9 peptides were purchased from AnaSpec, Inc. (Fremont, CA). The sequence is ARTKQTAR-K(me_x)-STGGKAPRKQLA (x = 0, 1, 2, 3).

3.2.2 Capillary Electrophoresis

Separation of non-fluorescent peptides was conducted on an Agilent 7100 CE system with a UV-visible diode-array detector. Data were acquired via ChemStation (Agilent Technologies, Santa Clara, CA). Samples were introduced into the LPA-coated capillary (50 μm inner diameter, 365 μm outer diameter, with an effective length of 26.5 cm) with a 50 mbar injection for 5 s. Separation was driven by an electric field of 571 V/cm with positive polarity. Separation experiments of fluorescently labeled peptides were performed using a Beckman Coulter ProteomeLab PA 800 (Beckman Coulter, Fullerton, CA) with a laser-induced fluorescence detector (λ_{exc} = 488 nm, λ_{em} = 520 nm). Samples were introduced into the LPA-coated capillary (50 μm inner diameter, 365 μm outer

diameter, with an effective length of 20 cm) with a 0.5 psi injection for 5 s. Separation was driven by an electric field of 662 V/cm with positive polarity. Data were acquired via 32Karat and analyzed via OriginPro 8.6.

3.2.3 Preparation of the Linear Polyacrylamide Coating

Bare fused-silica capillaries (50 μm i.d., 365 μm o.d.) were purchased from Polymicro Technologies (Phoenix, Arizona). The inner wall of the bare fused silica capillary was coated with linear polyacrylamide based on a protocol from Zhu et al.[23] with several modifications, described as following. The mixture of acrylamide and ammonium persulfate was degassed under the vacuum and flushed through the capillary with nitrogen. The sealed capillary was then incubated in an oven at 50 °C for 30 minutes. After rinsing excess reagents with water, the capillary was dried with nitrogen and stored at room temperature. The tip of the capillary was not etched.

3.2.4 Separation Performance on Linear Polyacrylamide-Coated Capillary

Non-fluorescent peptides were separated on an Agilent 7100 CE system with a UV-visible diode-array detector. Data were acquired via ChemStation (Agilent Technologies, Santa Clara, CA). Samples were introduced into an LPA-coated capillary (50 μm inner diameter, 365 μm outer diameter, with an effective length of 26.5 cm) with a 50 mbar injection for 5 s. Separation was driven by an electric field of 571 V/cm with positive polarity.

3.2.5 Synthesis and Purification of 11-Amino Acid Peptides

Amino acids were sequenced using Peptide Synthesizer CSBio CS336H on FMOC-rink amide MBHA resin. UHPLC was performed on a Dionex system: UltiMate 3000

pump and variable wavelength detector. A C-18 reversed phase column (5 μm diameter, 100 Å, 250 × 21.2 mm) was used. Solvent A was 0.1% TFA in water and solvent B was 0.1% TFA in acetonitrile when using the gradient solvent system: solvent B (0−40%) in solvent A from the 0- to 7-minute mark at a flow rate of 3.0 mL/ min, solvent B (40−75%) in solvent A from 7- to 30-minute mark at a flow rate of 8.0 mL/min, and solvent B (75-100%) in solvent A from the 30- to 40-minute mark at a flow rate of 15.0 mL/min. Data acquisition was completed on the Chromeleon 7.2 Chromatography Data System software. Fractions were collected with a Dionex UltiMate 3000 Automated Fraction Collector. The mass of each peptide was determined using MALDI-TOF MS. 0.5 μL of each fraction and 2.5 μL of matrix (saturated α-CHCA in a 1:1 ratio of acetonitrile and 0.1% formic acid in water) were mixed before spotting each sample on a stainless steel Opti-TOF 96-target plate. Each spot was left to dry before introduction into the mass spectrometer. MS spectra were acquired in a positive reflector mode using the AB Sciex 5800 TOF/TOF proteomics analyzer. Solvent from the peptide fractions was then removed, and samples were lyophilized.

3.2.6 Enzyme Activity and Inhibition Assays

The lysine methyltransferase assay was carried out using synthesized and fluorescently labeled peptides: H3 (1-11) peptide with sequence FAM-ARTKQTARKST and H3S10p with sequence FAM-ARTKQTARK-pS-T. Ten μM of FAM-labeled H3 (1-11), FAM-labeled H3S10p, or a mixture of the two was incubated with 0.25 μM human recombinant G9a protein (Sigma-Aldrich, St. Louis, MO) in the reaction buffer (500 μM SAM, 0.1 Mg^{2+} in 20 mM tris pH 9.0) at room temperature. The reaction mixture was

injected *in situ* into the LPA-coated capillary (50 μm inner diameter, 365 μm outer diameter) at time intervals between 0 and 3 hours. The separation buffer was 2 μM CX6 for labeled H3 (1-11) and 10 μM CX6 for labeled H3S10p in 10 mM phosphate buffer, pH 7.4.

The kinase assay was carried out using synthesized and fluorescently labeled peptides: H3 (1-11) peptide with sequence FAM-ARTKQTARKST and H3K9me$_2$ with sequence FAM-ARTKQTAR-K(me$_2$)-ST. Ten μM of FAM-labeled H3 (1-11), FAM-labeled H3K9me$_2$, or a mixture of the two was incubated with 0.01 μg/μL Aurora B kinase (Sigma-Aldrich, St. Louis, MO) in the reaction buffer (20 μM ATP, 0.1 Mg^{2+} in 20 mM tris pH 7.4) at room temperature. For the peptide mixture, 0.005 μg/μL Aurora B was used for 3 hours instead. The reaction mixture was injected in situ into the LPA-coated capillary (50 μm inner diameter, 365 μm outer diameter) at time intervals between 0 and 4 hours. The separation buffer was 2 μM CX6 in 10 mM phosphate buffer, pH 7.4. A parallel inhibitor experiment was performed with 2.5 nM AZD1152-hydroxyquinazoline pyrazol anilide (Sigma-Aldrich, St. Louis, MO), 10 μM FAM-labeled H3 (1-11), and 0.005 μg/μL Aurora B kinase in the reaction buffer (20 μM ATP, 0.1 Mg^{2+} in 20 mM tris pH 7.4) at room temperature.

3.2.7 Matrix-Assisted Laser Desorption/Ionization Time-of-Flight Mass Spectrometry Analysis

The enzymatic assays were performed as described above. Aliquots were removed and deactivated by direct addition to the matrix solution. The matrix solution was prepared to form a saturated solution with α-cyano-4-hydroxycinnamic acid (CHCA) in a 1:1 ratio

of acetonitrile and 0.1% formic acid. A 1:1 ratio of matrix and sample was spotted on a stainless steel Opti-TOF 96-target plate and left to dry before inserting into the mass spectrometer. MS spectra were acquired in positive reflector mode using the AB Sciex 5800 TOF/TOF proteomics analyzer with laser irradiation at a repetition frequency of 1000 Hz.

3.2.8 Calculations

The tailing factor (t) was calculated with the following equation:

$$t = \frac{w_{5.0}}{t_w \cdot 2} \qquad \textbf{Equation 3.1}$$

where $w_{5.0}$ = peak width at 5% of peak height (min.) and t_w = distance (min.) between peak front and peak center.

In order to assess the separation performance, the resolution (R) was calculated with the following equation:

$$R = \frac{2\,(t_2 - t_1)}{w_1 + w_2} \qquad \textbf{Equation 3.2}$$

where t_1 and t_2 are the migration times of peaks 1 and 2, respectively. Furthermore, w_1 and w_2 are the base peak widths of peaks 1 and 2, respectively.

3.3 Results and Discussion

3.3.1 Enzymes of Interest and Their Peptide Substrates

The present work focused on G9a and Aurora B kinase, which exhibit PTM crosstalk activities. G9a is a histone methyltransferase that has primarily been studied for

its role in embryonic stem cell differentiation,[24] but it is also correlated with metastatic cancer when overexpressed.[25] The enzyme's activity is dependent on the SET domain, which uses SAM as the source of a methyl group[26] to dimethylate lysine 9 and lysine 27. In order for methylation to proceed on lysine 9, G9a requires at least the following amino acid sequence: TARKSTG.[22] It has been revealed that phosphorylation on serine 10 can reduce the activity of G9a to methylate lysine 9.[19,22]

On the other hand, a nearby methylated lysine residue can impact phosphorylation on serine, which can occur during catalysis by Aurora B kinase. This protein involved in the regulation of mitosis events[27] during which it can phosphorylate serine 10 and serine 28. Dimethylation on lysine 9 can have an antagonistic effect on the activity of Aurora B kinase.[18,19] Other residues like arginine at position 8 are vital for its activity as well, which is affected if lysine 9, threonine 11, and lysine 14 are substituted with alanine.[28] Aurora B has an important role in the regulation of kinetochore to microtubule attachment,[29] so inhibition of it can interfere with this process. Both G9a and Aurora B kinase can act on histone proteins but on more than one residue; therefore, we employed histone peptides as the enzyme substrates. Furthermore, the targeted sequence includes lysine 9 and serine 10, both of which are involved in crosstalk events with G9a and Aurora B kinase. In order to study the crosstalk for these two enzymes, it is demanded to separate the methylated peptides with or without phosphorylation, and the phosphorylated peptides with or without methylation. The host assisted-CE method we reported previously should then be further developed to accommodate such needs.

We chose to synthesize the peptides for the flexibility in placing multiple modifications at different amino acid sites; however, the yield is limited by the peptide length. A minimum of seven amino acids is required for the G9a substrate[22] while a minimum of ten amino acids is required for the Aurora B kinase substrate;[28] thus, we synthesized peptides with 11 amino acids that included the target residues, lysine 9 and serine 10 (Table 3.1). Furthermore, we fluorescently labeled the peptides to improve detection sensitivity. However, the labeling molecule carboxyfluorescein (FAM) is comprised of a mixture of both isomers, 5-FAM and 6-FAM, in order to reduce the cost; these cannot be seen in the MALDI spectrum due to them bearing the same molecular weight (Figure 3.1), but CE can resolve the two isomers. Nevertheless, four peptide substrates for the two selected enzymes could be subjects in an enzyme crosstalk study.

Table 3.1 Peptide sequences of FAM-labeled H3 (1-11) peptides

Peptide	**Sequence**
H3K9me_0	FAM-ARTKQTARKST
H3K9me_2	FAM-ARTKQTAR-K(me_2)-ST
H3K9me_0S10p	FAM-ARTKQTARK-pS-T
H3K9me_2S10p	FAM-ARTKQTAR-K(me_2)-pS-T

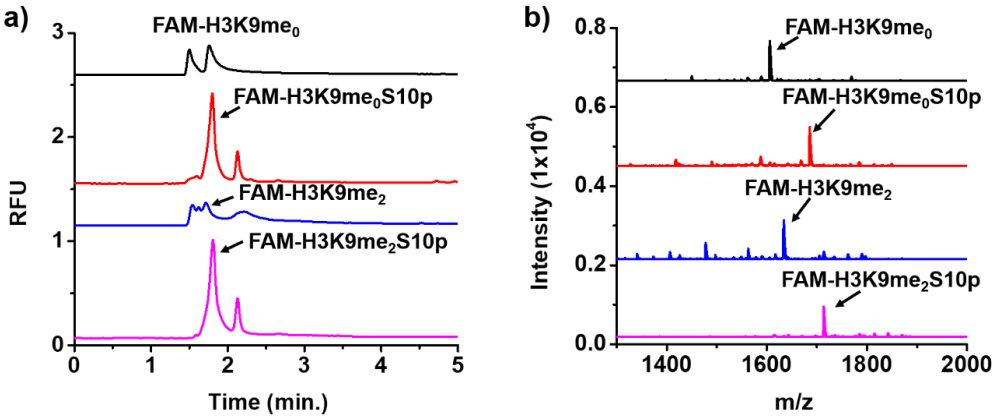

Figure 3.1 Purity of each peptide shown in (a) a CE electropherogram and (b) a MALDI spectrum.

3.3.2 Capillary Coating to Prevent Peptide Adsorption

The selected targets of the model enzymes, G9a and Aurora B kinase, are histone peptides. Many histone peptides have isoelectric points typically in the range of 10 to 12. In neutral running buffers, they carry positive charges and can be easily adsorbed to the negatively charged silanol groups via electrostatic attraction, which makes it necessary to coat the wall to prevent peak distortion and sample loss. In addition, a capillary coating can minimize fluctuation in electroosmotic flow (EOF), which could be induced by adsorption of the added host molecules. Covering the capillary wall can produce more reproducible migration for accurate analyte identification and quantification, which are required for enzyme assays. Coatings can either be dynamic or permanent. Dynamic coating requires the addition of coating materials to the running buffer, which also contains the synthetic hosts in our host-assisted CE method. This would make the buffer system complicated and reduce repeatability of separation. Therefore, we chose the permanent coating approach in our work.

In the previous chapter, we used the commercially available, pre-cut capillary coated by polyvinyl alcohol (PVA), which reduced peptide adsorption to the capillary wall and yielded satisfactory resolution of the histone peptides with varied methylation. However, the batch-to-batch reproducibility of the commercially available capillaries is not controllable. Thus, we carried out an in-lab coating of the capillaries using linear polyacrylamide (LPA) in the present work. Like PVA coating, LPA is neutral and hydrophilic, and it prevents adsorption of both cationic peptides and hydrophobic synthetic hosts. Various buffers, including solvents with surfactants,[30] can be used in LPA-coated capillaries. Like PVA-coated capillaries, LPA-coated capillaries are compatible with buffers in a wide pH range, inclusive of pH 10 and below. These features make the LPA-coated capillaries compatible with diverse synthetic hosts—specifically, the calixarene- and cucurbituril-based hosts used in our work.

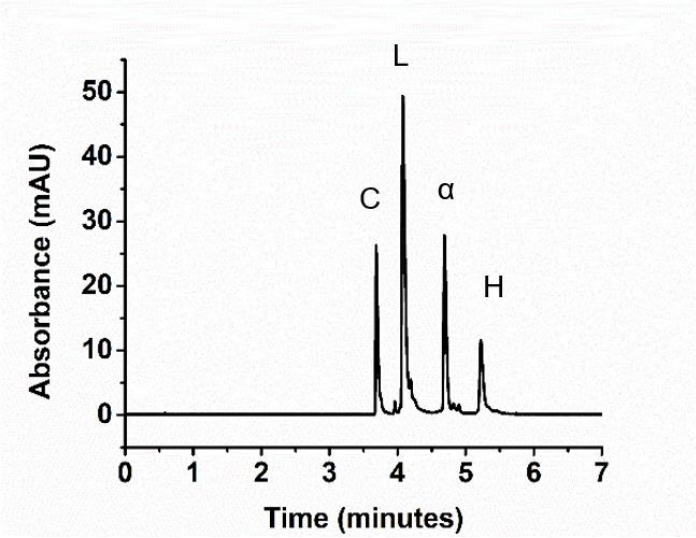

Figure 3.2 Separation of a standard protein mixture in an LPA-coated capillary. C = cytochrome c, L = lysozyme, α = α-lactalbumin, and H = hemoglobin. [Protein] = 0.25 mg/mL, background electrolyte = 50 mM phosphate buffer, pH 2.8.

Table 3.2 Average migration times, peak areas, and tailing factors (triplicate measurements) for standard proteins in linear polyacrylamide (LPA)-coated capillaries

Protein	**Migration Time (min)**		**Peak Area (mAU x min)**		**Tailing Factor**	
	Average	RSD (%)	Average	RSD (%)	Average	RSD (%)
Cytochrome c	3.72	1.2	62.9	0.6	4.1	0.3
Lysozyme	4.11	1.2	154.8	2.2	2.4	0.2
α-lactalbumin	4.73	1.3	77.8	1.6	1.9	0.1
Hemoglobin	5.28	1.5	39.0	6.2	2.2	0.1

We adopted the protocol reported by Dovichi's group to produce the LPA-coated capillaries.[23] In this protocol, 3-(trimethoxysilyl)propyl methacrylate, a bifunctional linker solution was injected into the capillary in order to activate the silanol groups for crosslinking with the polymer. Subsequently, the acrylamide monomer and ammonium persulfate initiator were introduced. Catalysts, such as tetramethylethylenediamine, can be used to promote polymerization. We used heat to catalyze the reaction, because the procedure is simpler and produces more consistent polymerization throughout the length of the capillary. To test the effectiveness of the coating, we injected a set of standard proteins ranging in pK_a values: cytochrome c, lysozyme, α-lactalbumin, and hemoglobin (Figure 3.2). Each protein was well separated from the others, and the relative standard

deviations for run-to-run migration times and peak areas were less than 10% with triplicate measurements (Table 3.2). More importantly, the basic proteins, lysozyme and cytochrome c, did not show significant peak tailing, although they had relatively larger tailing factors (Equation 3.1) than the acidic lactalbumin or the neutral hemoglobin. The slight coating could indicate some coating heterogeneity, but the coating was sufficient for reproducible migrations times and peak areas.

Table 3.3 Average migration times and peak areas (triplicate measurements) for 21-amino acid H3K9me$_{0-3}$ peptides in LPA-coated capillaries

Peptide	**Migration Time (min)**		**Peak Area (mAU x min)**	
	Average	RSD (%)	Average	RSD (%)
H3K9me$_0$	6.67	0.1	167.8	8.6
H3K9me$_1$	7.79	0.1	187.7	8.3
H3K9me$_2$	9.15	0.2	216.3	8.3
H3K9me$_3$	10.14	0.2	350.5	28.7

In order to demonstrate the separation capability of synthetic receptors in an LPA-coated capillary, we also tested the separation of the unlabeled H3K9me$_{0-3}$ peptides with CX4 in phosphate buffer at pH 3.0, a condition we used with the PVA-coated capillary. The relative standard deviations for each peptide's migration time and peak area were all less than 10% except for H3K9me$_3$ (Table 3.3). As shown in Figure 3.3, the separation of K9 peptides was comparable between the PVA- and LPA-coated capillaries. Overall, the

tailing factors and resolution values (R) in the LPA-coated capillary were similar to that of the commercial capillary.

3.3.3 Optimization of Separation

The enzyme crosstalk study requires baseline separation of peptides with a different number of modifications, so the separation conditions need to be optimized. Since the fluorescence of the FAM label is dependent on pH and would not fluoresce at pH 3.0, we chose to carry out the separation at pH 7.4 (Figure 3.4). As demonstrated in the previous chapter, CX4, CX6, and CB7 are effective in separating methylated and unmethylated small guests and peptides. All three synthetic hosts have electron-rich rims and hydrophobic cavities (Figure 3.5). While the negatively charged CX4 and CX6 both bind

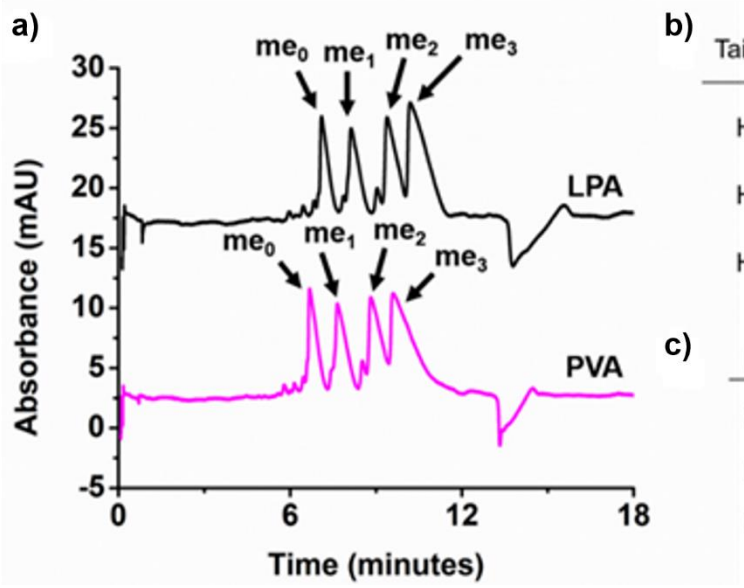

b)

Tailing Factor	PVA	LPA
H3K9me$_0$	1.5	1.9
H3K9me$_1$	1.6	1.6
H3K9me$_2$	2.6	1.9

c)

Resolution	PVA	LPA
H3K9me$_{0,1}$	1.0	1.2
H3K9me$_{1,2}$	1.1	1.4
H3K9me$_{2,3}$	0.4	0.6

Figure 3.3 (a) H3K9me$_{0\text{-}3}$ peptide separation in linear polyacrylamide (LPA)-coated and polyvinyl alcohol (PVA)-coated capillaries. Values for the tailing factor, t, (b) and resolution, R, (c) for 21-amino acid H3K9me$_{0\text{-}3}$ peptides in PVA- and LPA-coated capillaries. t was calculated using Equation 3.1 while R was calculated using Equation 3.2. The sequence of the peptide is ARTKQTAR-K(me$_x$)-STGGKAPRKQLA (x = 0, 1, 2, 3). [peptide] = 50 μM.

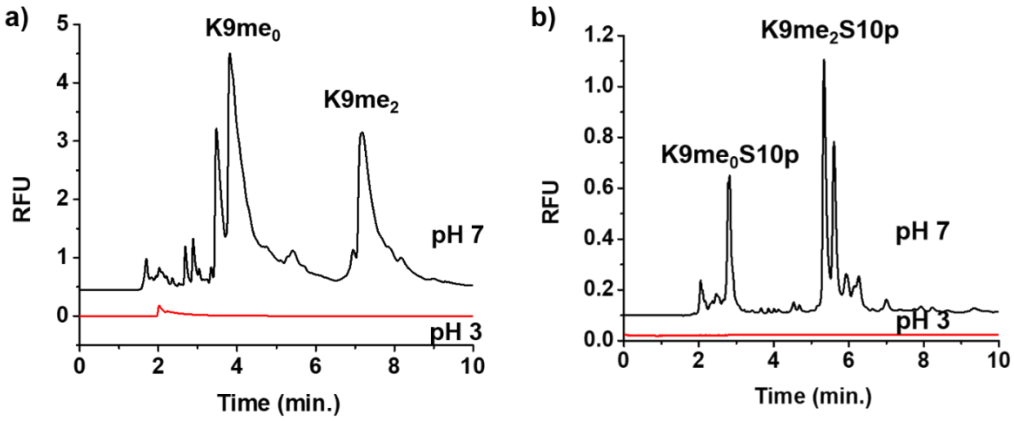

Figure 3.4 Separation of H3K9me$_{0,2}$ peptides (a) and H3K9me$_{0,2}$S10p peptides (b) in pH 3.0 and pH 7.4.

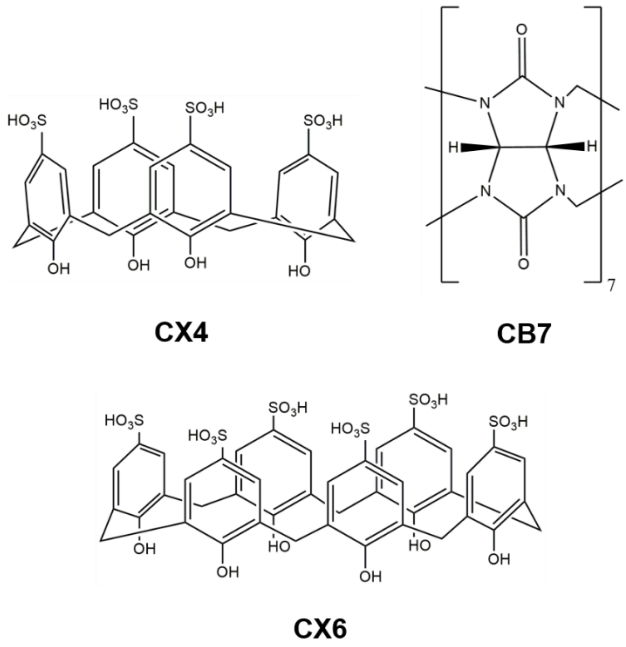

Figure 3.5 Structures of synthetic receptors: 4-tetrasulfonatocalix[4]arene (CX4), 4-hexasulfonatocalix[6]arene (CX6), and cucurbit[7]uril (CB7).

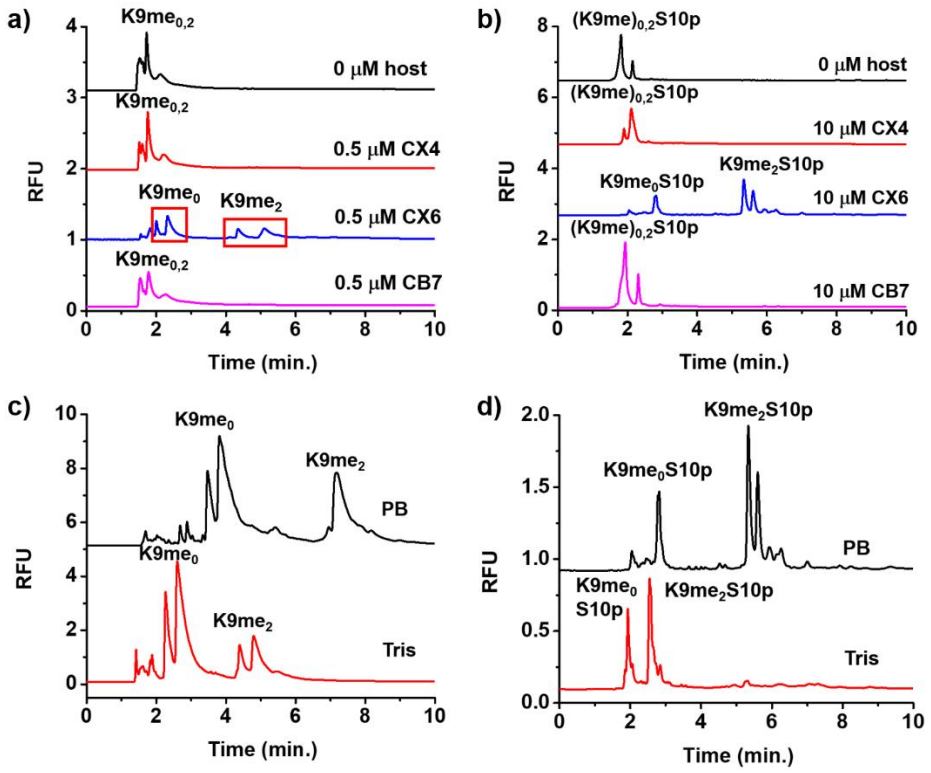

Figure 3.6 (a) Separation of H3K9me$_{0,2}$ peptides in 0 μM host, 0.5 μM CX4, 0.5 μM CX6, and 0.5 μM CB7 in 10 mM phosphate buffer, pH 7.4. (b) Separation of H3K9me$_{0,2}$S10p peptides in 0 μM host, 10 μM CX4, 10 μM CX6, and 10 μM CB7 in 10 mM phosphate buffer, pH 7.4. Separation of H3K9me$_{0,2}$ peptides (c) or H3K9me$_{0,2}$S10p peptides (d) with CX6 in 10 mM phosphate buffer and 10 mM tris buffer at pH 7.4.

to methylated lysine via cation-π interactions, neutral CB7 interacts with methylated lysine through the carbonyl groups to form ion-dipole interactions.[31] Besides the interaction differences, there is variability in separation performance between the synthetic receptors. While the calixarenes can separate all methylation levels, CB7 is less effective in separating them. In an uncoated capillary, CB7 causes a reduction in EOF unlike the calixarene hosts; however, this phenomenon is circumvented by the coated capillary. CX6 has the added benefit of flexibility[32] as well as a more negative charge, which can induce a larger mobility shift and increased separation. Out of all the previously tested synthetic

host molecules, CX6 resulted in the best resolution between all peptides with different methylation levels.

To confirm the optimal receptor type, we tested the separation performance of each synthetic host, kept at the same molar concentration, in the background electrolyte (Figures 3.6a,b). With the inclusion of 0.5 μM CX4 or CB7 in the running buffer, H3 and H3K9me$_2$ were not separated; however, the addition of 0.5 μM CX6 led to separation of the two peptides. A neutral marker only migrates with the addition of pressure during separation, which indicates that the EOF was eliminated by the LPA coating; thus, the electrophoretic migration is the same as the apparent mobility. Due to the preference of CX6 for methylation, H3K9me$_2$ had a slower electrophoretic migration compared to the unmethylated counterpart. CX6 induces a larger mobility shift and is the most flexible out of the chosen hosts to accommodate the peptide size. The same phenomenon occurred when separating H3K9me$_0$S10p and H3K9me$_2$S10p. With the addition of CX6, the peptide pair was well resolved. However, a higher concentration of 10 μM CX6 was required to better separate the peptides from the fluorescent peptide fragments that may have been produced during synthesis (Figure 3.7).

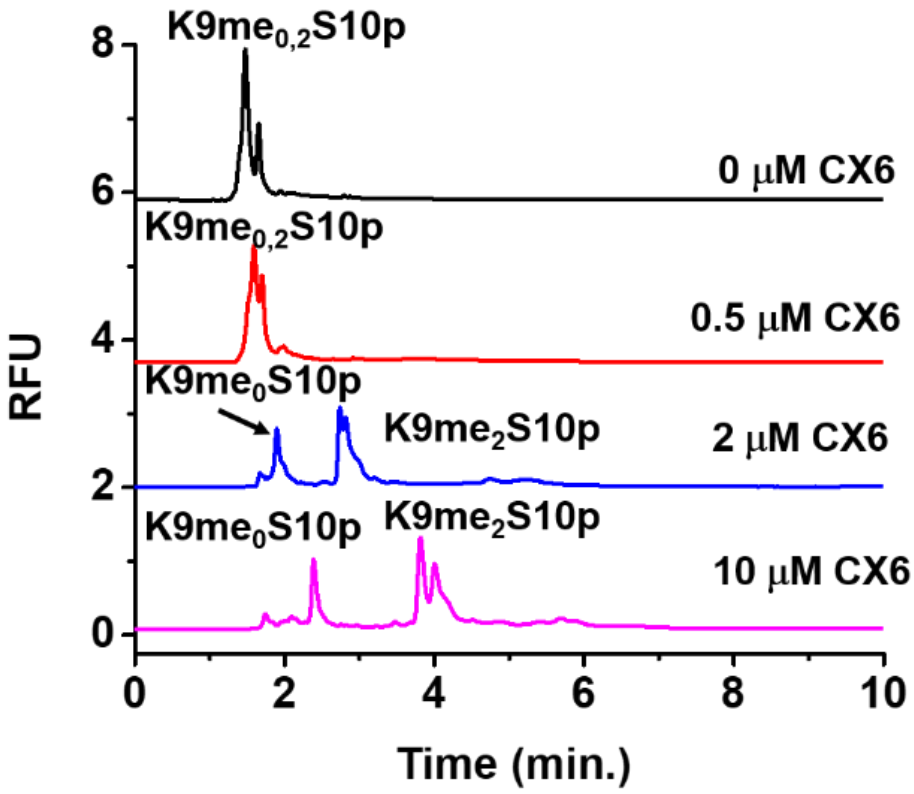

Figure 3.7 Optimization of H3K9me$_{0,2}$S10p separation in various concentrations of CX6, ranging from 0 μM to 10 μM CX6.

Table 3.4 Resolution of H3 (1-11) peptide peaks in phosphate and tris buffers[a]

Peptide Pair	**Phosphate**	**Tris**
H3K9me$_{0,2}$	3.4	2.4
H3K9me$_{0,2}$S10p	5.1	1.0

[a] For resolution calculation when isomer peaks (originated from the isomeric FAM) were present, the later migrating isomer peak of the first peptide and the earlier migrating isomer peak of the second peptide were used.

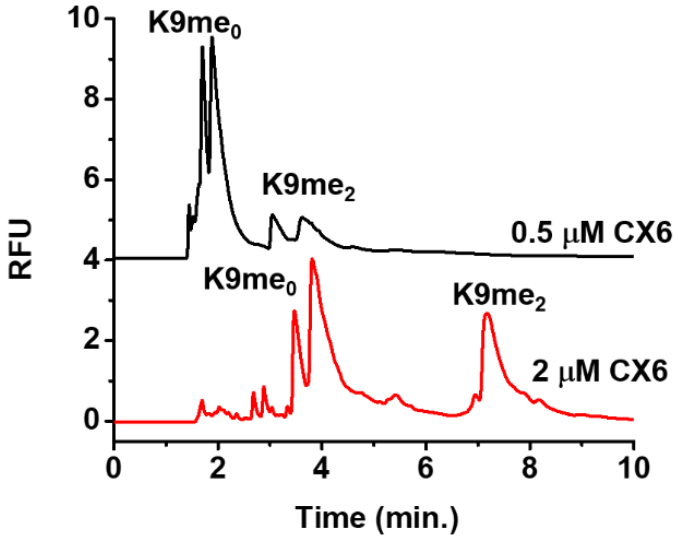

Figure 3.8 Comparison of H3K9me$_{0,2}$ peptide separation in 0.5 μM vs. 2 μM CX6.

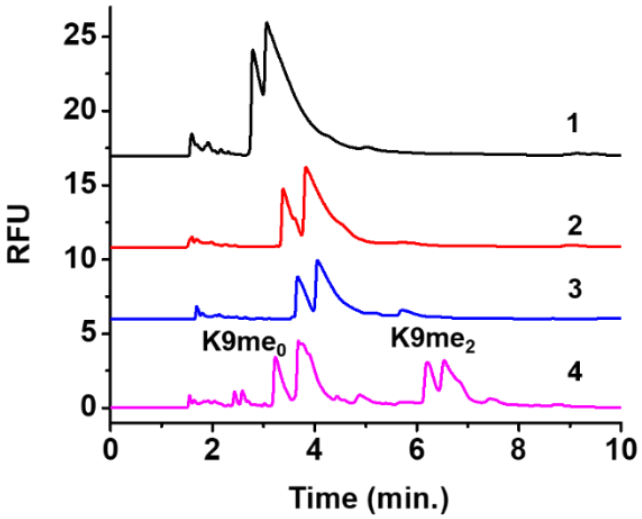

Figure 3.9 Controls for G9a reaction with H3K9me$_0$. Trace 1 – 10 μM H3K9me$_0$ peptide; trace 2 – 10 μM H3K9me$_0$ peptide with cofactors (500 μM SAM, 0.1 mM Mg^{2+}); trace 3 - 10 μM H3K9me$_0$ peptide with cofactors (500 μM SAM, 0.1 mM Mg^{2+}) and 0.25 μM deactivated G9a; trace 4 – H3K9me$_2$ spiked into reaction of 10 μM H3K9me$_0$ peptide with cofactors (500 μM SAM, 0.1 mM Mg^{2+}) and 0.25 μM deactivated G9a.

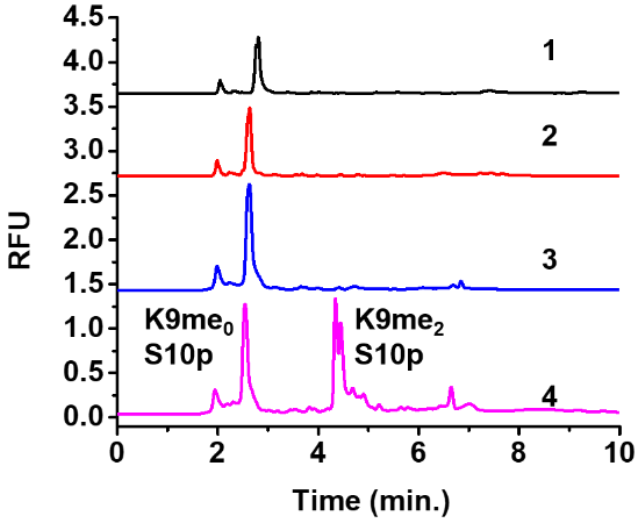

Figure 3.10 Controls for G9a reaction with H3K9me$_0$S10p. Trace 1 – 10 μM H3K9me$_0$S10p peptide; trace 2 – 10 μM H3K9me$_0$S10p peptide with cofactors (500 μM SAM, 0.1 mM Mg^{2+}); trace 3 - H3K9me$_0$S10p peptide with cofactors (500 μM SAM, 0.1 mM Mg^{2+}) and deactivated 0.25 μM G9a; trace 4 - H3K9me$_2$S10p spiked into reaction of H3K9me$_0$S10p peptide with cofactors (500 μM SAM, 0.1 mM Mg^{2+}) and deactivated 0.25 μM G9a

After choosing the optimal host type, we tested the effect of buffer composition on the separation capability of CX6 (Figure 3.6c,d). Tris and phosphate buffers were chosen since pH 7.4 is within their buffering ranges. H3 and H3K9me$_2$ were separated by CX6 in Tris buffer, however, the peptide migration shifts were less than those in phosphate buffer. CX6 may behave differently in Tris buffer, which contains an amine group akin to the side chain in lysine. For both the H3K9me$_{0,2}$ and H3K9me$_{0,2}$S10p pairs, the resolution, calculated with Equation 3.2 was higher in phosphate buffer than in Tris buffer (Table 3.4). For calculating the resolution when isomer peaks were involved, the later migrating isomer peak of the first peptide and the earlier migrating isomer peak of the second peptide were used.

3.3.4 Lysine Methylation Comparison Assay of Non-modified and Modified Peptides

In order to improve the resolution between multiple peptides in the G9a methylation assay, we used a higher concentration of CX6 (i.e., 2 μM) (Figure 3.8). We injected several controls, including a deactivated G9a reaction with spiked dimethylated product, to determine the migration order (Figures 3.9 and 3.10). Minimal influence from the cofactors and the deactivated enzyme to the migration and separation of the methylated and unmethylated peptides was observed. When the real enzyme traction mixture was analyzed, both the mono- and di-methylated peptide peak showed up at the reaction time of 30 min.

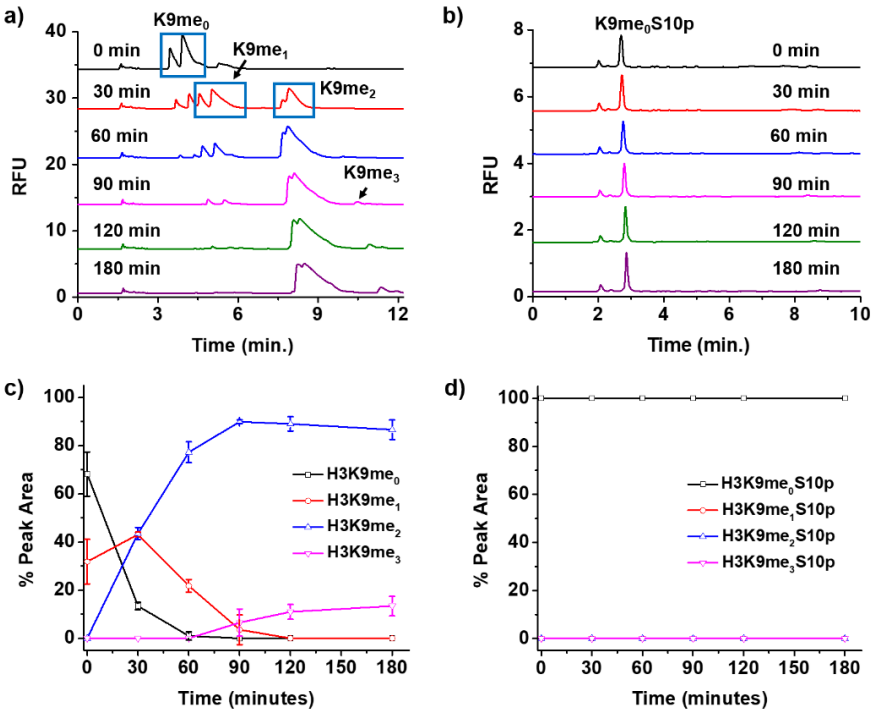

Figure 3.11 (a) Separation of the H3K9me$_0$ substrate and products, H3K9me$_{1\text{-}3}$, during a G9a methyltransferase reaction over time. (b) Progression of the G9a reaction with H3K9me$_0$S10p as a substrate over time. (c) Percent peak area (H3K9me$_x$; x=0,1,2,3; peak area over the total peak area) versus time using electropherogram data. (d) % peak area (H3K9me$_x$S10p; x=0,1,2,3; peak area over the total peak area) versus time using electropherogram data. Reaction conditions: [peptide] = 10 μM, [G9a] = 0.25 μM, [SAM] = 500 μM, [Mg^{2+}] = 0.1 mM in 20 mM tris pH 9.0 at room temperature.

As shown in Figure 3.11a, most of the peptide became dimethylated. There is a pair of peaks that starts to appear at the 90-minute mark, and this matches the MALDI peak at 1648 m/z (Figure 3.12a), which is the mass of the trimethylated peptide. G9a predominantly mono- and demethylates lysine 9;[33] however, it can trimethylate lysine 9 at a slower rate after the substrate and intermediary are exhausted[34,35] and if left overnight.[36]

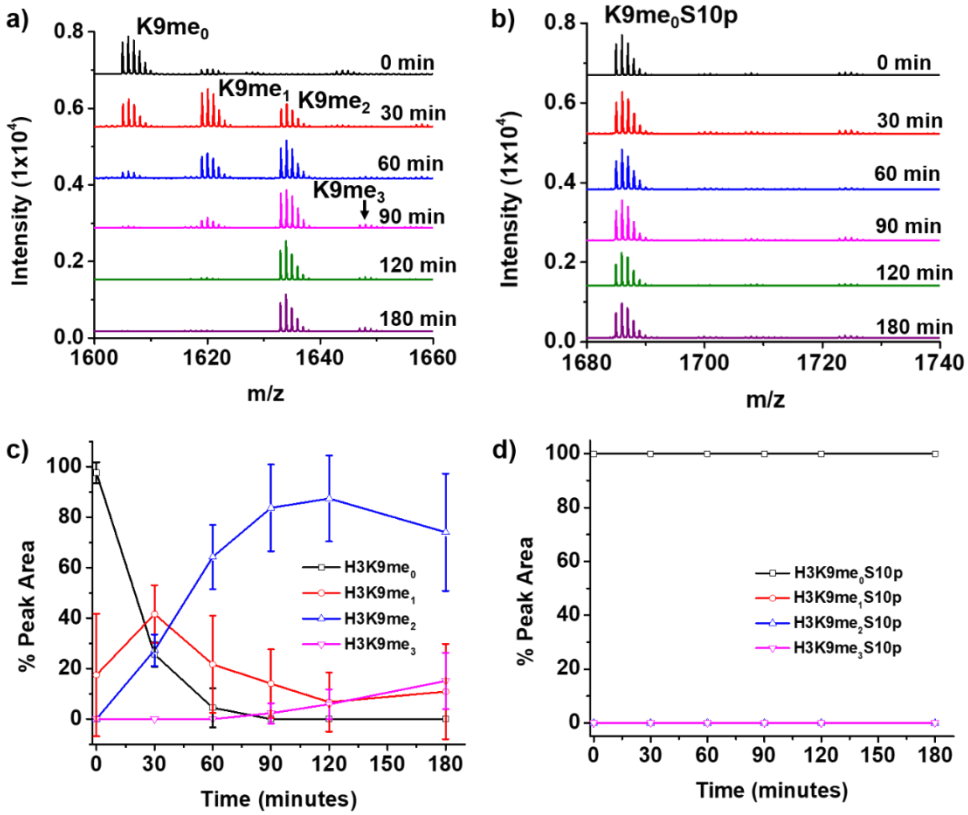

Figure 3.12 (a) MALDI-TOF/TOF spectra with H3K9me$_0$ substrate and products of H3K9me$_{1\text{-}3}$ during a G9a methyltransferase reaction over time. (b) MALDI-TOF/TOF spectra for progression of G9a methyltransferase reaction with H3K9me$_0$S10p as a substrate over time. (c) % peak area (H3K9me$_x$; x=0,1,2,3; peptide peak over the total peak area) versus time using MALDI-TOF/TOF data. (d) % peak area (H3K9me$_x$S10p; x=0,1,2,3; peptide peak over the total peak area) versus time using MALDI-TOF/TOF data. Reaction conditions: [peptide] = 10 μM, [G9a] = 0.25 μM, [SAM] = 500 μM, [Mg^{2+}] = 0.1 mM in 20 mM tris pH 9.0 at room temperature.

Remarkably, there was no product peak even after three hours (Figures 3.11b and 3.12b) when incubating G9a with the substrate, H3K9me$_0$S10p. Adjacent to lysine 9, phosphorylated serine 10 blocked G9a activity, which matches previous literature reports.[20–22] From the CE and MALDI data, we plotted the percent peak area, which is the H3K9me$_x$ peak area over the total peak area, against the reaction time (Figures 3.11c and 3.12c). The percentages between the two methods are similar except that the MALDI results have higher standard deviations compared to the CE results. While MALDI can have a quick turnaround time and high-throughput capabilities, it can suffer interference from salts and contaminants, resulting in crystallization variations on the MALDI plate;[37] therefore, quantitation requires the use of internal standards. Although CE requires fluorescent labeling of samples to produce low detection limits, it has several advantages: in situ monitoring (i.e., no quenching treatment of the reaction), low sample input volume in nanoliters, and reliable quantitation. The initial unmethylated substrate was converted within an hour and the H3K9me$_1$ intermediate was only present in smaller percentages compared to H3K9me$_2$, denoting that the dominant reaction was dimethylation. On the other hand, the phosphorylated peptide showed no difference in peak area over time (Figures 3.11d and 3.12d). Possible explanations for the inhibitory effect of the phosphate group could be its steric hindrance or repulsion that affects the conformation of the residues.

3.3.5 Phosphorylation Comparison Assay of Non-modified and Modified Peptides and Inhibition Assay

We then investigated an opposite situation in which lysine methylation can affect kinase activity. Monitoring the reaction by CE still required CX6 in the background electrolyte so that the peptides could be resolved (Figure 3.13). Controls for identifying the peaks confirmed the migration order of the product and substrate (Figures 3.14 and 3.15). Both H3 and H3K9me$_2$ were well phosphorylated (Figures 3.16), and there was a 25% difference in kinase activity between the two reactions at the 4-hour mark (Figure 3.17a). Again, the MALDI results do not represent the same trend, which can be caused by crystallization growth effects on signal intensities as mentioned earlier (Figure 3.18).

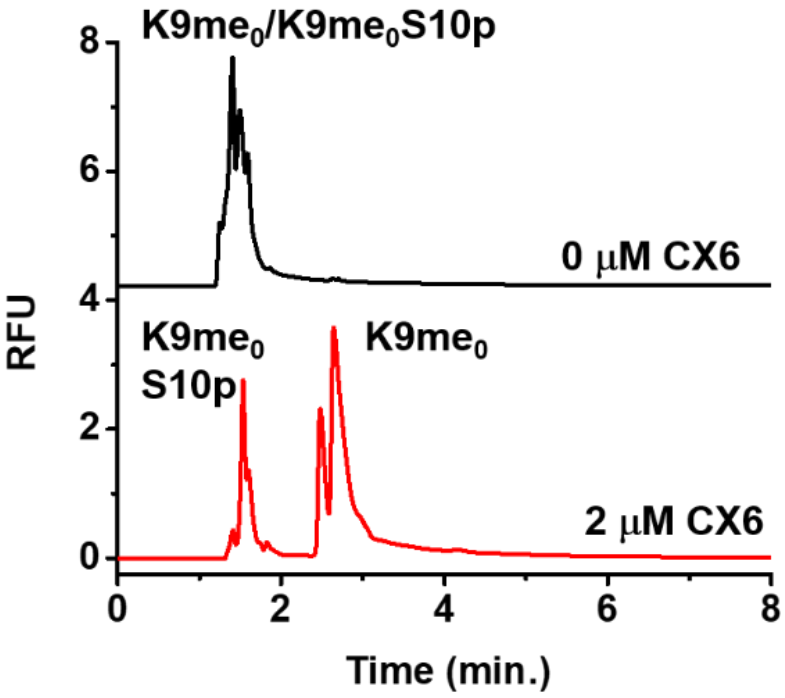

Figure 3.13 Comparison of H3K9me$_0$ and H3K9me$_0$S10p separation in 0 μM and 2 μM CX6.

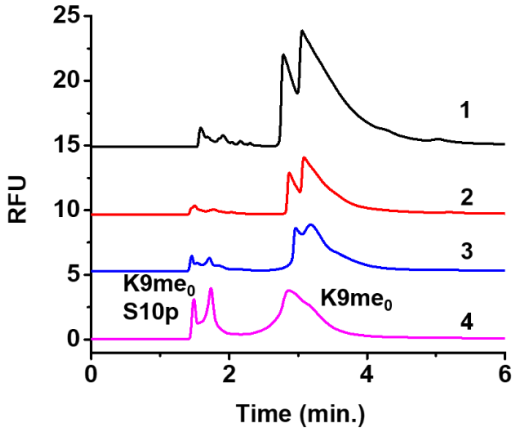

Figure 3.14 Controls for Aurora B kinase reaction with H3K9me$_0$. Trace 1 – 10 μM H3K9me$_0$ peptide; trace 2 – 10 μM H3K9me$_0$ peptide with cofactors (20 μM ATP, 0.1 mM Mg^{2+}); trace 3 - 10 μM H3K9me$_0$ peptide with cofactors (20 μM ATP, 0.1 mM Mg^{2+}) and 0.005 μg/μL deactivated Aurora B kinase; trace 4 - H3K9me$_0$S10p spiked into reaction of 10 μM H3K9me$_0$ peptide with cofactors (20 μM ATP, 0.1 mM Mg^{2+}) and 0.005 μg/μL deactivated Aurora B kinase.

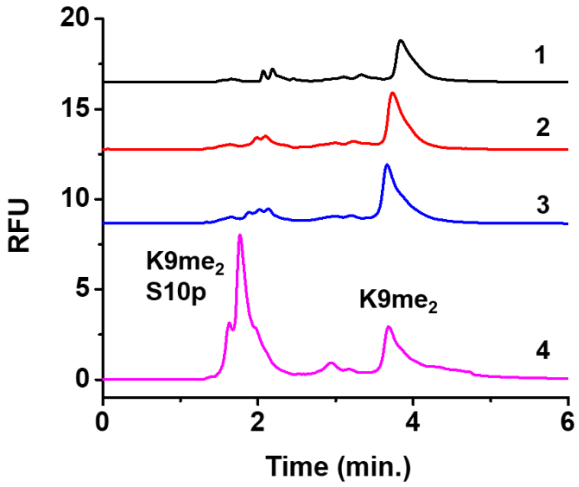

Figure 3.15 Controls for Aurora B kinase reaction with H3K9me$_2$. Trace 1 – 10 μM H3K9me$_2$ peptide; trace 2 – 10 μM H3K9me$_2$ peptide with cofactors (20 μM ATP, 0.1 mM Mg^{2+}); trace 3 - 10 μM H3K9me$_2$ peptide with cofactors (20 μM ATP, 0.1 mM Mg^{2+}) and 0.005 μg/μL deactivated Aurora B kinase; trace 4 - H3K9me$_2$S10p spiked into reaction of 10 μM H3K9me$_2$ peptide with cofactors (20 μM ATP, 0.1 mM Mg^{2+}) and 0.005 μg/μL deactivated Aurora B kinase.

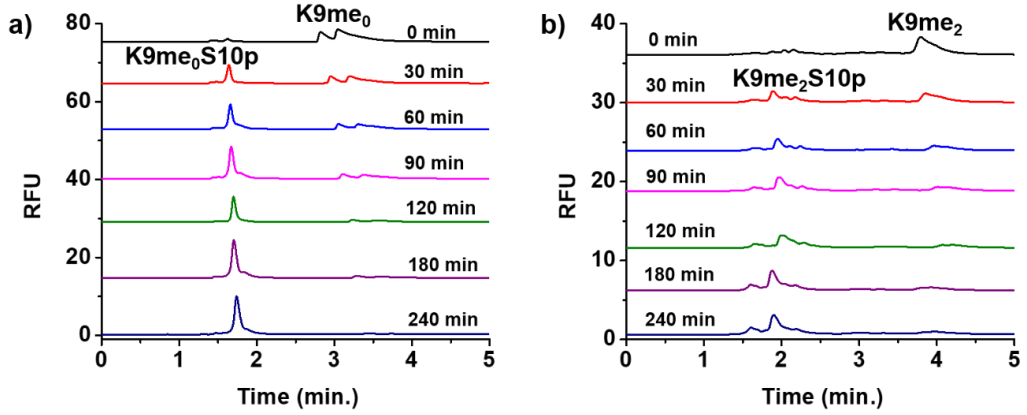

Figure 3.16 (a) Separation of H3K9me$_0$ substrate and H3K9me$_0$S10p product during an Aurora B kinase reaction over time. (b) Separation of H3K9me$_2$ substrate and H3K9me$_2$S10p product during an Aurora B kinase reaction over time. Reaction conditions: [peptide] = 10 µM, [ATP] = 20 µM, [Mg^{2+}] = 0.1 mM, [Aurora B] = 0.005 µg/µL in 20 mM tris pH 7.4 at room temperature.

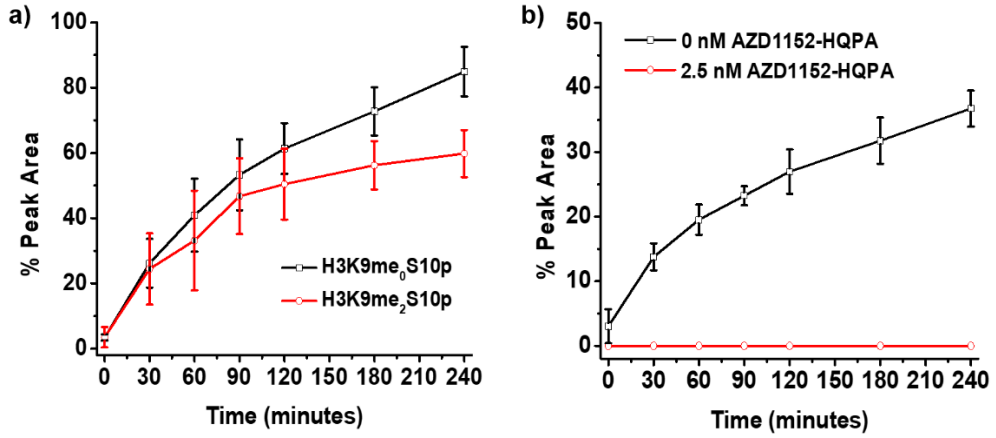

Figure 3.17 (a) % peak area (H3K9me$_x$S10p, x=0,2 peak area over the total peak area) versus time using electropherogram data from the Aurora B kinase reaction. (b) % peak area (H3K9me$_0$S10p peak area over the total peak area) versus time in the presence and absence of the AZD1152-HQPA inhibitor during an Aurora B kinase reaction. Reaction conditions: [peptide] = 10 µM, [ATP] = 20 µM, [Mg^{2+}] = 0.1 mM, [Aurora B] = 0.005 µg/µL (a) or 0.01 µg/µL (b), [AZD1152-HQPA] = 0 or 2.5 nM in 20 mM tris pH 7.4 at room temperature.

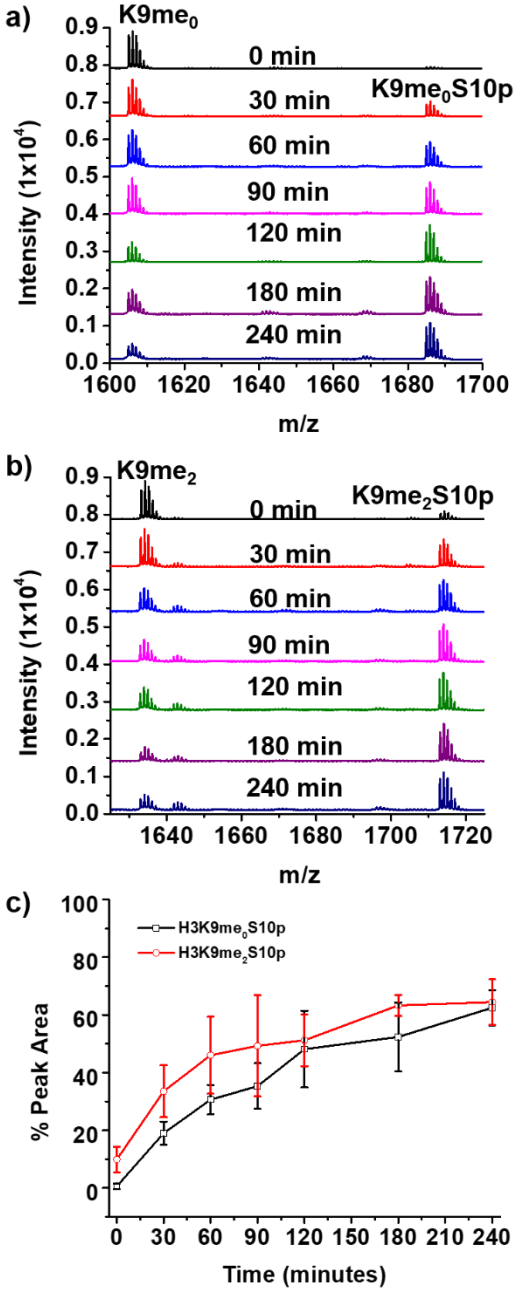

Figure 3.18 (a) MALDI-TOF/TOF spectra with H3K9me$_0$ substrate and H3K9me$_0$S10p product during an Aurora B kinase reaction over time. (b) MALDI-TOF/TOF spectra with H3K9me$_2$ substrate and H3K9me$_2$S10p product during an Aurora B kinase reaction over time. (c) % peak area (H3K9me$_x$S10p; x=0,2; peptide peak over the total peak area) versus time using MALDI data. Reaction conditions: [peptide] = 10 μM, [ATP] = 20 μM, [Mg^{2+}] = 0.1 mM, [Aurora B] = 0.005 μg/μL in 20 mM tris pH 7.4 at room temperature.

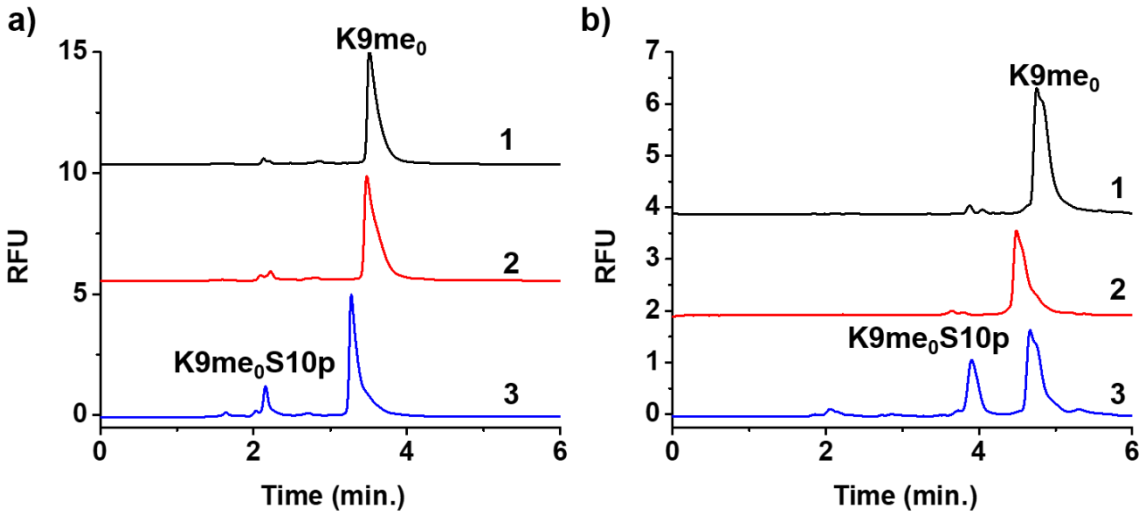

Figure 3.19 Controls for Aurora B kinase reaction for H3K9me$_0$ peptide with (a) 0 or (b) 2.5 nM of AZD1152-HQPA inhibitor. Trace 1 – 10 μM H3K9me$_0$ peptide with cofactors (20 μM ATP, 0.1 mM Mg^{2+}); trace 2 - 10 μM H3K9me$_2$ peptide with cofactors (20 μM ATP, 0.1 mM Mg^{2+}) and 0.01 μg/μL deactivated Aurora B kinase; trace 3- H3K9me$_0$S10p peptide spiked into reaction of 10 μM H3K9me$_2$ peptide with cofactors (20 μM ATP, 0.1 mM Mg^{2+}) and 0.01 μg/μL deactivated Aurora B kinase

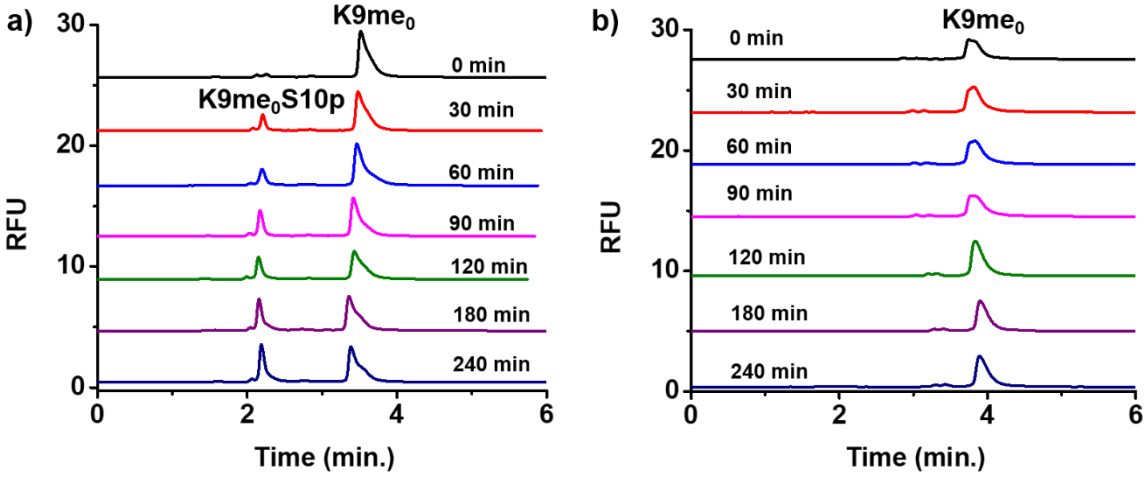

Figure 3.20 (a) Separation of H3K9me$_0$ substrate and H3K9me$_0$S10p product after Aurora B kinase reaction over time with 0 nM AZD1152-HQPA inhibitor. (b) Progression of Aurora B kinase reaction with H3K9me$_0$ and 2.5 nM AZD1152-HQPA. Reaction conditions: [peptide] = 10 μM, [ATP] = 20 μM, [Mg^{2+}] = 0.1 mM, [Aurora B kinase] = 0.1 μg/μL in 20 mM tris pH 7.4 at room temperature.

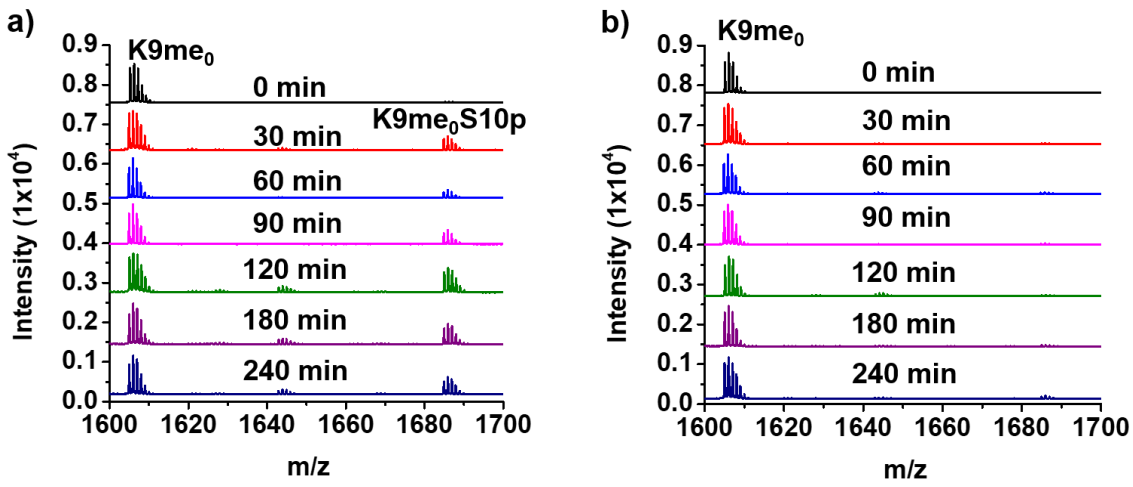

Figure 3.21 (a) MALDI-TOF/TOF spectra with H3K9me$_0$ substrate and H3K9me$_0$S10p product during an Aurora B kinase reaction over time with 0 nM AZD1152-HQPA. (b) MALDI-TOF/TOF spectra with H3K9me$_0$ substrate during an Aurora B kinase reaction over time with 2.5 nM AZD1152-HQPA. Reaction conditions: [peptide] = 10 μM, [ATP] = 20 μM, [Mg^{2+}] = 0.1 mM, [Aurora B kinase] = 0.1 μg/μL, [AZD1152-HQPA] = 0 or 2.5 nM in 20 mM tris pH 7.4 at room temperature

After analysis of an antagonistic effect, we observed another event of enzyme activity interference. Targeting the active ATP-binding pocket in Aurora B kinase,[38] AZD1152-HQPA is a selective inhibitor[39,40] with a K_i of 0.36 nmol/L.[40] We confirmed the migration order of the peptides to accurately identify the peaks in the enzymatic assay (Figure 3.19). While the phosphorylation reaction progressed without inhibitor, there was no formation of the product in the inhibitor reaction (Figures 3.17b, 3.20, and 3.21).

3.3.6 Enzyme Crosstalk Study with a Mixture of Substrates

After successfully monitoring enzyme reactions with one substrate, we proceeded to examine each enzyme reaction in more competitive environments. We conducted the G9a methyltransferase reaction with a mixture of the unphosphorylated (H3K9me$_0$) and

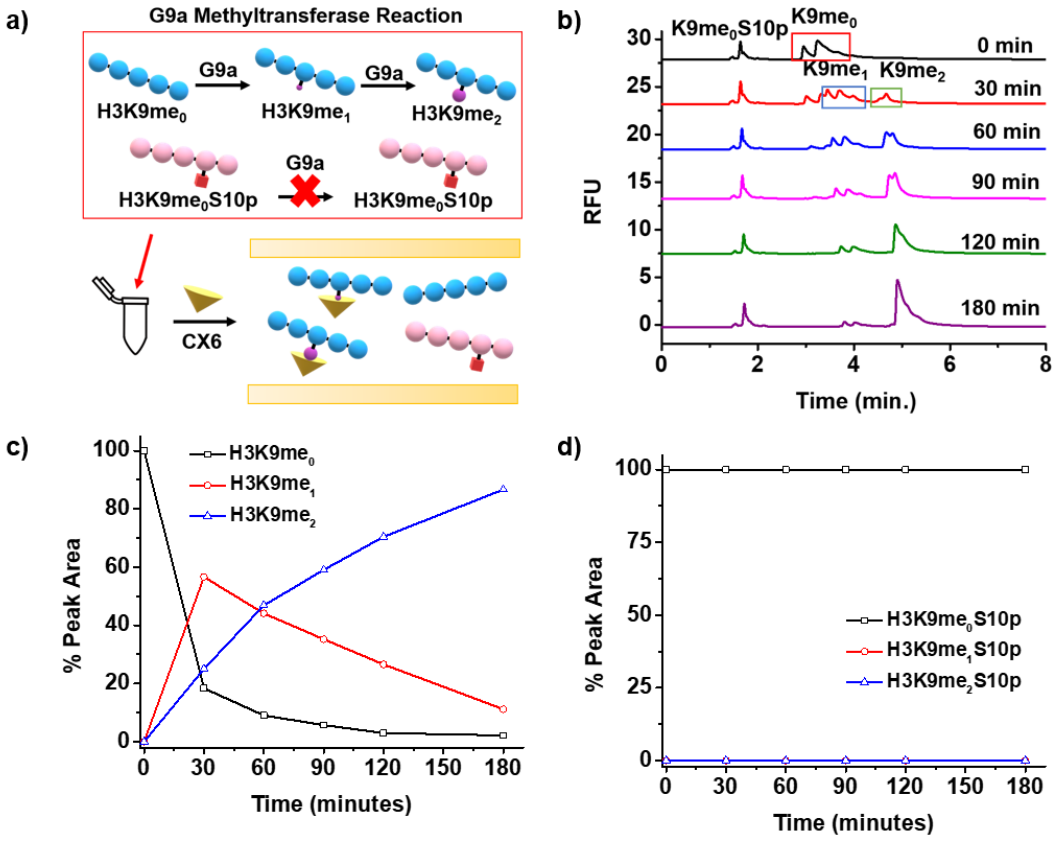

Figure 3.22 (a) Schematic for the separation of unphosphorylated and phosphorylated peptides as well as their products during a G9a methyltransferase reaction over time. (b) Separation of H3K9me$_0$ and H3K9me$_0$S10p substrates and their products during a G9a reaction over time. (c) % peak area (H3K9me$_x$; x=0,1,2; peak area over the total peak area) versus time for the G9a substrate mixture reaction. (d) % peak area (H3K9me$_x$S10p; x=0,1,2; peak area over the total peak area) versus time for the G9a substrate mixture reaction. Reaction conditions: [H3K9me$_0$] = 10 μM, [H3K9me$_0$S10p] = 30 μM, [G9a] = 0.25 μM, [SAM] = 500 μM, [Mg^{2+}] = 0.1 mM in 20 mM tris pH 9.0 at room temperature.

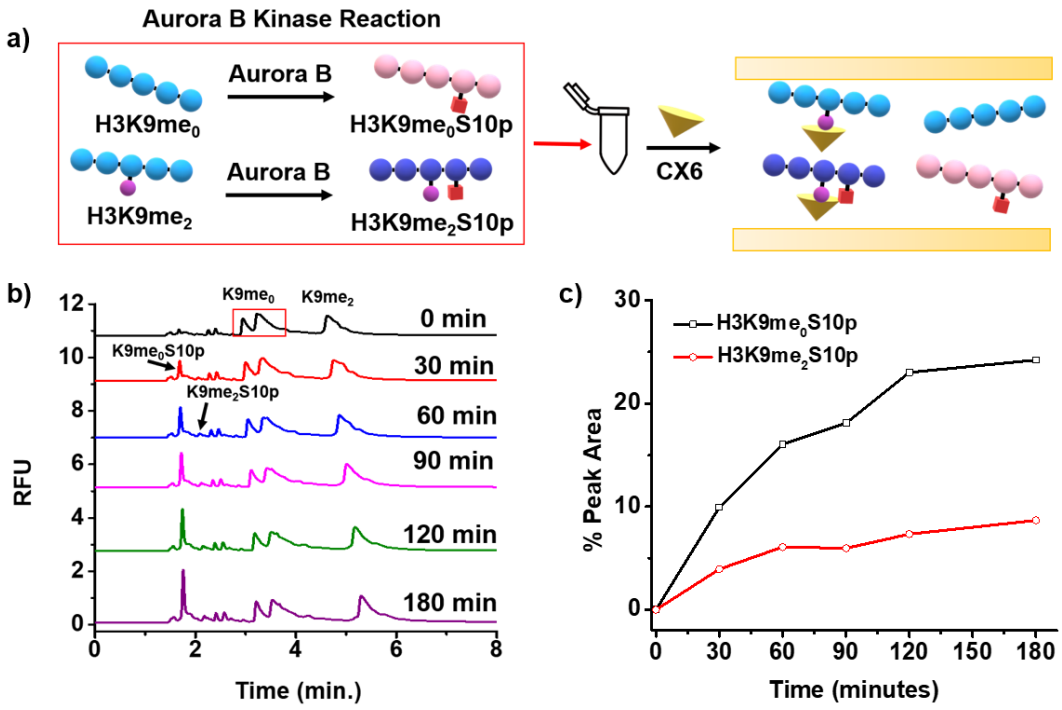

Figure 3.23 (a) Schematic for the separation of unmethylated and methylated peptides as well as their products during an Aurora B kinase reaction over time. (b) Separation of $H3K9me_0$ and $H3K9me_2$ substrates and their products during an Aurora B reaction over time. (c) % peak area ($H3K9me_xS10p$; x=0,2; peak over the total peak area) versus time for the Aurora B kinase substrate mixture reaction. Reaction conditions: [peptide] = 10 µM, [ATP] = 20 µM, [Mg^{2+}] = 0.1 mM, [Aurora B] = 0.005 µg/µL in 20 mM tris pH 7.4 at room temperature

phosphorylated ($H3K9me_0S10p$) histone peptides (Figure 3.22). As expected, the modified histone peptide was not methylated as the peak area of the phosphorylated peptide did not change. On the other hand, the reaction for the unmodified histone peptide proceeded. In addition, we subjected a mixture of unmethylated and dimethylated histone peptides to phosphorylation by Aurora B (Figure 3.23). There was a 15% peak area ratio difference between the two reactions, which is less than that of the independent reactions; this can be explained by the expected degradation of the enzyme over time in storage. Still, we

observed a difference in enzyme activity when both substrates are present. Both the high resolution of CE and the selectivity of the synthetic receptor made it possible to simultaneously observe PTM enzyme reactions of a substrate mixture.

3.4 Conclusions

In this chapter, we were able to monitor the activity of different enzyme reactions using our method of host-assisted capillary electrophoresis. The combination of receptor selectivity and separation by CE enhances the technique's efficacy in an enzymatic assay. The use of a permanent coating (LPA) on the inner capillary wall can improve the efficiency of separating multiply charged positive peptides. After optimization of the method, we were able to apply it to monitoring reactions of different enzymes such as G9a methyltransferase and Aurora B kinase. We analyzed the activities of G9a and Aurora B kinase with individual substrates or competitive substrate mixtures (i.e., unmodified and modified peptide pairs) to observe enzyme activity differences in the presence of an antagonistic PTM. Host-assisted CE introduces several advantages of simultaneous monitoring of the substrate, intermediates, and product as well as in situ analysis that doesn't necessitate quenching of the reaction. The assay has shown to be effective for the study of other potential antagonistic PTM pairs as well as synergistic ones in a cell lysate—a more complex, biological environment.

3.5 References

(1) Fischle, W.; Wang, Y.; Allis, C. D. Histone and Chromatin Cross-Talk. *Curr. Opin. Cell Biol.* **2003**, 172–183.

(2) Vlaming, H.; Welsem, T.; Graaf, E. L.; Ontoso, D.; Altelaar, A. M.; San-Segundo, P. A.; Heck, A. J.; Leeuwen, F. Flexibility in Crosstalk between H2B Ubiquitination and H3 Methylation in Vivo . *EMBO Rep.* **2014**, *15* (11), 1220–1221.

(3) Altaf, M.; Utley, R. T.; Lacoste, N.; Tan, S.; Briggs, S. D.; Côté, J. Interplay of Chromatin Modifiers on a Short Basic Patch of Histone H4 Tail Defines the Boundary of Telomeric Heterochromatin. *Mol. Cell* **2007**, *28* (6), 1002–1014.

(4) Zhang, Y. Y.; Mei, Z. Q.; Wu, J. W.; Wang, Z. X. Enzymatic Activity and Substrate Specificity of Mitogen-Activated Protein Kinase P38α in Different Phosphorylation States. *J. Biol. Chem.* **2008**, *283* (39), 26591–26601.

(5) Kim, Y.; Tanner, K. G.; Denu, J. M. A Continuous, Nonradioactive Assay for Histone Acetyltransferases. *Anal. Biochem.* **2000**, *280* (2), 308–314.

(6) Gowher, H.; Zhang, X.; Cheng, X.; Jeltsch, A. Avidin Plate Assay System for Enzymatic Characterization of a Histone Lysine Methyltransferase. *Anal. Biochem.* **2005**, *342* (2), 287–291.

(7) Cheung, P.; Tanner, K. G.; Cheung, W. L.; Sassone-corsi, P.; Denu, J. M.; Allis, C. D. Synergistic Coupling of Histone H3 Phosphorylation and Acetylation in Response to Epidermal Growth Factor Stimulation. **2000**, *5*, 905–915.

(8) Horiuchi, K. Y.; Eason, M. M.; Ferry, J. J.; Planck, J. L.; Walsh, C. P.; Smith, R. F.; Howitz, K. T.; Ma, H. Assay Development for Histone Methyltransferases. *Assay Drug Dev. Technol.* **2013**, *11* (4), 227–236.

(9) Scriba, G. K. E.; Belal, F. Advances in Capillary Electrophoresis-Based Enzyme Assays. *Chromatographia* **2015**, *78* (15–16), 947–970.

(10) Dawson, J. F.; Boland, M. P.; Holmes, C. F. B. A Capillary Electrophoresis-Based Assay for Protein Kinases and Protein Phosphatases Using Peptide Substrates. *Anal. Biochem.* 1994, pp 340–345.

(11) Lee, K. J.; Mwongela, S. M.; Kottegoda, S.; Borland, L.; Nelson, A. R.; Sims, C. E.; Allbritton, N. L. Determination of Sphingosine Kinase Activity for Cellular Signaling Studies. *Anal. Chem.* **2008**, *80* (5), 1620–1627.

(12) Lee, J.; Perez, L.; Liu, Y.; Wang, H.; Hooley, R. J.; Zhong, W. Separation of Methylated Histone Peptides via Host-Assisted Capillary Electrophoresis. *Anal. Chem.* **2018**, *90* (3), 1881–1888.

(13) Beshara, C. S.; Jones, C. E.; Daze, K. D.; Lilgert, B. J.; Hof, F. A Simple Calixarene Recognizes Post-Translationally Methylated Lysine. *ChemBioChem* **2010**, *11* (1), 63–66.

(14) Garnett, G. A. E.; Starke, M. J.; Shaurya, A.; Li, J.; Hof, F. Supramolecular Affinity Chromatography for Methylation-Targeted Proteomics. *Anal. Chem.* **2016**, *88* (7), 3697–3703.

(15) Gamal-Eldin, M. A.; MacArtney, D. H. Selective Molecular Recognition of Methylated Lysines and Arginines by Cucurbit[6]Uril and Cucurbit[7]Uril in Aqueous Solution. *Org. Biomol. Chem.* **2013**, *11* (3), 488–495.

(16) Liu, Y.; Perez, L.; Mettry, M.; Easley, C. J.; Hooley, R. J.; Zhong, W. Self-Aggregating Deep Cavitand Acts as a Fluorescence Displacement Sensor for Lysine Methylation. *J. Am. Chem. Soc.* **2016**, *138* (34), 10746–10749.

(17) Liu, Y.; Perez, L.; Gill, A. D.; Mettry, M.; Li, L.; Wang, Y.; Hooley, R. J.; Zhong, W. Site-Selective Sensing of Histone Methylation Enzyme Activity via an Arrayed Supramolecular Tandem Assay. *J. Am. Chem. Soc.* **2017**, *139* (32), 10964–10967.

(18) Liu, Y.; Lee, J.; Perez, L.; Gill, A. D.; Hooley, R. J.; Zhong, W. Selective Sensing of Phosphorylated Peptides and Monitoring Kinase and Phosphatase Activity with a Supramolecular Tandem Assay. *J. Am. Chem. Soc.* **2018**, *140* (42), 13869–13877.

(19) Rea, S.; Eisenhaber, F.; O'Carroll, D.; Strahl, B. D.; Sun, Z.-W.; Schmid, M.; Opravil, S.; Mechtler, K.; Ponting, C. P.; Allis, C. D.; et al. Regulation of Chromatin Structure by Site-Specific Histone H3 Methyltransferases. *Nature* **2000**, No. x, 593–599.

(20) Duan, Q.; Chen, H.; Costa, M.; Dai, W. Phosphorylation of H3S10 Blocks the Access of H3K9 by Specific Antibodies and Histone Methyltransferase IMPLICATION IN REGULATING CHROMATIN DYNAMICS AND EPIGENETIC INHERITANCE. *J. Biol. Chem.* **2008**, *283* (48), 33585–33590.

(21) Rathert, P.; Dhayalan, A.; Murakami, M.; Zhang, X.; Tamas, R.; Jurkowska, R.; Komatsu, Y.; Shinkai, Y.; Cheng, X.; Jeltsch, A. Protein Lysine Methyltransferase G9a Acts on Non-Histone Targets. *Nat. Chem. Biol.* **2008**, *4* (6), 344–346.

(22) Chin, H. G.; Pradhan, M.; Estève, P. O.; Patnaik, D.; Evans, T. C.; Pradhan, S. Sequence Specificity and Role of Proximal Amino Acids of the Histone H3 Tail on Catalysis of Murine G9a Lysine 9 Histone H3 Methyltransferase. *Biochemistry* **2005**, *44* (39), 12998–13006.

(23) Zhu, G.; Sun, L.; Dovichi, N. J. Thermally-Initiated Free Radical Polymerization for Reproducible Production of Stable Linear Polyacrylamide Coated Capillaries, and Their Application to Proteomic Analysis Using Capillary Zone Electrophoresis-Mass Spectrometry. *Talanta* **2017**, *263* (2), 219–227.

(24) Tachibana, M.; Sugimoto, K.; Nozaki, M.; Ueda, J.; Ohta, T.; Ohki, M.; Fukuda, M.; Takeda, N.; Niida, H.; Kato, H.; et al. G9a Histone Methyltransferase Plays a Dominant Role in Euchromatic Histone H3 Lysine 9 Methylation and Is Essential for Early Embryogenesis. **2002**, *3*, 1779–1791.

(25) Casciello, F.; Windloch, K.; Gannon, F.; Lee, J. S. Functional Role of G9a Histone Methyltransferase in Cancer. *Front. Immunol.* **2015**, *6* (SEP), 3–9.

(26) Fontecave, M.; Atta, M.; Mulliez, E. S -Adenosylmethionine : Nothing Goes to Waste. *Trends Biochem. Sci.* **2004**, *29* (5), 1–7.

(27) Shannon, K. B.; Salmon, E. D. Chromosome Dynamics: New Light on Aurora B Kinase Function. *Curr. Biol.* **2002**, *12* (13), 458–460.

(28) Sugiyama, K.; Sugiura, K.; Hara, T.; Sugimoto, K.; Shima, H.; Honda, K.; Furukawa, K.; Yamashita, S.; Urano, T. Aurora-B Associated Protein Phosphatases as Negative Regulators of Kinase Activation. *Oncogene* **2002**, *21* (20), 3103–3111.

(29) Muñoz-Barrera, M.; Monje-Casas, F. Increased Aurora B Activity Causes Continuous Disruption of Kinetochore-Microtubule Attachments and Spindle Instability. *Proc. Natl. Acad. Sci. U. S. A.* **2014**, *111* (38), E3996–E4005.

(30) Beneito-Cambra, M.; Anres, P.; Vial, J.; Gareil, P.; Delaunay, N. Stability and Effectiveness of Linear Polyacrylamide Capillary Coating to Suppress EOF in Acidic Media in the Presence of Surfactants, Ionic Liquids and Organic Modifiers. *Talanta* **2016**, *150*, 546–552.

(31) Isaacs, L. Stimuli Responsive Systems Constructed Using Cucurbit[n]Uril-Type Molecular Containers. *Acc. Chem. Res.* **2014**, *47* (7), 2052–2062.

(32) Perret, F.; Lazar, A. N.; Coleman, A. W. Biochemistry of the Para-Sulfonato-Calix[n]Arenes. *Chem. Commun.* **2006**, No. 23, 2425–2438.

(33) Tachibana, M.; Sugimoto, K.; Fukushima, T.; Shinkai, Y. SET Domain-Containing Protein, G9a, Is a Novel Lysine-Preferring Mammalian Histone Methyltransferase with Hyperactivity and Specific Selectivity to Lysines 9 and 27 of Histone H3. *J. Biol. Chem.* **2001**, *276* (27), 25309–25317.

(34) Osipovich, O.; Milley, R.; Meade, A.; Tachibana, M.; Shinkai, Y.; Krangel, M. S.; Oltz, E. M. Targeted Inhibition of V (D) J Recombination by a Histone Methyltransferase. *Nat. Immunol.* **2004**, *5* (3), 309–316.

(35) Collins, R. E.; Tachibana, M.; Tamaru, H.; Smith, K. M.; Jia, D.; Zhang, X.; Selker, E. U.; Shinkai, Y.; Cheng, X. In Vitro and in Vivo Analyses of a Phe/Tyr Switch Controlling Product Specificity of Histone Lysine Methyltransferases. *J. Biol. Chem.* **2005**, *280* (7), 5563–5570.

(36) Patnaik, D.; Hang, G. C.; Estève, P. O.; Benner, J.; Jacobsen, S. E.; Pradhan, S. Substrate Specificity and Kinetic Mechanism of Mammalian G9a Histone H3 Methyltransferase. *J. Biol. Chem.* **2004**, *279* (51), 53248–53258.

(37) Cohen, S. L.; Chait, B. T. Influence of Matrix Solution Conditions on the MALDI-MS Analysis of Peptides and Proteins. *Anal. Chem.* **1996**, *68* (1), 31–37.

(38) Sessa, F.; Villa, F. Structure of Aurora B-INCENP in Complex with Barasertib Reveals a Potential Transinhibitory Mechanism. *Acta Crystallogr. F Struct. Biol. Commun.* **2014**, *70* (3), 294–298.

(39) Tang, A.; Gao, K.; Chu, L.; Zhang, R.; Yang, J.; Zheng, J. Aurora Kinases : Novel Therapy Targets in Cancers. *Oncotarget* **2017**, *8* (14), 23937–23954.

(40) Wilkinson, R. W.; Odedra, R.; Heaton, S. P.; Wedge, S. R.; Keen, N. J.; Crafter, C.; Foster, J. R.; Brady, M. C.; Bigley, A.; Brown, E.; et al. Cancer Therapy : Preclinical AZD1152 , a Selective Inhibitor of Aurora B Kinase , Inhibits Human Umor Xenograft Growth by Inducing Apoptosis. *Clin. Cancer Res.* **2007**, *13* (12), 3682–3689.

Chapter 4: Investigation of Interactions with Deep Cavitands in Capillary Electrophoresis

4.1 Introduction

Water soluble deep cavitands have been increasingly used in recent years in application such as fluorescence displacement assays[1–3] and biomimetic studies.[4–7] In comparison to the calixarene- and cucurbituril-based hosts that we have used in previous chapters, cavitands have a deeper cavity. Like calixarene hosts, their binding is based on cation-π, electrostatic, hydrogen bond, and hydrophobic interactions. Deep cavitands can interact with a variety of targets, such as small guest fluorophores,[1] metal cations,[8] surfactants,[9] peptides,[1] and proteins.[4] Besides their versatility, deep cavitands can be modified more easily than other hosts, and they are easier and cheaper to produce in the lab. With these benefits in consideration, it would be useful to investigate host-guest interactions even further.

Separation techniques allow for detection of multiple analytes simultaneously, which can help with rapid screening of different host-guest interactions and faster assessment of the utility of the synthetic receptors. Calixarene-based hosts have been used in chromatography,[10] but it does require functionalization to the column. However, capillary electrophoresis (CE) is a fast, open-channel separation technique with several benefits, such as high resolution and low reagent and sample consumption. In addition, it has been demonstrated in previous chapters that simple addition of synthetic receptors to the separation buffer of CE is possible.

Among the wide range of potential targets, peptides with post-translational modifications can be discriminated by deep cavitands. These modifications are vital to many cellular events including metabolism,[11,12] protein folding,[13] and signaling transduction.[14] As epigenetic factors, histone PTMs are important to identify and study as they have significant roles in cell function; furthermore, some PTMs are correlated with the onset of disease.[15,16] Thus, studying these modifications can contribute to diagnosis and drug discovery. Some PTMs introduce only small changes that make separation challenging. For instance, lysine can be methylated to various degrees, ranging from monomethylation to trimethylation, and this addition of a methyl group confers only a small change in hydrophobicity, pK_a, charge, and size. Even with this difficulty, cavitands have been able to differentiate between the various methylation levels. Cavitands were also proven to be sensitive to the surrounding environment on peptides; binding of synthetic receptors can depend on the adjacent amino acid residues, which makes cavitands more comprehensively selective.[2]

In the previous chapters, we discussed the use of calixarene- and cucurbituril-based synthetic receptors in capillary electrophoresis. Here, we introduce cavitands, resorcinarene-based receptors that can bind to many different types of analytes. We studied the interactions of cavitand hosts with various small guests and proteins in CE. We were able to identify potential targets, small molecules and proteins, to better understand the behavior of these synthetic receptors in CE. Specifically, we observed potential binding of cavitand to histone protein H3K9(me_3), which can be relevant in future analysis of histone variants.

4.2 Materials and Methods

4.2.1 General

Cavitands **1**[17] and **2-3**[18] as well as guests **1-4**[1,19] were synthesized according to literature procedures. 4-Tetrasulfonatocalix[4]arene, cucurbit[7]uril hydrate, *trans*-4-[4-(dimethylamino)styryl]-1-methylpyridinium iodide, cytochrome c, lysozyme, transferrin, apo-transferrin, histidine, trypsin from porcine pancreas, 3-(trimethoxysilyl)propyl methacrylate, acrylamide, and ammonium persulfate were purchased from Sigma-Aldrich (St. Louis, MO). 4-Hexasulfonatocalix[6]arene hydrate was purchased from Alfa Aesar (Tewksbury, MA). Bovine serum albumin was purchased from Research Products International (Mount Prospect, IL). Recombinant histone H3.3 and recombinant histone H3K9me3 (MLA) were purchased from Active Motif (Carlsbad, CA). All samples and separation buffers were made using ultrapure water (18 MΩ) from a Direct-Q Water Purification System (Millipore Sigma, Billerica, MA).

4.2.2 Capillary Electrophoresis

Separation of fluorescent guests and non-fluorescent proteins was performed on an Agilent 7100 CE system with a UV-visible diode-array detector. Data were obtained using ChemStation (Agilent Technologies, Santa Clara, CA). Samples were introduced with a pressure injection of 50 mbar for 5 seconds into an LPA-coated capillary (50 μm inner diameter, 365 μm outer diameter, with an effective length of 26.5 cm) unless otherwise specified. The electric field was 571 V/cm with positive polarity during separation. Separation of small fluorescent guests were performed using a Beckman Coulter ProteomeLab PA 800 (Beckman Coulter, Fullerton, CA) with a laser-induced fluorescence

detector (λ_{exc} = 488 nm, λ_{em} = 520 nm). Samples were introduced into the LPA-coated capillary (50 μm inner diameter, 365 μm outer diameter, 20 cm effective length) with a 0.5 psi injection for 5 s. Separation was driven by an electric field of 662 V/cm with positive polarity. Data were obtained with 32Karat and analyzed with OriginPro 8.6.

4.2.3 Preparation of the Linear Polyacrylamide Coating

Bare fused-silica capillaries (50 μm i.d., 365 μm o.d.) were purchased from Polymicro Technologies (Phoenix, Arizona). The inner wall of the bare fused silica capillary was coated with linear polyacrylamide based on a protocol from Zhu et al.[20] with several modifications. The mixture of polymer and initiator was degassed via vacuum pressure and then introduced to the capillary with nitrogen. The capillary was sealed and then incubated in an oven at 50 °C for 30 minutes. After flushing the unreacted reagents, the capillary was dried with nitrogen and stored at room temperature.

4.3 Results and Discussion

4.3.1 Testing the compatibility of cavitands with different capillaries

Cavitands **1**-**3** are synthetic hosts that have been investigated in this study (Figure 4.1). All three host molecules are resorcinarene-based, and they each have a hydrophobic cavity. The "feet" of cavitand can be modified to increase solubility without affecting the binding portion in the upper rim of the structure. Cavitand **1** is negatively charged when above the pK_a of carboxylate groups on the rim. Cavitand **2** has a neutral rim and positively charged imidazolyl groups on the feet. Like cavitand **2**, cavitand **3** also has a neutral rim but positively charged pyridyl groups on the feet. Cavitand can either be flat in a "kite"

shape or folded in a “vase” conformation. The latter occurs when a guest is bound to the inner cavity. Cavitands have various interactions with guest molecules including the following: electrostatic, hydrogen bond, hydrophobic, and van der Waals. Potential guests include those with lysine methylation as well as larger biomolecules with hydrophobic portions.

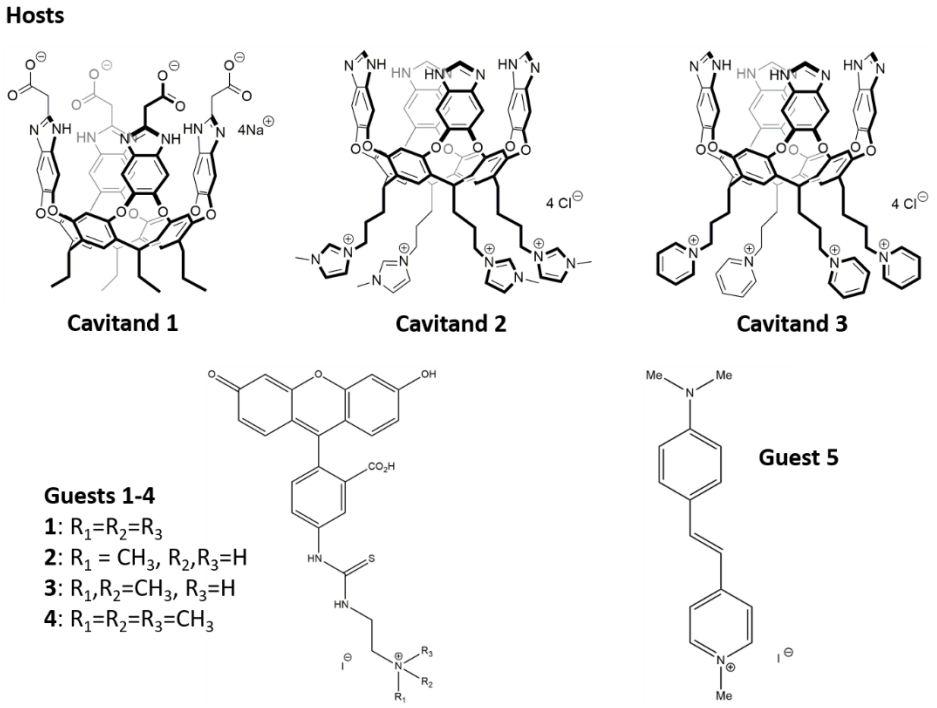

Figure 4.1 Structures of cavitands **1-3** and guest **1-5**.

Due to the possibility of cavitands interacting with the inner wall of the capillary, the use of cavitands in CE is challenging. Most often, a coating is employed in the inner wall of the capillary to reduce adsorption of samples. This is due to the ionization of weakly acidic silanol groups on the inner capillary wall in typical separation conditions (i.e., above pK_a of silanol at 4.5). A coating can either be dynamic or permanent: dynamic coatings

establishes an equilibrium at the interface of liquid-solid surface while permanent coatings are composed of irreversibly attached materials. With the use of dynamic coatings such as lipid bilayers, synthetic receptors can still adsorb to the coating material, which will affect separation efficiency by reducing the concentration of the hosts in solution. Permanent coatings avoid this issue and have improved reproducibility for long term usage. Furthermore, the need to replenish the coating material after each run is eliminated. There is still not much known about the behavior of cavitands in CE, so it is important to test individual cavitand response in this environment without the presence of guests.

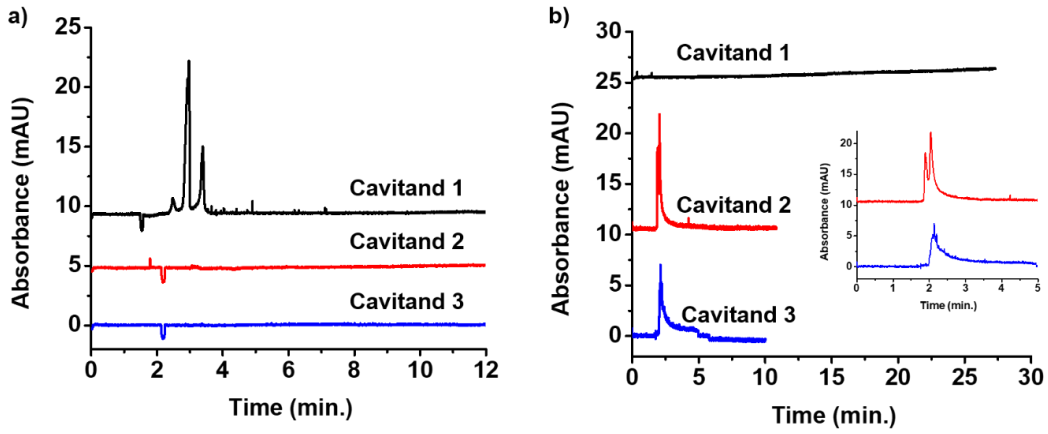

Figure 4.2 (a) Injection of cavitands **1-3** in bare fused silica capillary. [Cavitand] = 100 µM; background electrolyte: 10 mM phosphate buffer, pH 7.4; separation voltage: 15 kV. (b) Injection of cavitands 1-3 in an LPA-coated capillary. [Cavitand] = 100 µM; background electrolyte: 10 mM phosphate buffer, pH 3.0; separation voltage: 20 kV with added 5 mbar pressure.

In order to test capillary compatibility of each cavitand, cavitands **1-3** were injected into two types of capillaries: bare fused silica (BFS) and permanently coated capillaries (Figure 4.2). While the peak for cavitand **1** appeared when using a BFS capillary, there was no presence of the peaks for cavitands **2** and **3**. At pH 7.4, the capillary's inner wall has

silanol groups that are negatively charged, which can adsorb cavitands **2** and **3** that contain permanently charged cationic feet. On the other hand, cavitand **1**'s carboxyl groups repel the negative silanol groups on the wall, enabling the host to migrate to the detection window. In order to rectify the situation with the positive cavitands, we injected all the cavitands individually in a linear polyacrylamide (LPA)-coated capillary. In addition to voltage application, we also applied a pressure of 5 mbar to obtain a reasonable migration time. LPA is a neutral, hydrophilic coating, which greatly reduces or eliminates the electroosmotic flow (EOF). To no avail, cavitand **1** did not appear in the electropherogram trace. The EOF is minimized with the presence of a coating due to reduction of the zeta potential on the wall, which creates a lack of a double diffuse layer to produce a bulk flow movement of buffer. Additionally, the carboxyl groups on the rim of cavitand **1** are neutralized at pH 3.0. These two factors cause cavitand to migrate slowly, which can help increase binding. However, the pH of the running buffer can be adjusted to ionize the carboxylate groups on the rim. In contrast, the positively charged cavitands **2** and **3** were able to migrate to the detection window.

4.3.2 Investigation of Cavitand Binding with Small Fluorescent Guests

After testing the compatibility of cavitands with different surfaces in CE, we then studied the potential interactions between guests **1-5** and cavitands **1-3** (Figure 4.1). As opposed to larger biomolecules, the small guests present a simpler system to test. In particular, guests **1-4** have the same structure except for the difference in the number of methyl groups on the binding handle. The option of having them synthesized allowed tuning of the

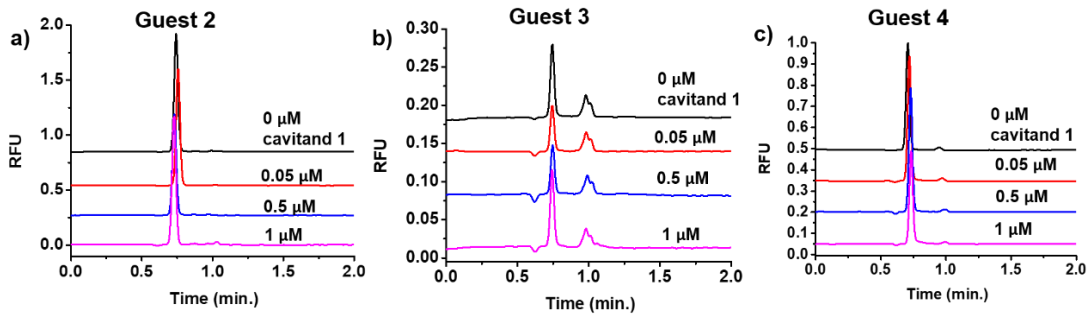

Figure 4.3 Injection of monomethylated guest **2** (a), dimethylated guest **3** (b), and trimethylated guest **4** (c) in the presence of 0-1 μM cavitand **1**. [guests **2**-**4**] = 50 nM; background electrolyte: 10 mM tris buffer, pH 7.4; separation voltage: 30 kV; bare fused silica capillary.

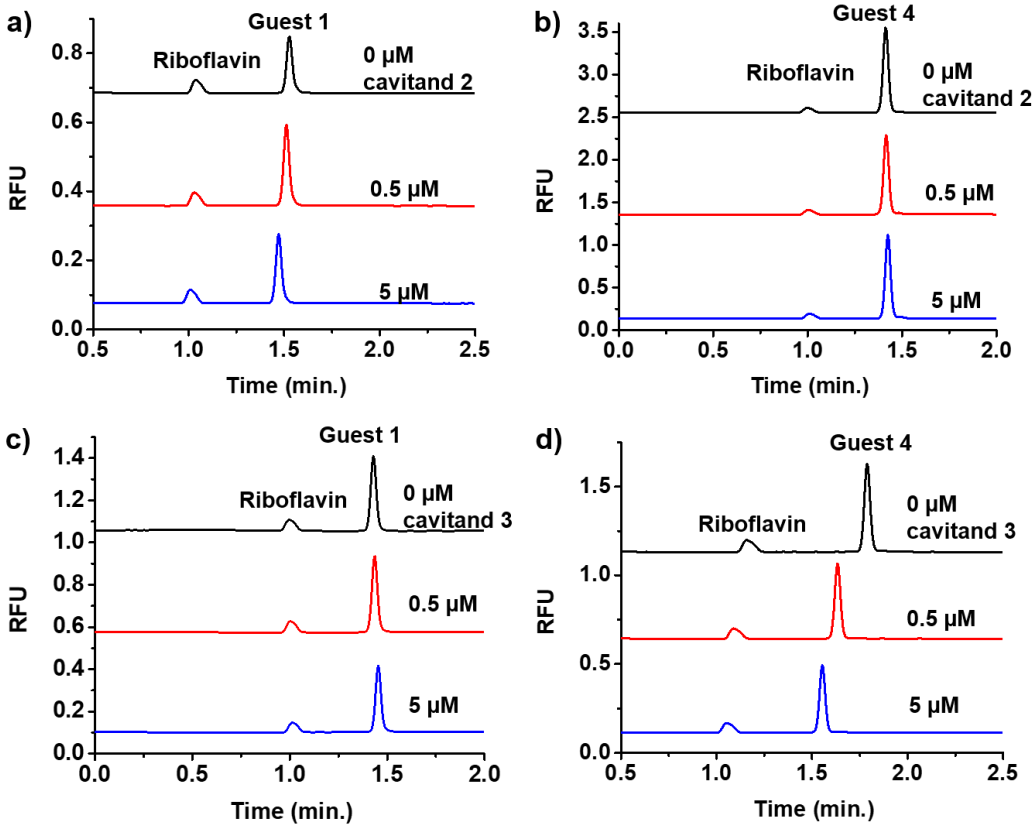

Figure 4.4 Injection of unmethylated guest **1** and trimethylated guest **4** in the presence of 0-5 μM cavitand **2** (a,b) and **3** (c,d). [guest **1**,**4**] = 50 nM; background electrolyte: 10 mM tris buffer, pH 7.4; separation voltage: 30 kV; bare fused silica capillary.

Table 4.1 Percent mobility change between guests **1** and **4** with various concentrations of cavitands **2** and **3**.

Concentration of Host (µM)	Cavitand 2	Cavitand 3
0 µM	3.7%	2.0%
0.5 µM	3.1%	1.7%
5 µM	3.0%	1.5%

fluorophore to carry multiple methylation levels, mimicking mono- to trimethylation in the lysine residue. In chapter 2, the focus was on the binding of guests **1-4** with calixarene and cucurbituril hosts; there were sufficient mobility shifts for each guest, making it possible to obtain dissociation constants for each complex. Herein, we first incorporated various concentrations of cavitand **1** in the running buffer; however, there was no variation in the migration time for guests **2-4** (Figure 4.3). In order to do a quicker screening, we compared unmethylated guest **1** and trimethylated guest **4**, which would have the highest mobility difference, to investigate potential interactions with the remaining cavitands **2** and **3** (Figure 4.4). There was variability in the guest migration time when using these positively charged cavitands in the LPA-coated capillary; thus, we included riboflavin as an internal standard in the sample to correct for the migration time. Unfortunately, there was no significant difference in the electrophoretic mobilities between guests **1** and **4** (Table 4.1). Guests **1-4** fit the amphiphilic profile in which one end is hydrophobic and the other end with the ammonium cation is hydrophilic. Cavitand will aggregate in the presence of such lipophilic guest molecules.[1,21] In this case, the concentrations of cavitand was not high

enough to induce aggregation of the synthetic hosts, which may be necessary to induce mobility shifts of the guests.

We then tried to use another small, cationic small molecule. *Trans*-4-[4-(dimethylamino)styryl]-1-methylpyridinium iodide (DSMI), referred to as guest **5** in this chapter, is a hemicyanine dye that has been used in studies with host molecules[22–24] including cavitand.[8,25–27] Due to the positively charged amine group it carries, guest **5** can bind to cavitands via cation-π interactions. We analyzed the mobility shift of guest **5** in the presence of various concentrations of cavitands **1-3**. There were some variations in the peak intensity of guest **5** that could possibly be due to guest adsorption to the capillary wall. Nonetheless, there were indications of binding when 50 µM of cavitands **1-3** were employed in separate runs (Figure 4.5). While the peak for guest **5** did not appear in the traces for 0-10 µM cavitand **1** or **3**, the absorbance of guest **5** increased at 50 µM cavitand **1** or **3**. Furthermore, there is slight peak broadening in these conditions. Without host in the background electrolyte, the peak for guest **5** is small (Figure 4.6a). With the addition of 50 µM cavitand **1** (i.e., 1:1 ratio with the guest), the peak area increases and the peak broadens.

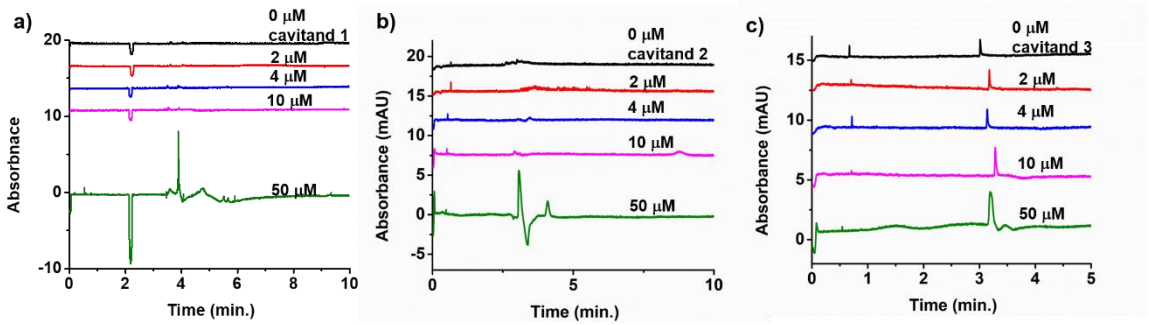

Figure 4.5 Injection of guest **5** in presence of various concentration of cavitands **1** (a), **2** (b), and **3** (c). Background electrolyte: 10 mM phosphate buffer, pH 7.4 (a) or 3.0 (b,c); separation voltage: 10 kV (a) or 15 kV (b,c); BFS capillary (a) or LPA-coated capillary (b,c).

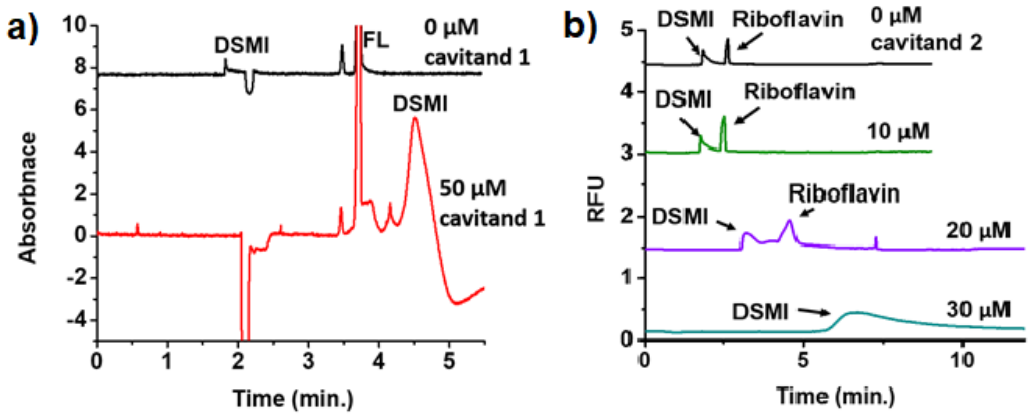

Figure 4.6 (a) Injection of guest 5 and internal standard, fluorescein, into 0 or 50 µM cavitand 1. [guest 5] = 50 µM; background electrolyte: 10 mM phosphate buffer, pH 7.4; separation voltage: 10 kV; bare fused silica capillary. (b) Injection of guest 5 in 0-30 µM cavitand 2. [Guest 5] = 2 µM; [riboflavin] = 1 µM; background electrolyte: 10 mM phosphate buffer, pH 7.4; separation voltage: 15 kV; linear-polyacrylamide capillary.

Furthermore, the migration time of guest **5** is delayed and appears after the peak for fluorescein, which is used as an internal standard. The inclusion of cavitand **1** in the running buffer also causes the intensity of the negative peak, appearing in both traces, to increase in magnitude. This is caused by the difference in absorbance between the running buffer and the water in the sample. Since water has a lower absorbance than phosphate buffer, it shows up as a negative peak. A negative peak is similar to a void peak in which there is absence of the analyte.[28] Furthermore, the intensity of the negative peak increases in the cavitand **1** trace due to cavitand increasing the background absorbance at 200 nm, as indicated by the host's absorbance in Figure 4.2.

Compared to cavitands **1**-**2**, cavitand **3** has poor water solubility; thus, we focused our studies more on cavitands **1** and **2**. Cavitand **2** also had poor water solubility, but we

were able to use fluorescence detection in order to use lower concentrations of this host. In addition, there is an added benefit of fluorescence detection in that it is more sensitive than absorbance detection. The use of cavitand **2** also required the LPA-coated capillary, which causes a reduced EOF. In this regard, we used a different internal standard, riboflavin, since negatively charged fluorescein would migrate very slowly.

Fluorescein is negatively charged at pH 7.4 so it would not have a reasonable migration time. As shown in Figure 4.6b, there is no shift in the migration time of guest **5** and the internal standard in the range of 0 to 10 μM of cavitand **2** in the background electrolyte. However, there is peak broadening for both molecules at 20 μM cavitand **2**. At 30 μM cavitand **2**, the peak for guest **5** is even more broad and riboflavin does not appear within this time window. Although riboflavin does not have a cationic group at neutral pH, the migration shift of the internal standard could be based on hydrophobic interactions with the synthetic receptor.

4.3.3 Potential Interactions of Proteins with Cavitand

Following the analysis in a simpler system with small molecule guests, we proceeded to study possible interactions of various proteins with cavitands **1** and **2**. As opposed to the small guests, proteins may be better options due to stronger hydrophobic interactions they can have with the cavity. In a biological setting, there can be other sequence-dependent interactions that help facilitate binding. Amino acids have a plethora of variation based on their isoelectric point, charge, hydrophobicity or hydrophilicity, and steric bulk, which contributes to the complexity of host-guest interactions. We injected a mixture of various proteins ranging in isoelectric points (Figure 4.7). Cytochrome c and

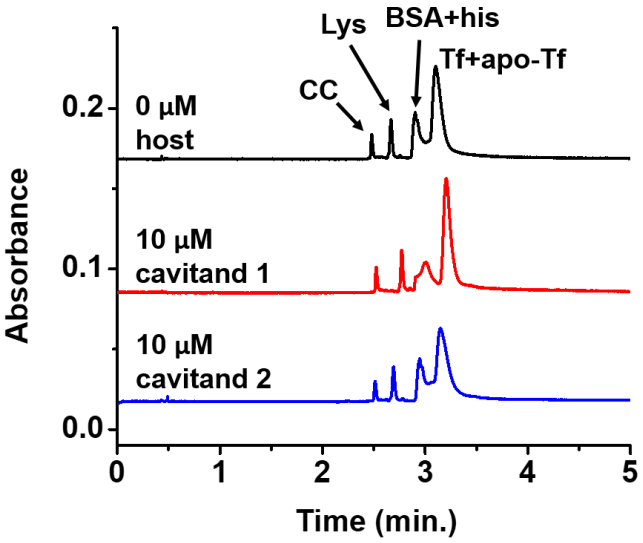

Figure 4.7 Separation of a standard protein mixtures in the presence of 0 µM host, 10 µM cavitand **1**, and 10 µM cavitand **2**. CC = cytochrome c, Lys = lysozyme, BSA = bovine serum albumin, his = histidine, Tf = transferrin, apo-Tf = apo-transferrin. [Protein] = 1 µM; [histidine] = 100 µM; background electrolyte: 10 mM phosphate buffer pH 3.0; separation voltage: 20 kV; linear-polyacrylamide capillary.

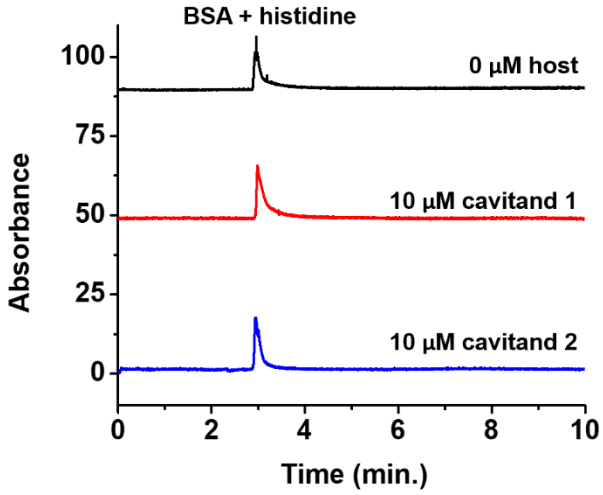

Figure 4.8 Injection of bovine serum albumin (BSA) and histidine in 0 µM host, 10 µM cavitand **1**, and cavitand **2**. [BSA] = 1 µM; [histidine] = 100 µM; background electrolyte: 10 mM phosphate buffer, pH 3.0; separation voltage: 20 kV; linear polyacrylamide-coated capillary.

lysozyme are basic proteins while bovine serum albumin (BSA) and the transferrin variants are acidic. However, we had to use a background electrolyte at acidic pH so all the proteins carry a positive charge, inducing fast migration times in the reduced EOF condition. We included an amino acid reference marker, histidine, which overlapped with BSA in the electropherogram. There was a slight shift in the electrophoretic mobility of BSA in the mixture of proteins. However, there was no change in the electrophoretic mobility of BSA when injecting it with the histidine marker alone (Figure 4.8).

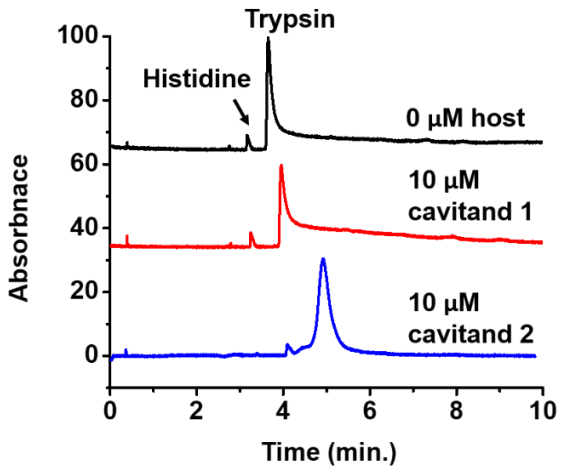

Figure 4.9 Injection of trypsin and reference marker histidine in 0 µM or 10 µM cavitand 1-2. [Trypsin] = 10 µM; [histidine] = 100 µM; background electrolyte: 10 mM phosphate buffer, pH 3.0; separation voltage: 20 kV; linear polyacrylamide capillary.

We studied the potential effects of cavitand on trypsin (Figure 4.9), which has been shown to interact with cavitand in the literature.[4] We used histidine as an internal standard again to correct any migration time shift. The addition of cavitand **1** did not change the overall migration time of trypsin. However, there was a shift in the migration time of trypsin as well as the internal standard when cavitand **2** was incorporated into the background electrolyte. While there was only a 1.44% mobility change comparing 0 and

10 µM cavitand **2**, there was a 27.3% change in electrophoretic mobility between 0 and 10 µM cavitand **1** (Table 4.2). Furthermore, there was a peak shape change, in terms tailing, of trypsin, when 10 µM cavitand **2** were present. The peak tailing was reduced with the presence of cavitand **2** when compared to the condition with cavitand **1** or no cavitand present.

Table 4.2 Electrophoretic mobility and percent mobility change of trypsin for cavitands 1 and 2.

	0 µM host	**10 µM cavitand 1**	**10 µM cavitand 2**
μ_{em} ($cm^2/V \cdot s$)	$-3.19 \times 10^{-5} \pm 1.4 \times 10^{-6}$	$-4.06 \times 10^{-5} \pm 2.8 \times 10^{-6}$	$-3.14 \times 10^{-5} \pm 4 \times 10^{-7}$
Mobility change (%)	0%	1.44%	27.3%

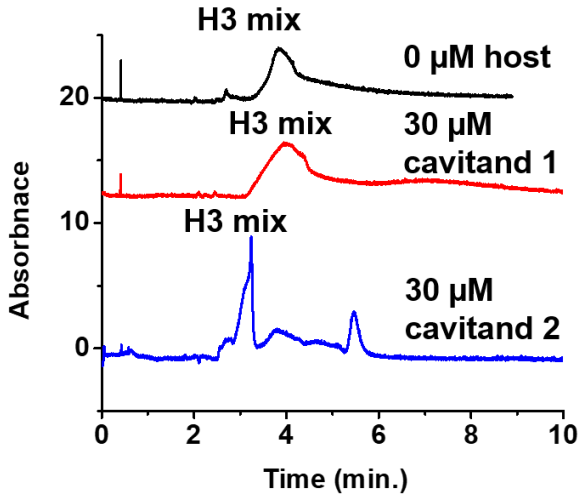

Figure 4.10 Injection of a H3.3 and H3K9me$_3$ protein mixture in 0 µM or 30 µM cavitands **1**-**2**. [Protein] = 3 µM; background electrolyte: 10 mM phosphate buffer, pH 3.0; separation voltage: 20 kV; linear polyacrylamide capillary.

After the attempt of separating several proteins with various isoelectric points, a more specific target, a protein containing lysine trimethylation, was tested. As shown in Figure 4.10, there was a slight change in the peak shape. Although there was no shift in the migration time, further optimization of buffer conditions, such as the cavitand concentration, can improve separation of these proteins. There is also the appearance of a second peak at 5.5 minutes when cavitand **3** was included in the running buffer. This could possibly be a protein degradation product, and the cavitand with imidazolyl feet can separate or enhance its peak. The lack of significant binding between the targets and the cavitand molecules could possibly be due to synthetic receptors still adsorbing to the capillary wall. Alternatively, mobility shift in the protein may not be significant when bound to the much smaller cavitand; this can be corroborated by the slight peak tailing of cavitands **2** and **3** in Figure 4.1.

4.4 Conclusions

In this chapter, we have studied the potential interactions between deep cavitands and various guests. Cavitands **1** and **2** have induced a mobility shift and increased the peak area of fluorescent guest **5** among the small guests. When studying protein interaction, it has been demonstrated that positively charged cavitand **2** can interact with trypsin based on the change in peak shape of the protein. In addition to unmodified proteins, cavitand binding with modified histone proteins can be studied. Although there was no separation between the unmethylated and trimethylated histone H3.3 proteins, there was a distinct change in peak shape. For the most promising proteins (i.e., trypsin and H3K9me$_3$ protein), further analysis must be performed to improve mobility shifts and CE separation. In the

future, the LPA-coated capillary can be employed in the analysis with positively charged proteins and guests; thus, adsorption of the targets can be reduced. However, an uncoated capillary can be utilized for studying negatively charged proteins and guests in order to obtain fast migration times and appearance of these peaks. There are several considerations to make when using cavitands in the background electrolyte.

4.5 References

(1) Liu, Y.; Perez, L.; Mettry, M.; Easley, C. J.; Hooley, R. J.; Zhong, W. Self-Aggregating Deep Cavitand Acts as a Fluorescence Displacement Sensor for Lysine Methylation. *J. Am. Chem. Soc.* **2016**, *138* (34), 10746–10749.

(2) Liu, Y.; Perez, L.; Mettry, M.; Gill, A. D.; Byers, S. R.; Easley, C. J.; Bardeen, C. J.; Zhong, W.; Hooley, R. J. Site Selective Reading of Epigenetic Markers by a Dual-Mode Synthetic Receptor Array. *Chem. Sci.* **2017**, *8* (5), 3960–3970.

(3) Liu, Y.; Perez, L.; Gill, A. D.; Mettry, M.; Li, L.; Wang, Y.; Hooley, R. J.; Zhong, W. Site-Selective Sensing of Histone Methylation Enzyme Activity via an Arrayed Supramolecular Tandem Assay. *J. Am. Chem. Soc.* **2017**, *139* (32), 10964–10967.

(4) Ghang, Y. J.; Perez, L.; Morgan, M. A.; Si, F.; Hamdy, O. M.; Beecher, C. N.; Larive, C. K.; Julian, R. R.; Zhong, W.; Cheng, Q.; et al. Anionic Deep Cavitands Enable the Adhesion of Unmodified Proteins at a Membrane Bilayer. *Soft Matter* **2014**, *10* (48), 9651–9656.

(5) Ghang, Y. J.; Lloyd, J. J.; Moehlig, M. P.; Arguelles, J. K.; Mettry, M.; Zhang, X.; Julian, R. R.; Cheng, Q.; Hooley, R. J. Labeled Protein Recognition at a Membrane Bilayer Interface by Embedded Synthetic Receptors. *Langmuir* **2014**, *30* (34), 10161–10166.

(6) Perez, L.; Ghang, Y. J.; Williams, P. B.; Wang, Y.; Cheng, Q.; Hooley, R. J. Cell and Protein Recognition at a Supported Bilayer Interface via in Situ Cavitand-Mediated Functional Polymer Growth. *Langmuir* **2015**, *31* (41), 11152–11157.

(7) Perez, L.; Mettry, M.; Hinman, S. S.; Byers, S. R.; McKeating, K. S.; Caulkins, B. G.; Cheng, Q.; Hooley, R. J. Selective Protein Recognition in Supported Lipid Bilayer Arrays by Tailored, Dual-Mode Deep Cavitand Hosts. *Soft Matter* **2017**, *13* (21), 3966–3974.

(8) Liu, Y.; Mettry, M.; Gill, A. D.; Perez, L.; Zhong, W.; Hooley, R. J. Selective Heavy Element Sensing with a Simple Host-Guest Fluorescent Array. *Anal. Chem.* **2017**, *89* (20), 11113–11121.

(9) Trembleau, L.; Rebek, J. Interactions between a Surfactant and Cavitand in Water Blur Distinctions between Host and Guest. *Chem. Commun.* **2004**, *4* (1), 58–59.

(10) Garnett, G. A. E.; Starke, M. J.; Shaurya, A.; Li, J.; Hof, F. Supramolecular Affinity Chromatography for Methylation-Targeted Proteomics. *Anal. Chem.* **2016**, *88* (7), 3697–3703.

(11) Fan, J.; Krautkramer, K. A.; Feldman, J. L.; Denu, J. M. Metabolic Regulation of Histone Post-Translational Modifications. *ACS Chem. Biol.* **2015**, *10* (1), 95–108.

(12) Newman, J. C.; He, W.; Verdin, E. Mitochondrial Protein Acylation and Intermediary Metabolism: Regulation by Sirtuins and Implications for Metabolic Disease. *J. Biol. Chem.* **2012**, *287* (51), 42436–42443.

(13) Xu, C.; Ng, D. T. W. Glycosylation-Directed Quality Control of Protein Folding. *Nat. Rev. Mol. Cell Biol.* **2015**, *16* (12), 742–752.

(14) Tang, X.; Gao, J. S.; Guan, Y. jie; McLane, K. E.; Yuan, Z. L.; Ramratnam, B.; Chin, Y. E. Acetylation-Dependent Signal Transduction for Type I Interferon Receptor. *Cell* **2007**, *131* (1), 93–105.

(15) Tryndyak, V. P.; Kovalchuk, O.; Pogribny, I. P. Loss of DNA Methylation and Histone H4 Lysine 20 Trimethylation in Human Breast Cancer Cells Is Associated with Aberrant Expression of DNA Methyltransferase 1, Suv4-20h2 Histone Methyltransferase and Methyl-Binding Proteins. *Cancer Biol. Ther.* **2006**, *5* (1), 65–70.

(16) Seligson, D. B.; Horvath, S.; Shi, T.; Yu, H.; Tze, S.; Grunstein, M.; Kurdistani, S. K. Global Histone Modification Patterns Predict Risk of Prostate Cancer Recurrence. *Nature* **2005**, *435* (7046), 1262–1266.

(17) Biros, S. M.; Ullrich, E. C.; Hof, F.; Trembleau, L.; Rebek, J. Kinetically Stable Complexes in Water: The Role of Hydration and Hydrophobicity.

(18) Mosca, S.; Yu, Y.; Rebek, J. Preparative Scale and Convenient Synthesis of a Water-Soluble, Deep Cavitand. *Nat. Protoc.* **2016**, *11* (8), 1371–1387.

(19) Liu, Y.; Liao, P.; Cheng, Q.; Hooley, R. J. Protein and Small Molecule Recognition Properties of Deep Cavitands in a Supported Lipid Membrane Determined by Calcination-Enhanced SPR Spectroscopy. *J. Am. Chem. Soc.* **2010**, *132* (30), 10383–10390.

(20) Zhu, G.; Sun, L.; Dovichi, N. J. Thermally-Initiated Free Radical Polymerization for Reproducible Production of Stable Linear Polyacrylamide Coated Capillaries, and Their Application to Proteomic Analysis Using Capillary Zone Electrophoresis-Mass Spectrometry. *Talanta* **2017**, *263* (2), 219–227.

(21) Li, V.; Ghang, Y.-J.; Hooley, R. J.; Williams, T. J. Non-Covalent Self Assembly Controls the Relaxivity of Magnetically Active Guests. *Chem. Commun. (Camb).* **2014**, *50* (11), 1375–1377.

(22) Korbakov, N.; Timmerman, P.; Lidich, N.; Urbach, B.; Sa'ar, A.; Yitzchaik, S. Acetylcholine Detection at Micromolar Concentrations with the Use of an Artificial Receptor-Based Fluorescence Switch. *Langmuir* **2008**, *24* (6), 2580–2587.

(23) Fernández-Abad, S.; Pessêgo, M.; Basílio, N.; García-Río, L. Counterion-Controlled Self-Sorting in an Amphiphilic Calixarene Micellar System. *Chem. - A Eur. J.* **2016**, *22* (19), 6466–6470.

(24) Sun, S.; Yuan, Y.; Li, Z.; Zhang, S.; Zhang, H.; Peng, X. Interaction of a Hemicyanine Dye and Its Derivative with DNA and Cucurbit[7]Uril. *New J. Chem.* **2014**, *38* (8), 3600–3605.

(25) Liu, Y.; Duan, Y.; Gill, A. D.; Perez, L.; Jiang, Q.; Hooley, R. J.; Zhong, W. Metal-Assisted Selective Recognition of Biothiols by a Synthetic Receptor Array. *Chem. Commun. (Camb).* **2018**, *54* (93), 13147–13150.

(26) Gill, A. D.; Perez, L.; Salinas, I. N. Q.; Byers, S. R.; Liu, Y.; Hickey, B. L.; Zhong, W.; Hooley, R. J. Selective Array-Based Sensing of Anabolic Steroids in Aqueous Solution by Host–Guest Reporter Complexes. *Chem. - A Eur. J.* **2019**, *25* (7), 1740–1745.

(27) Gill, A. D.; Hickey, B. L.; Wang, S.; Xue, M.; Zhong, W.; Hooley, R. J. Sensing of Citrulline Modifications in Histone Peptides by Deep Cavitand Hosts. *Chem. Commun.* **2019**, *55* (88), 13259–13262.

(28) Sebille, B.; Thuaud, N.; Tillement, J. P. Equilibrium Saturation Chromatographic Method for Studying the Binding of Ligands to Human Serum Albumin by High-Performance Liquid Chromatography. Influence of Fatty Acids and Sodium Dodecyl Sulphate on Warfarin-Human Serum Albumin Binding. *J. Chromatogr. A* **1979**, *180* (1), 103–110.

Chapter 5 Conclusions and Future Developments

5.1 Conclusions

This dissertation has focused on the succession of a host-assisted capillary electrophoresis (host-assisted CE) method for selectively separating biomolecules with post-translational modifications (PTMs). In addition, we were able to form a library of different synthetic receptors to employ in CE, and we applied our method to various PTM enzymes.

In chapter 2, we developed a host-assisted capillary electrophoresis method in order to selectively discriminate between different lysine methylation levels.[1] We first tested our method with small molecules that contained methyl binding handles, which provided a simple system to study. From this experiment, we compared affinity measurements for different combinations of hosts and guests. We kept one host, 4-tetrasulfonatocalix[4]arene (CX4), the same, and CX4 bound most strongly to the trimethylated guest; in addition, the dissociation constant increased when there were fewer methyl groups on the binding handle. When comparing the affinity of different hosts for the trimethylated guest, cucurbit[7]uril had the strongest binding. Furthermore, all three receptors had comparatively stronger affinities for the H3K27(me_3) peptide than for the small molecule guests, which suggests that there are external influences from the surrounding sequence of the peptides. In contrast to the results from the small molecule study, 4-hexasulfonatocalix[6]arene (CX6) resulted in the best resolution when separating peptides. The combination of the high resolution in CE as well as the excellent selectivity of the synthetic hosts resulted in well-separated peptides. We were able to demonstrate the

applicability to an enzyme assay and monitor the activity of lysine demethylases, KDM6B and JMJD2E, as a proof-of concept. Furthermore, monitoring the effect of the 2,4-PDCA inhibitor on the activity of both lysine demethylases was successful.

In chapter 3, we expanded the applicability of the host-assisted CE method to other enzymes, such as G9a methyltransferase and Aurora B kinase. A coated capillary is a vital tool when injecting basic histone peptides as it prevents the adsorption of these samples to the negatively charged capillary wall; therefore, we coated the capillary wall with linear polyacrylamide (LPA). The LPA-coated capillary was found to be stable in the presence of synthetic receptors, calixarenes and cucurbiturils. In the literature, LPA-coatings have only been previously tested with other buffer additives, such as surfactants and ionic liquids.[2] After testing the coating's compatibility with the macrocycles, we successfully monitored the activities of G9a and Aurora B kinase with unmodified and modified peptide substrates. Through host-assisted CE, we saw antagonistic effects of phosphorylated serine 10 and dimethylated lysine 9 on G9a and Aurora B kinase activity, respectively Furthermore, our method demonstrated simultaneous monitoring of enzyme reactions for multiple substrates. Our research showed that host-assisted CE can analyze crosstalk activity between different PTMs, and there is possibility of expanding the use of this method to other crosstalk activity and monitoring synergistic effects between histone marks.

In chapter 4, we investigated potential small molecule and protein guests for cavitands as alternative synthetic receptors. In contrast to CX4, CX6, and CB7, cavitands have a deeper cavity to encompass an analyte. Although there wasn't significant binding

between the selected guests and the different cavitand hosts, we still found some indication of binding cavitands **1** and **2** with *trans*-4-[4-(Dimethylamino)styryl]-1-methylpyridinium iodide (DSMI). Furthermore, there was a change in the peak shape of trypsin when adding cavitand **2** to the background electrolyte as well as a reduction in peak tailing with both cavitands **1** and **2**; this indicates other forms of interactions with cavitands, including hydrogen bonding, hydrophobic, and electrostatic interactions. When trying to separate the unmethylated and trimethylated histone H3 protein pair, the peak shape changed when including the positively charged cavitand 2 in the background electrolyte. When injecting the protein, it is important to note that the protein is large in comparison to cavitand: cavitands are around 1.5 kDa, while proteins can range upward from 10 kDa. In addition, the charge of the protein is very large in acidic conditions; therefore, the complex will not differ much in charge compared to the free protein, which can cause the binding shift to be small. Although the separation is challenging, further optimization can be performed in order to improve the resolution. The peak shape changes in the trypsin and H3 proteins indicate that there is some form of binding that is occurring.

5.2 Future Developments

The low solubility in water was a challenge in obtaining efficient separation with cavitands **2** and **3** from chapter 4; however, a great benefit in using cavitands is the tunability of the rim and feet to enhance selectivity and render the structure appropriate for the method conditions at hand. In addition to the cavitands introduce in chapter 4, there are several alternative cavitand structures currently available (Figure 5.1).

Tetraphosphonate cavitands have been developed by the Dalcanale group;[3] in this structure, the positioning of the phosphonate groups are directed towards the center of the cavity. These cavitands have different interactions with methylated species, including cation-dipole, cation-π, and hydrogen bonding interactions.[3] Cavitand **4** is one variation of tetraphosphonate cavitand that includes pyridyl groups on the feet and phosphonate groups on the rim, both of which improve water solubility of this molecule (Figure 5.1). Aside from this property, a unique characteristic of this host is its selectivity for a lower methylation state (i.e., monomethylation).[4] Other synthetic hosts that have been reported to have affinity for lysine methylation usually have a preference for higher levels of methylation.[5–7]

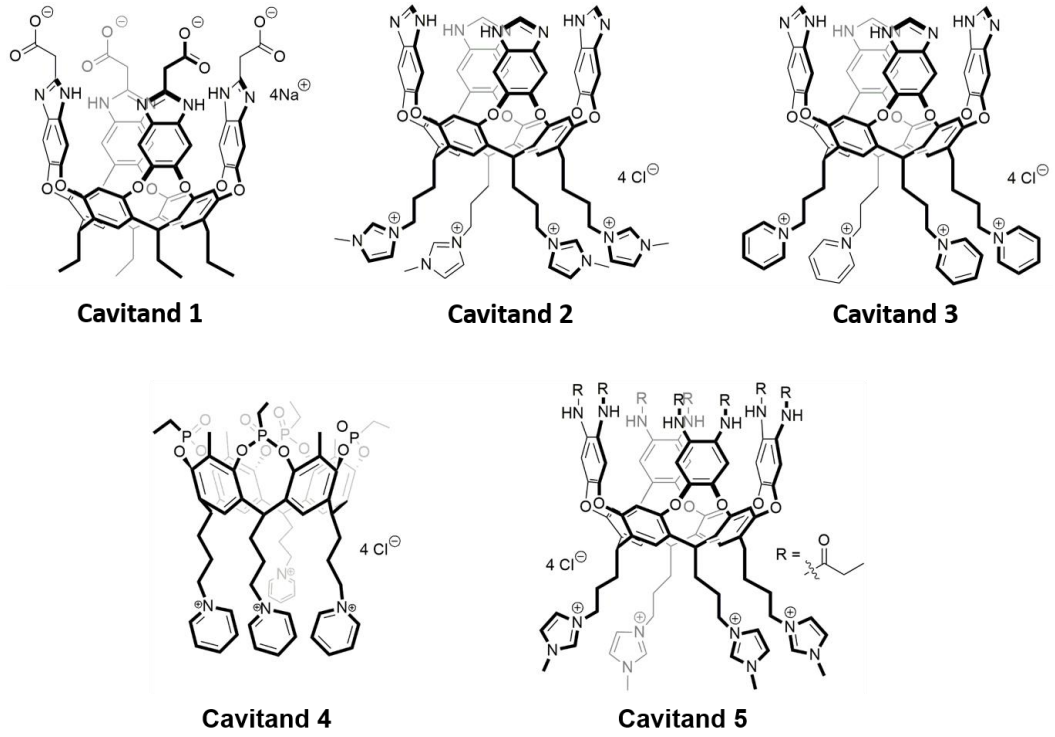

Figure 5.1 Structures of cavitands **1**-**5**.

We performed a quick test with 21-amino acid H3K9 peptides that we used in chapter 2. When injecting a mixture of nonmethylated and monomethylated H3K9 peptides, the two peptides co-migrate in the separation buffer without synthetic receptor. With the presence of cavitand **4**, there was an increasing migration time shift with an increase in the concentration of cavitand **4** (Figure 5.2). There is a split peak in the trace

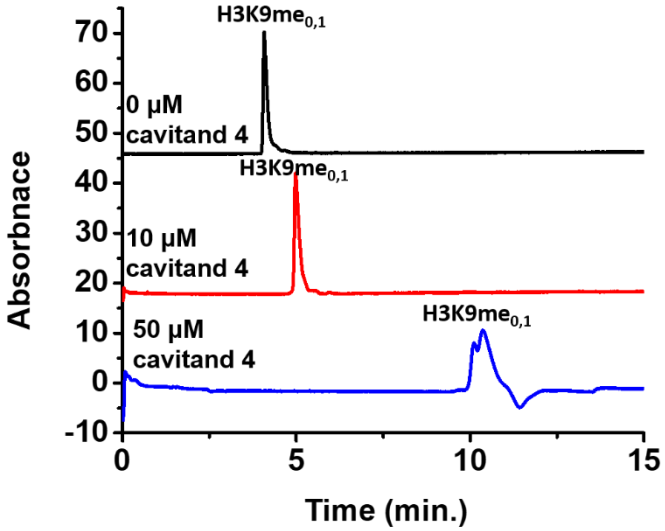

Figure 5.2 Injection of H3K9me$_{0,1}$ (1-21) peptide mixture in the presence of 0-50 μM cavitand **4**. [Peptide] = 20 μM; background electrolyte: 10 mM phosphate buffer, pH 3.0; separation voltage: 20 kV with the addition of 5 mbar; linear polyacrylamide capillary.

with 50 μM; however, the appearance of splitting is not an indication of the two peptides separating. When each peptide was injected individually in the presence of 50 μM cavitand **4**, split peaks were still present for each peptide (Figure 5.3a); this could be attributed to the two forms of cavitand **4**, as shown when the host was injected as a sample in Figure 5.3b. Although there was no separation of the H3K9me$_{0,1}$ pair, there was a peak broadening effect in the 50 μM cavitand **4** condition, which can indicate some interaction between the host and the peptides. The broadening effect could be a result of slow kinetics and an

unstable complex. In addition, all the receptor molecules may not be spending the same amount of time in the complexed form.[8,9] In this effect, the conditions should be customized further in order to resolve the peptides. For example, we can increase the amount of time that the peptide and cavitand remain in the complexed form.

As an improved version of cavitand **2** from chapter 4, a water-soluble octamide cavitand (i.e., cavitand **5** in Figure 5.1) that is synthesized by the Hooley group can be another alternative.[10] There are additional hydrogen bond points on the octamide rim of the synthetic receptor that improves solubility in water. In combination with the cavitand **1**-**3** from chapter 4, we can form a direct combinatorial library for screening guests.

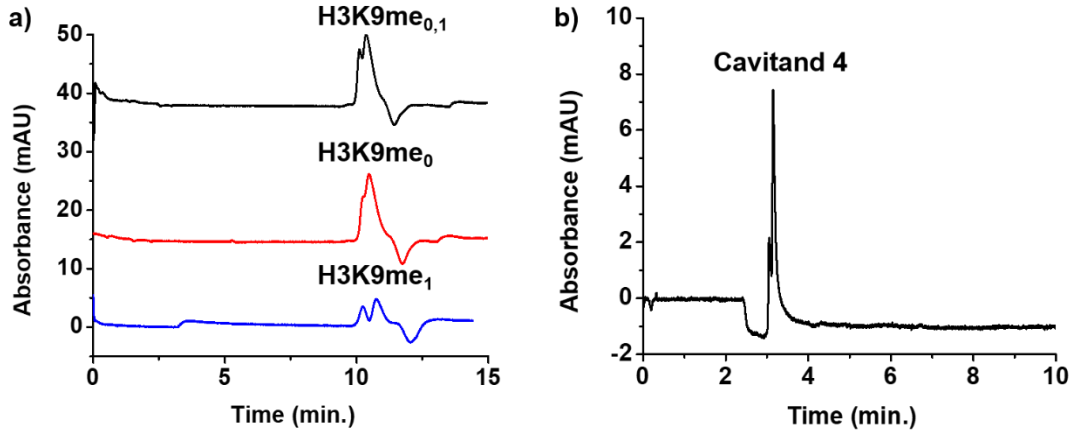

Figure 5.3 (a) Injection of H3K9me$_{0,1}$ as a mixture or individually in 50 μM cavitand **4**. [Peptide] = 20 μM; background electrolyte: 10 mM phosphate buffer, pH 3.0; separation voltage: 20 kV with added 5 mbar; linear-polyacrylamide capillary. (b) Injection of 100 μM cavitand **4** in 10 mM phosphate buffer, pH 3.0. Separation voltage: 20 kV with added 5 mbar; linear polyacrylamide capillary.

Aside from using other cavitands, we can focus on optimizing an affinity capillary electrophoresis (ACE) method to improve the binding of guests to cavitand. For the

calixarene and cucurbituril derivatives that were tested in chapters 2 and 3, there was a shift in migration time for the small guests and the peptides when bound to the synthetic receptors in the running buffer, which indicates fast kinetics at play. However, cavitands may be undergoing slow kinetics in their interaction, at least with the fluorescein-derivative guests (i.e., guests **1**-**4** in chapter 4). We can increase the time of the host and guest in a complex form by pre-incubating cavitands and guests **1**-**4** before introducing the sample into the capillary. This process is called pre-equilibrium CZE. In addition to pre-incubation of the complex, we can include the receptor in the background electrolyte to reduce dissociation of the complex. Furthermore, there may not be a large mobility shift when observing the binding of cavitand to various proteins. Cavitand **1** has previously been used in CE except it was in the presence of a lipid, 1-palmitoyl-2-oleoyl-sn-glycero-3-phosphocholine (POPC).[11] We can incorporate cavitand into lipid micelles[12] to induce a larger mobility shift in the proteins.

5.3. References

(1) Lee, J.; Perez, L.; Liu, Y.; Wang, H.; Hooley, R. J.; Zhong, W. Separation of Methylated Histone Peptides via Host-Assisted Capillary Electrophoresis. *Anal. Chem.* **2018**, *90* (3), 1881–1888.

(2) Beneito-Cambra, M.; Anres, P.; Vial, J.; Gareil, P.; Delaunay, N. Stability and Effectiveness of Linear Polyacrylamide Capillary Coating to Suppress EOF in Acidic Media in the Presence of Surfactants, Ionic Liquids and Organic Modifiers. *Talanta* **2016**, *150*, 546–552.

(3) Pinalli, R.; Brancatelli, G.; Pedrini, A.; Menozzi, D.; Hernández, D.; Ballester, P.; Geremia, S.; Dalcanale, E. The Origin of Selectivity in the Complexation of N-Methyl Amino Acids by Tetraphosphonate Cavitands. *J. Am. Chem. Soc.* **2016**, *138* (27), 8569–8580.

(4) Bontempi, N.; Biavardi, E.; Bordiga, D.; Candiani, G.; Alessandri, I.; Bergese, P.; Dalcanale, E. Probing Lysine Mono-Methylation in Histone H3 Tail Peptides with an Abiotic Receptor Coupled to a Non-Plasmonic Resonator. *Nanoscale* **2017**, *9* (25), 8639–8646.

(5) Liu, Y.; Perez, L.; Mettry, M.; Easley, C. J.; Hooley, R. J.; Zhong, W. Self-Aggregating Deep Cavitand Acts as a Fluorescence Displacement Sensor for Lysine Methylation. *J. Am. Chem. Soc.* **2016**, *138* (34), 10746–10749.

(6) Gill, A. D.; Perez, L.; Salinas, I. N. Q.; Byers, S. R.; Liu, Y.; Hickey, B. L.; Zhong, W.; Hooley, R. J. Selective Array-Based Sensing of Anabolic Steroids in Aqueous Solution by Host–Guest Reporter Complexes. *Chem. - A Eur. J.* **2019**, *25* (7), 1740–1745.

(7) Beshara, C. S.; Jones, C. E.; Daze, K. D.; Lilgert, B. J.; Hof, F. A Simple Calixarene Recognizes Post-Translationally Methylated Lysine. *ChemBioChem* **2010**, *11* (1), 63–66.

(8) Heegaard, N. H. H.; Nilsson, S.; Guzman, N. A. Affinity Capillary Electrophoresis: Important Application Areas and Some Recent Developments. *J. Chromatogr. B Biomed. Appl.* **1998**, *715* (1), 29–54.

(9) Heegaard, N. H. H. Determination of Antigen-Antibody Affinity by Immuno-Capillary Electrophoresis. *J. Chromatogr. A* **1994**, *680* (2), 405–412.

(10) Gill, A. D.; Hickey, B. L.; Wang, S.; Xue, M.; Zhong, W.; Hooley, R. J. Sensing of Citrulline Modifications in Histone Peptides by Deep Cavitand Hosts. *Chem. Commun.* **2019**, *55* (88), 13259–13262.

(11) Ghang, Y. J.; Perez, L.; Morgan, M. A.; Si, F.; Hamdy, O. M.; Beecher, C. N.; Larive, C. K.; Julian, R. R.; Zhong, W.; Cheng, Q.; et al. Anionic Deep Cavitands Enable the Adhesion of Unmodified Proteins at a Membrane Bilayer. *Soft Matter* **2014**, *10* (48), 9651–9656.

(12) Schramm, M. P.; Hooley, R. J.; Rebek, J. Guest Recognition with Micelle-Bound Cavitands. *J. Am. Chem. Soc.* **2007**, *129* (31), 9773–9779.